

NASA/TM–2014-218507



Multi-Mission System Analysis for Planetary Entry (M-SAPE) Version 1

*Jamshid Samareh and Louis Glaab
Langley Research Center, Hampton, Virginia*

*Richard G. Winski
Binera, Inc., Yorktown, Virginia*

*Robert W. Maddock
Langley Research Center, Hampton, Virginia*

*Anjie L. Emmett
Analytical Mechanics Associates, Inc., Hampton, Virginia*

*Michelle M. Munk
Langley Research Center, Hampton, Virginia*

*Parul Agrawal, Steve Sepka, Jose Aliaga,
Kerry Zarchi, and Nancy Mangini
Ames Research Center, Moffett Field, California*

*Scott Perino and Javid Bayandor
Virginia Polytechnic Institute and State University, Blacksburg, Virginia*

*Charles Liles
Old Dominion University, Norfolk, Virginia*

August 2014

NASA STI Program . . . in Profile

Since its founding, NASA has been dedicated to the advancement of aeronautics and space science. The NASA scientific and technical information (STI) program plays a key part in helping NASA maintain this important role.

The NASA STI program operates under the auspices of the Agency Chief Information Officer. It collects, organizes, provides for archiving, and disseminates NASA's STI. The NASA STI program provides access to the NASA Aeronautics and Space Database and its public interface, the NASA Technical Report Server, thus providing one of the largest collections of aeronautical and space science STI in the world. Results are published in both non-NASA channels and by NASA in the NASA STI Report Series, which includes the following report types:

- **TECHNICAL PUBLICATION.** Reports of completed research or a major significant phase of research that present the results of NASA Programs and include extensive data or theoretical analysis. Includes compilations of significant scientific and technical data and information deemed to be of continuing reference value. NASA counterpart of peer-reviewed formal professional papers, but having less stringent limitations on manuscript length and extent of graphic presentations.
- **TECHNICAL MEMORANDUM.** Scientific and technical findings that are preliminary or of specialized interest, e.g., quick release reports, working papers, and bibliographies that contain minimal annotation. Does not contain extensive analysis.
- **CONTRACTOR REPORT.** Scientific and technical findings by NASA-sponsored contractors and grantees.

- **CONFERENCE PUBLICATION.** Collected papers from scientific and technical conferences, symposia, seminars, or other meetings sponsored or co-sponsored by NASA.
- **SPECIAL PUBLICATION.** Scientific, technical, or historical information from NASA programs, projects, and missions, often concerned with subjects having substantial public interest.
- **TECHNICAL TRANSLATION.** English-language translations of foreign scientific and technical material pertinent to NASA's mission.

Specialized services also include organizing and publishing research results, distributing specialized research announcements and feeds, providing information desk and personal search support, and enabling data exchange services.

For more information about the NASA STI program, see the following:

- Access the NASA STI program home page at <http://www.sti.nasa.gov>
- E-mail your question to help@sti.nasa.gov
- Fax your question to the NASA STI Information Desk at 443-757-5803
- Phone the NASA STI Information Desk at 443-757-5802
- Write to:
STI Information Desk
NASA Center for AeroSpace Information
7115 Standard Drive
Hanover, MD 21076-1320

NASA/TM–2014-218507



Multi-Mission System Analysis for Planetary Entry (M-SAPE) Version 1

*Jamshid Samareh and Louis Glaab
Langley Research Center, Hampton, Virginia*

*Richard G. Winski
Binera, Inc., Yorktown, Virginia*

*Robert W. Maddock
Langley Research Center, Hampton, Virginia*

*Anjie L. Emmett
Analytical Mechanics Associates, Inc., Hampton, Virginia*

*Michelle M. Munk
Langley Research Center, Hampton, Virginia*

*Parul Agrawal, Steve Sepka, Jose Aliaga,
Kerry Zarchi, and Nancy Mangini
Ames Research Center, Moffett Field, California*

*Scott Perino and Javid Bayandor
Virginia Polytechnic Institute and State University, Blacksburg, Virginia*

*Charles Liles
Old Dominion University, Norfolk, Virginia*

National Aeronautics and
Space Administration

Langley Research Center
Hampton, Virginia 23681-2199

August 2014

Acknowledgments

M-SAPE project is a multidisciplinary analysis and design activity, and the project would have been impossible to do without the help of many experts. The authors would like to thank the following people: Howard Abston (LaRC), Sasan Armand (LaRC), James Arnold (ARC), Nikki Bauer (GT), Robert Braun (GT), Juan Cruz-Ayoroa (GT), Artem Dyakonov (LaRC), Bob Gershman (JPL), Robin Hardy (LaRC), Kimberly Halom (LARSS), Chris Johnston (LaRC), Daniel Lyons (JPL), Richard Mattingly (JPL), Michelle Munk (LaRC), Erik Nilsen (JPL), Dinesh Prabhu (LaRC), Jeremy Shidner (LaRC), Aaron Siddens (VT), Brandon Smith (GT), Erick Sturm (JPL), Ken Sutton (LaRC), Chris Tanner (GT), John Theisinger (LaRC), and Ethiraj Venkatapathy (ARC).

The use of trademarks or names of manufacturers in this report is for accurate reporting and does not constitute an official endorsement, either expressed or implied, of such products or manufacturers by the National Aeronautics and Space Administration.

Available from:

NASA Center for AeroSpace Information
7115 Standard Drive
Hanover, MD 21076-1320
443-757-5802

TABLE OF CONTENTS

List of Figures	v
List of Tables	viii
Nomenclature	ix
Summary	1
1.0 Introduction	2
1.1 MMEEV Description	3
1.2 M-SAPE Description	5
2.0 M-SAPE System	5
2.1 Multidisciplinary Systems Analysis	6
2.2 M-SAPE Tool Architecture	7
2.3 Web Portal	8
2.4 Web Portal Development and Operational Approach	12
2.5 Sample Web Portal Results	13
3.0 M-SAPE Modules	17
3.1 Parametric Vehicle Module	17
3.1.1 Inputs	18
3.1.2 Rules and Constraints.....	18
3.1.3 Validation.....	19
3.1.4 Geometry and Mass Sizing.....	21
3.1.5 Impact Analysis.....	26
3.1.6 Structural Analysis.....	28
3.2 Flight Mechanics Module	30
3.3 Aerodynamic Module	33
3.3.1 Summary of Data Sources.....	33
3.3.2 Rarefied and Hypersonic Aero Data.....	34
3.3.3 Supersonic Aero Data	36
3.3.4 Transonic Aero Data.....	36
3.3.5 Subsonic Aero Data	37
3.3.6 Summary of all Static Data across the Mach Number Range.....	37
3.3.7 MMEEV Dynamic Data.....	38
3.4 Aerothermal Module	42
3.4.1 Vehicle Geometries	42
3.4.2 CFD Methodology.....	43
3.4.3 CFD Results	44
3.5 TPS Sizing Module	54
3.5.1 Background	54
3.5.2 MER Model Development	55
3.6 Thermal Soak Module	58
3.6.1 Finite Element Model Development.....	60
3.6.2 Entry Environments and Boundary Conditions.....	64

3.6.3 Temperature Predictions in Entry Vehicle Design.....	66
3.6.4 Parametric Thermal Soak Model Development for M-SAPE.....	67
3.6.5 Summary and Future work.....	69
4.0 Sample Results	69
5.0 Conclusion	72
6.0 Future Development and opportunities for collaboration	73
7.0 References.....	74

LIST OF FIGURES

Figure 1. Sample Return Earth Entry Vehicles (left to right: Genesis, Stardust, Hayabusa, and Phobos-Grunt).....	2
Figure 2. MSR Vehicle Concept.....	4
Figure 3. Time into Design Process	5
Figure 4. Design Structure Matrix for M-SAPE	7
Figure 5. M-SAPE Flow Chart	9
Figure 6. M-SAPE System Integration	10
Figure 7. M-SAPE System Integration Example (UML Sequence Diagram).....	11
Figure 8. Screenshot of M-SAPE Database Query and Results.....	14
Figure 9. Screenshot of M-SAPE Contour Plot.....	15
Figure 10. Screenshot of M-SAPE Sample Single Run Results.....	16
Figure 11. Sample Vehicle Models	17
Figure 12. Flow Chart for Parametric Vehicle Model.....	20
Figure 13. Geometry Models for MSR and Non-MSR Vehicles.....	22
Figure 14. Non-MSR Vehicle Assumptions	23
Figure 15. MSR Vehicle Assumptions.....	23
Figure 16. MSR and/or Non-MSR Vehicle Parameters.....	24
Figure 17. MSR and/or Non-MSR Vehicle Parameters (Close Up)	24
Figure 18. MSR Vehicle Parameters	25
Figure 19. Impact G's Assuming Ground Penetration.....	27
Figure 20. Required foam Thickness and Compression Strength	28
Figure 21. A Biplane Cross Section View of the Finite-Element Model of Impact Sphere.....	29
Figure 22. Finite-Element Model of EEV for Launch and Entry	30
Figure 23. Model Integration into POST2, MSL Example.....	31
Figure 24. MMEEV Representative Trajectory	33
Figure 25. MMEEV Supersonic, Hypersonic, and Rarefied Flow Pitching Moment at 0.2D cm	34
Figure 26. CFD Computer Flow field at 100 Degrees Angle of Attack.....	35
Figure 27. Time History Data for Several Trajectories with Different CGs (Cms). Baseline CG=0.2D.....	37
Figure 28. MMEEV Normal Force Coefficient for All Mach Numbers.....	38
Figure 29. MMEEV Pitching Moment and Axial Force Coefficients for All Mach Numbers.....	40
Figure 30. MMEEV Pitch Damping Data from M=0.5 to 2.1.....	41
Figure 31. Geometries are Superimposed.....	43
Figure 32. Mach Contour for the v1 Geometry.....	45
Figure 33. Correlated Heat Flux with Varying Velocity as Compared to DPLR and Sutton-Graves.....	45
Figure 34. Correlated Heat Flux with Varying Entry Path Flight angles as Compared to DPLR and Sutton-Graves.....	46
Figure 35. Correlated Heat Flux with Varying Ballistic Coefficient as Compared to DPLR and Sutton-Graves.....	46

Figure 36. Stagnation Point Heat Flux along a Trajectory for v2 Geometry.....	47
Figure 37. Stagnation Point Heat Flux along a Trajectory	48
Figure 38. Mach Contour after Grid Adaption for the v2 Geometry.....	48
Figure 39. Mach Contour after Grid Adaption for the v3 Geometry.....	49
Figure 40. Stagnation Pressure for v1 Geometry.	50
Figure 41. Stagnation Pressure for v3 Geometry.	51
Figure 42. Non-dimensionalized Shoulder Heat Flux as a Function of Mach Number for the v3 Geometry.....	51
Figure 43. Heat Flux Comparison between Laminar and Fully Turbulent Solutions at an Early Point in the Trajectory	52
Figure 44. Heat Flux Comparison Between Laminar and Fully Turbulent Solutions at Peak Heating along the Trajectory.....	53
Figure 45. Time History of the Maximum Value of Momentum Thickness Reynolds Number for the v3 Geometry	53
Figure 46. Different Phases of Earth Entry Vehicle and Time Span for Thermal Soak Inside the Vehicle.....	59
Figure 47. MMEEV Thermal Soak Model Geometry.....	61
Figure 48. Finite Element Mesh with Component Sets.....	62
Figure 49. Materials Map for Baseline Thermal Analysis.....	63
Figure 50. Trajectory Space with Selected Trajectories	65
Figure 51. Figure 51. Sample M-SAPE Trade Space for MSR Model	71
Figure 52. Galahad EEV Concept (Maddock et al. 2010).....	71
Figure A1. MMEEV Aero Database for Rarefied Flow Conditions. Moment Reference Point is the Vehicle theoretical Nose Apex.....	A-1
Figure A2. MMEEV Aero Database for M=24. Moment Reference Point is the Vehicle theoretical Nose Apex.....	A-2
Figure A3. MMEEV Aero Database for M=9.8. Moment Reference Point is the Vehicle theoretical Nose Apex.....	A-3
Figure A4. MMEEV Aero Database for M=3.98. Moment Reference Point is the Vehicle Theoretical Nose Apex.....	A-4
Figure A5. MMEEV Aero Database for M=1.3. Moment Reference Point is the Vehicle theoretical Nose Apex.....	A-5
Figure A6. MMEEV Aero Database for M=1.15. Moment Reference Point is the Vehicle Theoretical Nose Apex	A-6
Figure A7. MMEEV Aero Database for M=0.85. Moment Reference Point is the Vehicle Theoretical Nose Apex	A-7
Figure A8. MMEEV Aero Database for M=0.75. Moment Reference Point is the Vehicle Theoretical Nose Apex	A-8
Figure A9. MMEEV Aero Database for M=0.6. Moment Reference Point is the Vehicle Theoretical Nose Apex	A-9
Figure A10. MMEEV Aero Database for M=0.5. Moment Reference Point is the Vehicle Theoretical Nose Apex	A-10
Figure B1. PICA-only MER GoF vs. FIAT-predicted PICA Thickness.....	B-2
Figure B2. Carbon Phenolic over ACC6 MER, GoF vs. FIAT-predicted PICA Thickness.....	B-4
Figure B3. SIRCA MER GoF.....	B-5
Figure B4. Acusil II MER GoF.....	B-6
Figure B5. SLA-561V MER GoF.....	B-7
Figure B6. LI900 MER GoF.....	B-10
Figure C1. The 256 Surface Body Points for Full body Aerothermal Analysis.....	C-1
Figure C2. Heat Flux Distribution along Vehicle at Peak Heating	C-1
Figure C3. DPLR Solutions with the Curve Fits Superimposed for the Low Heat Load Trajectory	C-2
Figure C4. Temperature Contours for the High Heat Load Trajectory	C-2
Figure C5. Temperature contours for the Low Heat Load Trajectory	C-3

Figure C6. Temperature Contours in the Probe after Touchdown.....	C-3
Figure C7. Peak Foam Temperature for the Two Trajectories	C-4
Figure C8. Payload temperature History and Peak Payload Temperature for Various Trajectories	C-4
Figure C9. Parametric Studies for Heat Flux Magnitude Variation for the High Heat Load Trajectory.....	C-5
Figure C10. Parametric Studies for Heat Flux Magnitude Variation for the Low Heat Load Trajectory	C-5
Figure C11. Peak Payload Temperature Variations with Head Load for a Given Vehicle Diameter	C-5
Figure C12. The GoF for Established Correlations for Peak Payload Temperature with Vehicle Diameter, Peak Stagnation Heat Flux and Head Load	C-6

LIST OF TABLES

Table 1. Mass Property Output Values	25
Table 2. Geopotential Coefficients	32
Table 3. Geometry Configurations	42
Table 4. CFD Trade Space for v1 Geometry	44
Table 5. Flight Trajectory Space Considered for the MERs	55
Table 6. Surface Heating and Pressure Ranges Found by Running FIAT over the 840 Trajectories	56
Table 7. Summary of MERs Model Development Data	57
Table 8. Summary of Arcjet, Galileo, Pathfinder, and MSL Materials Test Data	59
Table 9. Thickness of the Subcomponents along the Vertical Centerline for MMEEV Vehicle	61
Table 10. Specific Heat Capacity of Rohacell-51	63
Table 11. Thermal Conductivity of Rohacell-51	64
Table 12. For PICA TPS	68
Table 13. For CP TPS	68
Table 14. Input Parameters for Case 1	70
Table 15. M-SAPE Results Compared with Dillman and Corliss 2008	70
Table 16. M-SAPE Results Compared with Maddock et al. 2010	72
Table B1. B1. Material Stack-up for Carbon Phenolic Atop Advanced Carbon-Carbon 6	B-1
Table B3. Vehicle Characteristics	B-1
Table B4. MER Summary	B-1
Table B5. Flight Trajectory Space and Correlation Details for the PICA-only MER	B-2
Table B6. Material Stack-up	B-3
Table B7. Flight Trajectory Space and Correlation Details for the Carbon Phenolic Atop ACC MER	B-3
Table B8. SIRCA MER Parameters	B-5
Table B9. Acusil II Parameters	B-6
Table B10. SLA-561V Parameters	B-7
Table B11. LI-900 MER Parameters	B-9

NOMENCLATURE

<i>a,b,c</i>	Power Law Fit Parameters
ACC	Advanced Carbon-Carbon
ACE	Aerothermal Chemical Equilibrium Computer Program
CAD	Computer Aided Design
CFD	Computational Fluid Dynamics
CEV	Crew Exploration Vehicle
CG	Center of Gravity
CMA	Charring Material Thermal Response and Ablation Program
DPLR	Data Parallel Line Relaxation
DSMC	Direct Simulated Monte Carlo
DAC	DSMC Analysis Code
EDL	Entry Descent and Landing
EEV	Earth Entry Vehicle
EFPA	Entry Flight Path Angle, absolute degrees
FE	Finite Element
FEA	Finite Element Analysis
FIAT	Fully Implicit Ablation and Thermal Response
GoF	Goodness of Fit
GRAM	Global Reference Atmospheric Model
HL	Heat Load, J/cm ²
<i>i</i>	Index of Data Point
IGES	Initial Graphics Exchange Specification
LaRC	Langley Research Center
LAURA	Langley Aeroheating Upwind Relaxation Algorithm
MER	Mass Estimating Relationship
MMEEV	Multi Mission Earth Entry Vehicle
M-SAPE	Multi Mission System Analysis for Planetary Entry
MSR	Mars Sample Return

<i>n</i>	Total Number of Data Points
OS	Operating System
PHP	PHP Hypertext Preprocessor
PICA	Phenolic Impregnated Carbon Ablator
POST	Program to Optimize Simulated Trajectories
PRA	Probabilistic Risk Assessment
Python	Platform-independent open-source programming language
qmax	Maximum (peak) Heat Flux of a Trajectory, W/ cm ²
R	Residual
SD	Standard Deviation
STAB	Standard Ablation Program
STEP	Standard for the Exchange of Product Model Data
TH	TPS Thickness
TPS	Thermal Protection System
TRL	Technology Readiness Level
UTTR	Utah Test and Training Range
V	Velocity, km/sec

SUMMARY

This report describes an integrated system for Multi-mission System Analysis for Planetary Entry (M-SAPE). The system in its current form is capable of performing system analysis and design for an Earth entry vehicle suitable for sample return missions. The system includes geometry, mass sizing, impact analysis, structural analysis, flight mechanics, TPS, and a web portal for user access. The report includes details of M-SAPE modules and provides sample results.

Current M-SAPE vehicle design concept is based on Mars sample return (MSR) Earth entry vehicle design, which is driven by minimizing risk associated with sample containment (no parachute and passive aerodynamic stability). By M-SAPE exploiting a common design concept, any sample return mission, particularly MSR, will benefit from significant risk and development cost reductions. The design provides a platform by which technologies and design elements can be evaluated rapidly prior to any costly investment commitment.

An important goal for M-SAPE is to provide an integrated environment such that a low fidelity system analysis and trade can be performed in hours (not weeks or months) with sufficient hooks to perform high-fidelity analysis in days. The system is designed to help analysts to gain a better understanding of various entry system concepts and their limitations. The role of discipline experts in the systems analysis process is indispensable and cannot be replaced by any tool. However, M-SAPE helps to improve the performance of the systems analysis team by automating and streamlining the process, and this improvement can reduce the errors resulting from manual data transfer among discipline experts. The process improves and accelerates design activities such as trade studies, sensitivity analyses, Monte Carlo analyses, and vehicle optimization.

Another goal of M-SAPE is to use existing software components, especially open-source software, to avoid unnecessary software development and licensing issues. M-SAPE is a loosely-coupled system that uses Python language (platform-independent open-source software) for integration. Development has relied heavily on the object-oriented programming capabilities available in Python. Modules are provided to interface with commercial and government off-the-shelf software components.

1.0 INTRODUCTION

In recent years, the sample return mission concept has gradually grown increased favor. The successes of the Stardust and the partial successes of the Genesis missions, and most recently, the Japanese Hayabusa mission, have clearly highlighted the advantages of bringing samples back to Earth where they can be studied in much greater detail by more powerful instruments, examined by a much wider scientific community, and preserved over an extended period of time. With growing interest in the Moon, asteroids, comets, and particularly Mars, more and more sample return missions are included into the space exploration roadmap. For example, the Planetary Science Decadal Survey, published in March 2011, includes several missions to return samples to Earth from around the Solar System.

There were many sample return missions in the past. Figure 1 shows several sample return Earth entry vehicles. The Soviets had several successful robotic lunar sample-return missions in the 1970s. The NASA Genesis project was a sample return mission that was launched in August of 2001 to collect a sample of solar wind and return it to Earth. In September of 2004, the Genesis Earth entry vehicle crashed in the Utah desert when the parachutes failed to deploy, and the planned mid-air retrieval could not be performed. Stardust was a NASA sample return mission launched in 1999 to collect cosmic dust. The Stardust entry vehicle successfully landed at the Utah Test and Training Range in 2006. Hayabusa was a Japanese mission that collected dust from an asteroid, and it landed in June of 2010 in the South Australian Outback. There is a plan for a follow-up mission for Hayabusa 2 scheduled for either 2014 or 2015. Phobos-Grunt was a Russian sample return mission to Phobos. The mission was launched in November of 2011, but a failure left the spacecraft stranded in low Earth orbit. China has a mission plan to return a lunar sample in 2017. There is also the Mars Sample Return (MSR) plan, which is the most challenging of all existing sample return plans. Mattingly and May 2011 provide the most up-to-date overview of this mission plan.

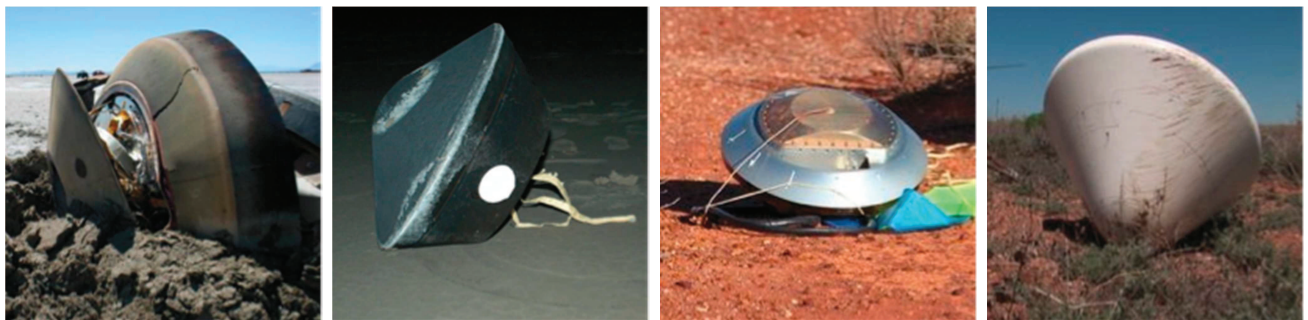


Fig. 1 Sample Return Earth Entry Vehicles (left to right: Genesis, Stardust, Hayabusa, and Phobos-Grunt)

The potential for terrestrial contamination from returned sample material could be a major driver for Earth Entry Vehicle (EEV) design. A planetary Entry, Descent, and Landing (EDL) system

typically consists of a heat shield for entry, a parachute for descent, and either retro rockets or airbags for landing. Mitcheltree et al. 1998 provide a discussion on two possible options for a reliable EEV design: either the design includes sufficient redundancy for each subsystem or eliminates the need for the subsystem. They propose a simple passive entry system solution that replaces the parachute and landing system with a hardened container surrounded by sufficient energy absorbing material to assure containment during ground impact. Dillman and Corliss 2008 continued refining Mitcheltree's model that is the basis for the EEV model used in the current study.

The Multi-Mission Earth Entry Vehicle (MMEEV) provides a highly reliable, yet flexible design concept, from which any sample return mission can benefit. Based on the MSR EEV design that was developed by minimizing risk associated with the loss of sample containment at Earth, the MMEEV concept provides a logical foundation upon which any individual mission can build an optimized design that meets their specific needs. Beginning from a single design concept ensures maximum commonality and feed-forward for all MMEEV users. The MMEEV concept provides a platform by which new technologies, design elements, and processes can be developed, tested, and even flown, prior to implementation on MSR. By leveraging common design elements and technology development, this approach could significantly reduce the risk and associated cost in development of not only the MSR EEV, but all sample return missions which utilize the MMEEV concept.

Maddock et al. 2008 provides the details of the MMEEV analysis, design, system components and the vehicle trade space for the Galahad asteroid sample return mission proposal submitted in response to the NASA New Frontiers solicitation. The second version of MMEEV is described in Maddock et al. 2011, where the initial tightly coupled MMEEV integration approach is introduced. The loosely coupled system integration was introduced in Samareh et al. 2012.

The NASA In-Space Propulsion Technologies (ISPT) Project, funded by the Science Mission Directorate, is continuing to conduct activities that will mature a class of vehicles in support of Earth entry, descent and landing mission phases. However, the ISPT Project funding level does not currently support a dedicated flight test prior to use of the MMEEV concept. The current strategy, therefore, is to mature vehicle critical characteristics for a range of MMEEVs to TRL 5-6 before the next Discovery or New Frontiers Announcement of Opportunity.

1.1 MMEEV Description

The Multi-Mission Earth Entry Vehicle (MMEEV) concept is based on the Mars Sample Return (MSR) EEV design originally developed at NASA LaRC in the 1990s for the 2003/2005 MSR Project (Figure 2). Development continued from 2000-2005 through focused technology development activities, including impact attenuation, sample containment, and aerodynamic performance. Development continued during 2005-2008 with NASA Langley internal funding. From 2008-2012, In-Space Propulsion Technology Program (ISPT) funded further development of the MMEEV system concept. During 2007-2008, a system analysis for planetary EDL (SAPE) (Samareh 2009) was developed with NASA Langley internal funds. The ISPT program continued funding development of MMEEV system analysis capability, which has since morphed into M-SAPE activity.

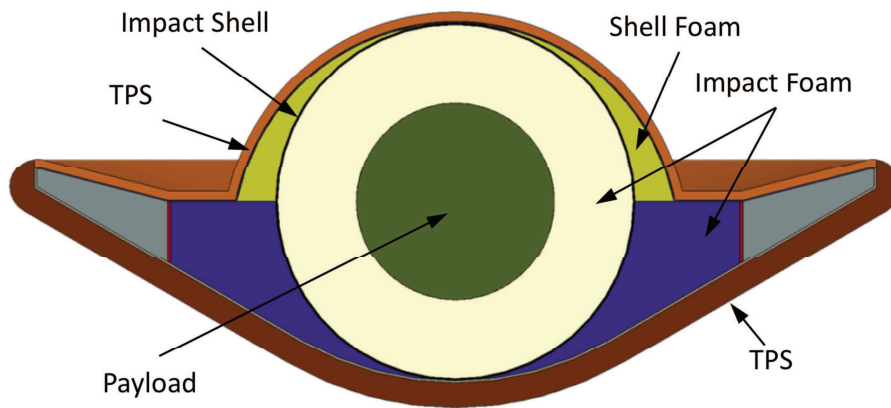


Figure 2. MSR Vehicle Concept

The MSR EEV design was driven by the mission's Probabilistic Risk Assessment (PRA) where (Earth) planetary protection and sample containment were the major drivers. This required the need to eliminate or minimize the use of active systems, as well as the strong drive to use heritage, high Technology Readiness Level (TRL) elements. In essence, the MSR EEV design was to be the most reliable vehicle humans could build.

This approach provided a logical starting point for any sample return mission. However, because the same level of reliability may not be needed by all missions due to variable planetary protection requirements, by using the MSR EEV design concept as a starting point, each mission could maximize reliability while also optimizing for specific mission needs. Although the MSR EEV baseline design has not changed dramatically since 2001, modifications were anticipated as new technologies and processes were made available. And that is where MMEEV came in.

The high reliability of the MSR EEV design can be attributed to two design principles, both of which were preserved in the MMEEV concept. The first of these design principles was eliminating all active systems, including the parachute. The combined reliability of parachutes and their required automated deployment systems is much lower than that needed to ensure sample containment for MSR. Also, parachute systems can be massive, thus increasing aeroheating and impact loads in the event of a parachute failure, and possibly reducing aerodynamic stability during entry by shifting the center of mass aft. They can also be difficult to package, which could complicate the sample transfer chain.

The second key design principle which the MMEEV preserved is the use of a well-known, highly tested, and flight proven aerodynamic forebody shape - the 60 degree, half-angle sphere cone. This forebody shape provides robust performance against a wide range of entry condition dispersions and atmospheric uncertainties. In addition, selecting an aftbody shape that provides for hypersonic stability upon atmospheric reentry is highly desirable. This allows for a reorientation capability, even when spin stabilized and entering the atmosphere backwards or tumbling due to attitude errors from spacecraft separation or meteoroid impact. Although, this particular capability is only needed for missions with very stringent planetary protection requirements, such as MSR, the concept was implemented on MMEEV and studied as a way to provide feed-forward to MSR.

To support this strategy, the software tool known as M-SAPE (Multi Mission System Analysis for Planetary Entry) has been created to assist in the development of a flexible Earth Entry Vehicle (EEV) design that can be utilized by multiple sample return missions.

1.2 M-SAPE Description

As the vehicle design process goes forward, designs are refined based upon information developed during the process. However, as shown in Figure 3, the later in the process this information becomes available, the more difficult and expensive it becomes to act upon the knowledge gained.

M-SAPE is a system analysis tool developed for use by planetary probe vehicle designers to make enough information available early in the design process to maintain design freedom while still improving the probability of mission success.

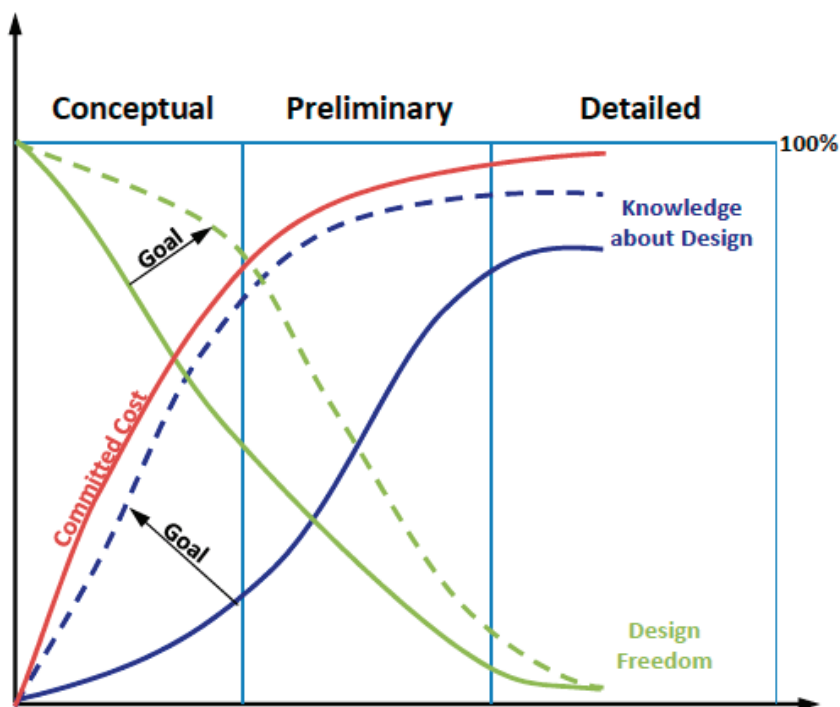


Figure 3. Time into Design Process (baseline is in solid lines and improved is in dotted lines)

2.0 M-SAPE SYSTEM

The purpose of systems analysis of an EEV is to gain a better understanding of various entry system concepts and their limitations. Systems analysis teams typically include systems engineers and discipline-specific experts in flight mechanics, aerodynamics,

aerothermodynamics, structural analysis, impact analysis, thermal soak, and thermal protection systems. The systems analysis process may take from several weeks to several years.

The NASA In-Space Propulsion Technology (ISPT) Program has funded a system analysis project for the development of Multi-Mission Earth Entry Vehicle (MMEEV) for the past several years. Maddock et al. 2008, 2010, and 2011; and Samareh et al. 2012 have documented the overall MMEEV project and its progress.

The implementation of the multidisciplinary analysis approach presented here is a modified version of the System Analysis for Planetary EDL (SAPE) code (Samareh 2012). This implementation is targeted for Multi-Mission Earth Entry Vehicles using SAPE (M-SAPE). The purpose of M-SAPE is to provide a variable-fidelity capability for conceptual and preliminary analysis within the same framework. M-SAPE uses Python language (platform-independent open-source software) for integration. The development has relied heavily on the object-oriented programming capabilities available in Python. M-SAPE has links to commercial and government off-the-shelf software modules (e.g., flight mechanics code, POST2). An important goal for M-SAPE is to provide an integrated environment such that a low fidelity system analysis and trade can be performed in minutes and hours (not days or weeks) with sufficient hooks to perform high-fidelity analysis in days. Another goal of M-SAPE is to use existing software modules, especially open-source software to avoid unnecessary software development and licensing issues.

As stated in Section 1.0, the M-SAPE goal is to develop a flexible Earth Entry Vehicle (EEV) design that can be utilized by multiple sample return missions. By preserving key common elements, the MMEEV concept provides a platform by which technologies, design elements, and processes can be developed and flight-tested prior to implementation on MSR. This approach could not only significantly reduce the risk and associated cost in development of the MSR EEV, but all sample missions that would benefit by leveraging common design elements.

2.1 Multidisciplinary Systems Analysis

Integrated multidisciplinary analysis tools improve the performance of the systems analysis team by automating and streamlining the process, and this improvement can reduce the errors resulting from manual data transfer among discipline experts. The process improves and speeds up the design activities such as trade studies, sensitivity analyses, Monte Carlo analyses, and vehicle optimization.

A multidisciplinary problem can be decomposed into a set of key disciplines. These discipline tools, in this paper referred to as modules, can be represented in matrix form using the Design Structure Matrix (DSM) approach. The matrix is a graphical approach for representing the interdependencies among the various modules. The DSM is a square matrix with the analysis modules positioned along the main diagonal. Figure 4 shows a DSM representation for the EEV integrated analysis tool that includes seven analysis modules: geometry, mass sizing, impact analysis, structural analysis, flight mechanics, TPS sizing, and thermal soak. For each analysis module shown along the DSM diagonal, relevant outputs are listed in the corresponding row; the inputs are listed in the corresponding column. For example, the required inputs for impact

analysis are the OML, mass, terminal velocity, and temperature field. Impact analysis outputs include an estimate for the mass of impact sphere as well as the required impact stroke. The data exchanges among modules below the DSM diagonal indicate a feedback loop. The DSM can be reordered to reduce the number of feedback loops or to exchange strong feedback loops with weaker ones.

Design or Dependency Structure Matrix for MMEEV

	Geometry Module	Mass Sizing	Impact Analysis	Structural Analysis	Flight Mechanics	Aerothermal	TPS Sizing	Thermal Soak
Geometry Module	Geometry	OML	OML	OML	OML	OML	OML	OML
Mass Sizing	Overall Size	Mass Sizing	Mass	Mass	Mass			
Impact Analysis	Energy Absorber Stroke	Energy Absorber Mass	Impact Analysis					
Structural Analysis		Structural Mass		Structural Analysis				
Flight Mechanics			Terminal Velocity	Entry Loads	Flight Mechanics	Environment		
Aerothermal						Aerothermal	Heat Rate	Heat Rate
TPS Sizing		TPS Mass					TPS Sizing	TPS Interface Condition
Thermal Soak			Temperature Field	Temperature Field				Thermal Soak

Columns are inputs, and Rows are outputs

Figure 4. Design Structure Matrix for M-SAPE

2.2 M-SAPE Tool Architecture

There are two approaches to implement a multidisciplinary analysis system: tightly-coupled or loosely-coupled. In a tightly-coupled implementation, the modules are integrated at the module levels. This type of implementation results in a system with faster execution time, but it is difficult to implement and maintain. In a loosely-coupled approach, the modules are integrated at the application levels. This type of coupling is relatively easy to implement, modify, and maintain. However, there is an additional computational overhead, albeit a very small one for this implementation. M-SAPE uses a loosely-coupled implementation approach.

The current M-SAPE implementation, geometry, mass sizing, impact analysis, and structural sizing are combined into a single integrated tool referred to as the parametric vehicle model. The aerodynamics model is incorporated into the flight mechanics tool. Figures 5 - 7 show M-SAPE implementation process from different perspectives.

As discussed before, M-SAPE is a loosely coupled, integrated problem with a strong feedback loop. The problem is solved using standard Gauss–Seidel approach, which has been very effective. Figure 5 shows a flowchart of M-SAPE overall solution process, which is broken into 10 major steps (numbered in the order they are processed):

1. Read and validate user inputs.
2. Create relevant M-SAPE Python objects.

3. Initialize objects and database.
4. Start Gauss–Seidel iterative process by calculating mass and volume based on available information.
5. Calculate trajectory. In early stages of convergence, a low-fidelity model is used. As convergence is reached, a high-fidelity model is used.
6. Calculate heating environment.
7. Calculate thermal soak response.
8. Calculate TPS thickness.
9. Assess M-SAPE model and convergence status.
10. Create a report and update database.
11. If convergence is not reached, go to step 5.
12. End of process.

Python language is used to wrap individual modules and integrate them together. Figure 6 shows an overview of M-SAPE implementation. Completed modules and connections are shown with solid lines, and those that are incomplete are shown with broken lines. The modules are designed to be independent, and interactions among them are managed by M-SAPE Driver that is also written in Python.

Figure 7 shows a typical module integration using POST as an example. The figure is a sequence diagram that is used in unified modeling language (UML). This sequence diagram involves four modules: M-SAPE Driver, Post Wrapper, M-SAPE Utilities, and POST executable. The diagram is executed from top to bottom and from left to right.

2.3 Web Portal

M-SAPE users access the software through a Web Portal. To run a vehicle design case, users must set vehicle characteristics and then select the “Run M-SAPE” button on the Web page.

The goal of M-SAPE Web Portal is to provide an intuitive, secure user interface and data-tracking system. The tool allows approved users to utilize the M-SAPE software in a web-enabled and secure environment. A PHP (Hypertext Preprocessor) user interface connected to a MySQL database on a NASA server was developed for this project. The PHP pages are accessible by a user’s browser as long as they are inside the NASA Langley firewall.

Users must provide credentials to access the M-SAPE Web Portal. They can then run the M-SAPE software for either a single entry vehicle analysis or a trade-space contour plot. They are also able to view and query previous M-SAPE data runs stored in the MySQL backend of the site (aka Database Module). There are over 80,000 unique entry vehicle designs stored in the M-SAPE Web Portal. This easy-to-use system grants vehicle designers the functionality to obtain preliminary information about possible probe designs while maintaining data security via user authentication and limiting access to data based on a user’s privileges.

The real strength of M-SAPE is its flexible handling of large amounts of data. System Administrators can upload massive datasets into the Database Module (via a PHP interface) where regular users can access, but not alter it.

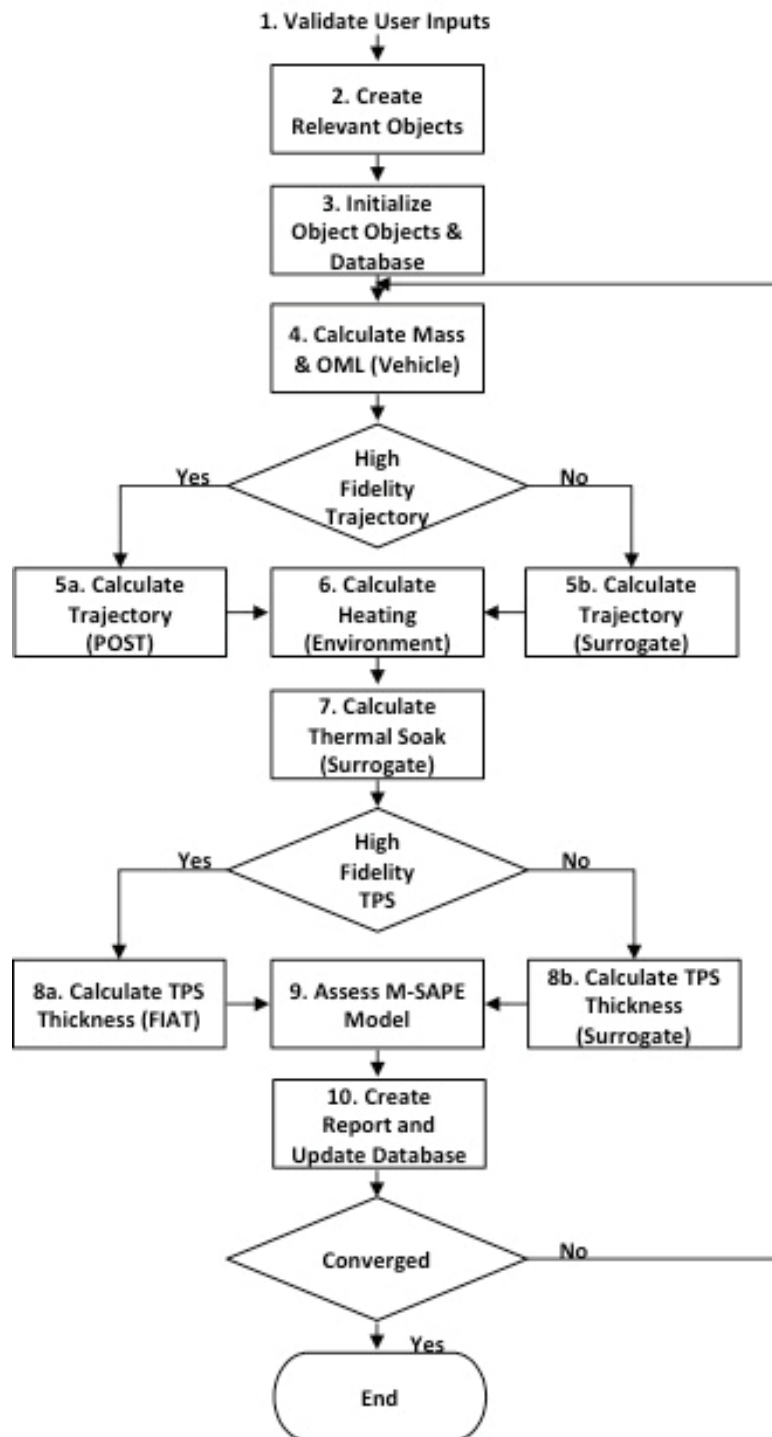


Figure 5. M-SAPE Flow Chart

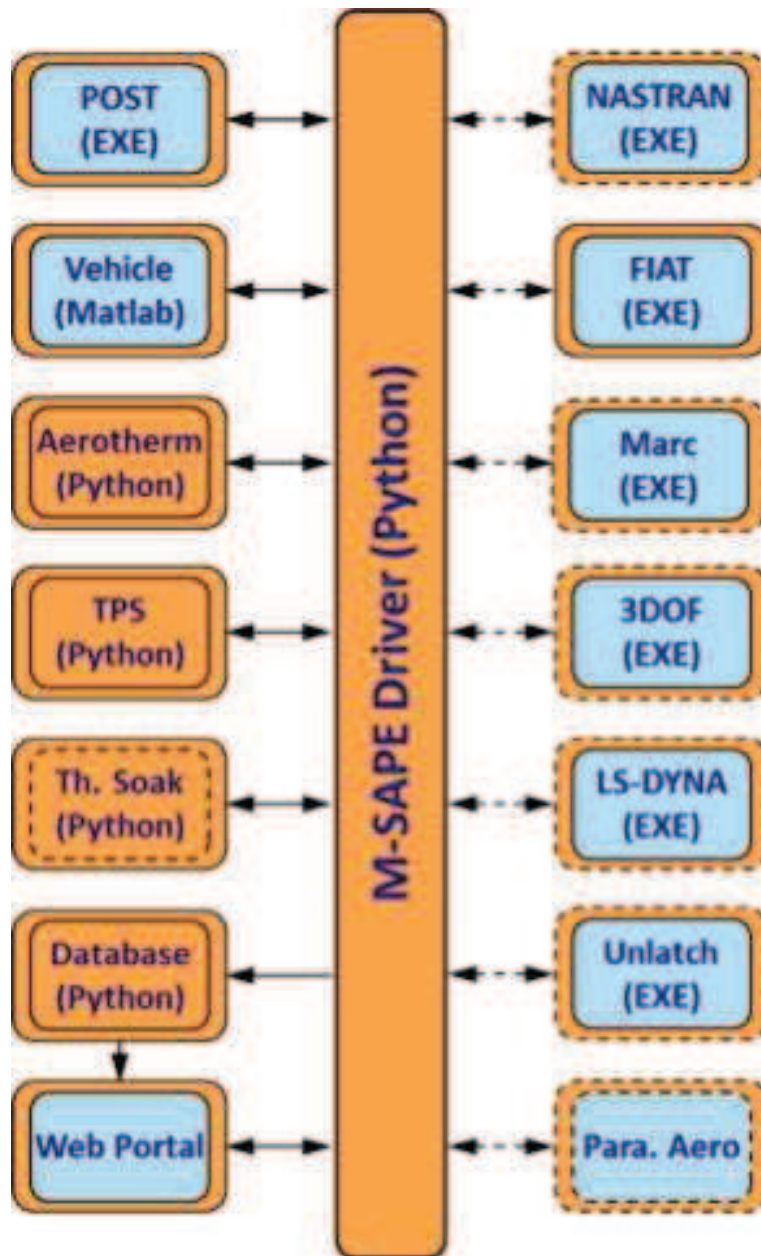


Figure 6. M-SAPE System Integration (modules in tan color are in Python and sky-blue color are in the native application language)

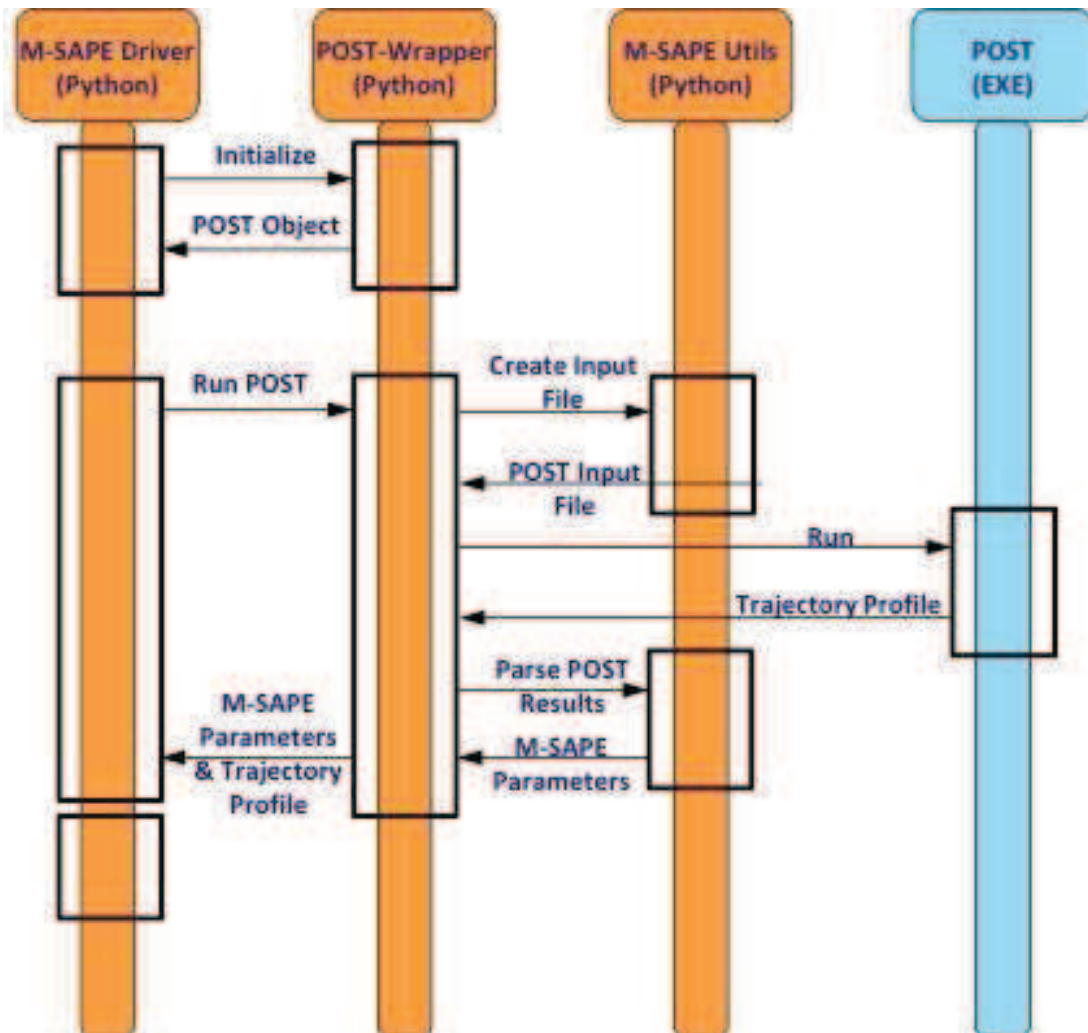


Figure 7. M-SAPE System Integration Example (UML Sequence Diagram)

The most obvious advantage of the Web Portal system is that it provides authorized users a secure access to M-SAPE, enabling more streamlined development of entry vehicle prototypes for a wider audience in the future.

2.4 Web Portal Development and Operational Approach

The M-SAPE Web Portal system was designed to be flexible and intuitive to use. It was also constructed to function on a wide array of operating systems (OS) such as Windows, Macintosh and Unix/Linux and software environments such as Internet Explorer, Google Chrome, Safari, Opera, and Mozilla Firefox. PHP was chosen as the code for developing this system because it is a server-side scripting language that provides a user-interface via common Internet browsers. PHP can also connect to a MySQL database stored on the server, allowing users to access previously stored data and update data without granting them full access to the database. Finally, PHP is capable of calling other code on its server. The Web Portal was designed to make calls to M-SAPE code written in Python and return the results.

The PHP pages built for the M-SAPE Web Portal are connected to a MySQL interface that is stored on a server. The PHP interface to the MySQL database can import, export, and display dynamic data. Datasets in different formats can be uploaded into the system. PHP identifies the format of the data based on the CSV file from which it is uploaded into the system. It then dynamically creates tables to store the information. For each new dataset created in the M-SAPE Web Portal, another storage table is created to identify what type of data is being stored in its associated table. Also, the M-SAPE PHP code identifies independent variables and creates indexes for each of these variables within the data storage tables. These indexes are vital for fast retrieval of queried data.

Once data is uploaded to M-SAPE web portal, users can query this information from a browser interface. The interface provides a mechanism for querying both numeric and nominal (i.e., text) data. M-SAPE also can export this data to the user's file system in the same format from which it was originally uploaded.

It proved to be a challenge to integrate the PHP interface with the preexisting Python code from the M-SAPE project. This had to be implemented for both the contour plotting functionality and the single-run M-SAPE Python function. The PHP pages which run the Python scripts on the server side have to record user inputs, export data from MySQL into a CSV file that Python can read, call the Python script while passing user inputs and the input CSV file location as command line arguments, and then display the results of the call. The primary difficulty when doing this is due to timing as some Python M-SAPE routines can take several minutes to run in some cases. So, to display the results, PHP opens a separate pop up window that continuously refreshes and checks to see if the Python results have been generated. Once the M-SAPE Python code outputs its results, the pop up window automatically shows the user the resulting page. The M-SAPE Web Portal also logs users' actions that an administrator can use for maintaining and debugging problems.

2.5 Sample Web Portal Results

As mentioned above, the web portal interface was built in PHP which can be opened in any common internet browser. Users can query the underlying MySQL database by entering query parameters into their browser and selecting a “Query” button on the displayed webpage. Figure 8 shows an example screenshot where a user has queried the M-SAPE database to find all stored examples of entry vehicles with a carbon-phenolic forebody TPS and an Accusil aftbody TPS.

This interface is designed to be intuitive and easy to use. Users can enter minimum and/or maximum values for numeric, independent variables as shown in Fig. 8. They can also select nominal, independent variables in the combo boxes displayed in the middle of the screenshot. The query returned by the system will be based on what the user has entered for these nominal and numeric variables. The number of results obtained by the query is displayed (in this case, it is 10,079 records), and the user has the option to export the results to a CSV file by clicking on the “Export Results to CSV” hyperlink.

The M-SAPE web portal also has the ability to display contour plots of dependent, numeric data as shown in Figure 9 using either a K-dimension tree (KD-tree) or neural network plot prediction methods. The neural network plotting method also has the ability to provide nominal output plot shading. Users must first select independent, nominal variables for the plot. They must then select which numeric, independent variables will be used in the X and Y axes of the plot. Next, specific values for the remaining numeric, independent variables must be entered, and the numeric, dependent variables which the user would like to see displayed in the plot must be selected. When this has been done, users can click a “Plot” button in their browser, and a pop-up window will appear which will continuously refresh until the contour plot is created. When the plot has been created by the underlying M-SAPE Python code on the server, it will automatically appear in the new pop-up window. Figure 9 shows an example of a contour plot where the Forebody Max Total Heat Rate, Max Entry Load, and Total Entry Mass have been plotted together.

Figure 10 shows a single run of the Python M-SAPE code from the Web Portal. For a single M-SAPE run, users must enter all desired values for nominal and numeric independent variables for the entry vehicle they want to design. The system will then test the validity of the vehicle design using the Python M-SAPE code on the server. A pop-up window will appear showing the results of the run. The results will include a cross-section of the entry vehicle design, a table showing details about the model and its performance, warnings about which variables had to be adjusted to close the user-desired design, and plots showing the vehicle’s altitude over time, total heat rate over time, deceleration over time, and altitude over relative velocity. A user’s previous M-SAPE results are stored in the Web Portal and can be accessed later by the user. The Web Portal also authenticates users on sign-in and tracks their use of the system.

The Web Portal provides a number of advantages. First, users have an easy access to M-SAPE. Second, the security of the M-SAPE software can be maintained at just one location. Third, the code for M-SAPE can be maintained and updated at just one site. M-SAPE also stores data securely behind the NASA firewall. It requires user authentication and grants hierarchical rights

based on whether or not users are also administrators. The Web Portal also tracks user actions and prevents unauthorized users from viewing the data and results stored in the MySQL database by specific users.

Entry Flight Path Angle (deg) -16/-3

Entry Velocity (m/s) 10000/16000

Input Shoulder Radius / Vehicle Radius 0.05/0.05

Input Vehicle Diameter (m) 0.6/2

Mass Convergence Criterion (kg) 0.001/0.001

Mass Margin 0.3/0.3

Max. Number of Iterations 20/20

Nose Radius / Vehicle Radius 0.75/0.75

Payload Diameter / Vehicle Diameter 0.2/0.6

Payload Mass (kg) 5/30

Radiative Heat Rate Margin 1/1

Acusil Aftbody TPS Concept

SuttonGraves Convective Heat Rate Model

CP Forebody TPS Concept

--Select Item-- MSR Mode

TauberSutton Radiative Heat Rate Model

My First Run Run Name

(3) Select the "Query" button below to launch the query:

Query

Export Results to CSV

There are 10079 cases available. Only the first 200 results are shown below. You may view all results by selecting **Export Results to CSV** above.

Adjusted Shoulder Radius (m)	Adjusted Shoulder Radius / Vehicle Radius	Adjusted Vehicle Diameter (m)	Aeroshell Type	Aftbody Angle (deg)	Aftbody Carrier Structure Density (kg/m ³)	Aftbody Carrier Structure Mass (kg)	Aftbody Carrier Structure Thickness (cm)	Aftbody Max Heat Rate (W/cm ²)	Aftbody TPS Concept	Aftbody TPS Density (kg/m ³)	Aftbody TPS Mass (kg)	Aftbody TPS Message	Aftbody TPS Thickness (cm)	Aftbody Total Heat Load (J/cm ²)	Attached Structure Depth (m)	Ballistic Coefficient at Impact (kg/m ²)	Body Foam Density (kg/m ³)	Convective Heat Rate Margin	Convective Heat Rate Model	Converged	Crust Load Limit (g's)
0.0264	0.088	0.6	Sphere-Cone	24.343	1522	0.339649	0.0561	11.90963836	Acusil	255	0.774684	None	0.807174267	174.2270674	0.142511	126.991	160	1.3	SuttonGraves	Yes	1500
0.0262	0.0654	0.8	Sphere-Cone	29.9592	1522	0.857409	0.0756	9.595643951	Acusil	255	1.394912	None	0.738532031	139.6400268	0.175746	108.263	160	1.3	SuttonGraves	Yes	1500
0.0261	0.0521	1	Sphere-Cone	23.8768	1522	1.61927	0.095	8.303656393	Acusil	255	2.060178	None	0.6975882	121.1530036	0.187417	100.572	160	1.3	SuttonGraves	Yes	1500
0.03	0.04	1.2	Sphere-	21.7778	1477	7.710107	0.1142	7.512109463	Acusil	255	2.802109	None	0.677191755	110.4667917	0.198071	98.225	160	1.3	SuttonGraves	Yes	1400

Figure 8. Screenshot of M-SAPE Database Query and Results

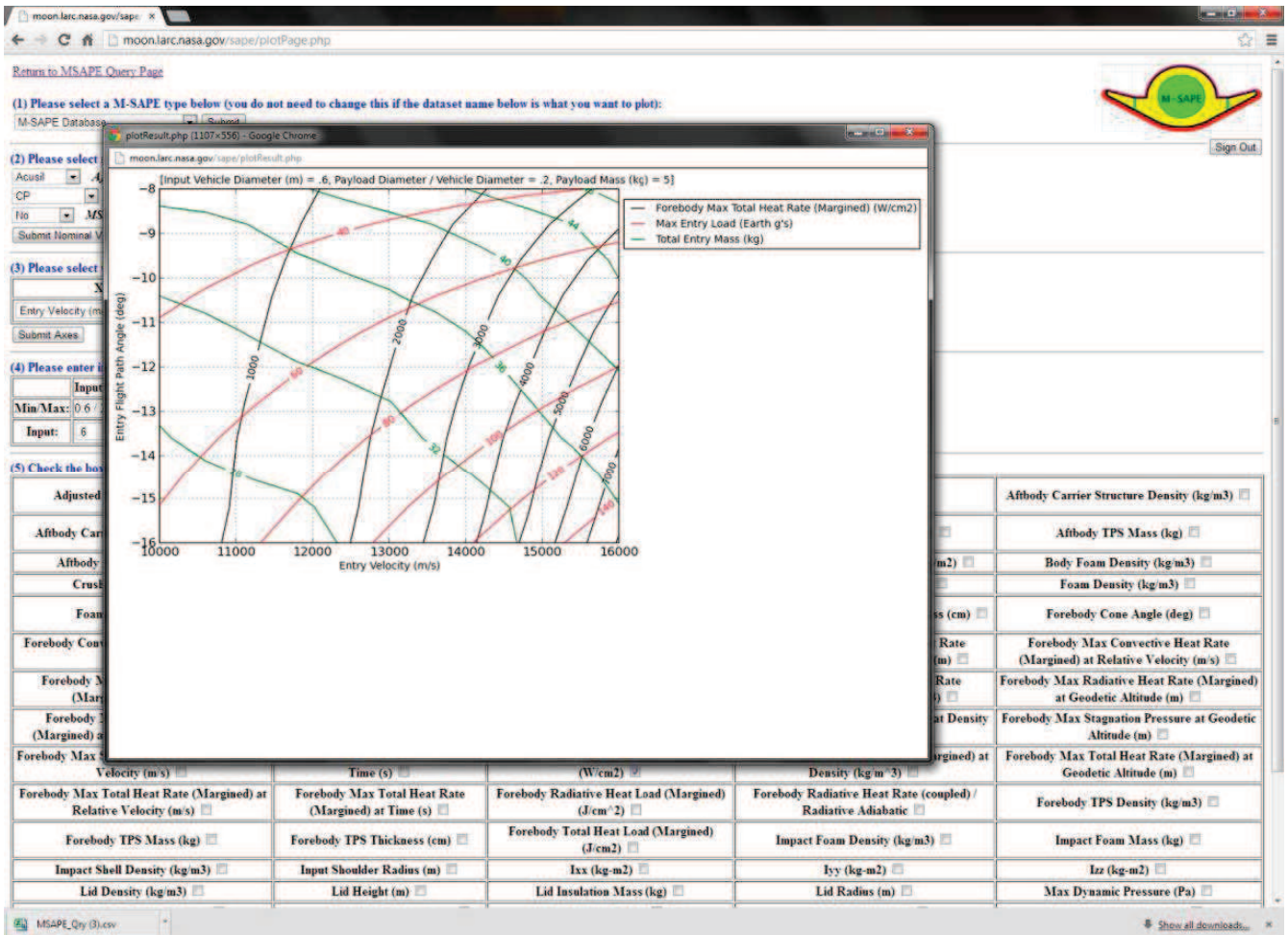


Figure 9. Screenshot of M-SAPE Sample Contour Plot

The Web Portal provides a number of advantages. First, users have an easy access to M-SAPE. Second, the security of the M-SAPE software can be maintained at just one location. Third, the code for M-SAPE can be maintained and updated at just one site. M-SAPE also stores data securely behind the NASA firewall. It requires user authentication and grants hierarchical rights based on whether or not users are also administrators. The Web Portal also tracks user actions and prevents unauthorized users from viewing the data and results stored in the MySQL database by specific users.

The M-SAPE Web Portal provides a structure within which users can securely access entry vehicle data. It grants access to M-SAPE Python code for users' analysis without giving them direct access to the underlying software. Appendix D contains a User Guide and step-by-step instructions on operating the Web Portal interface.

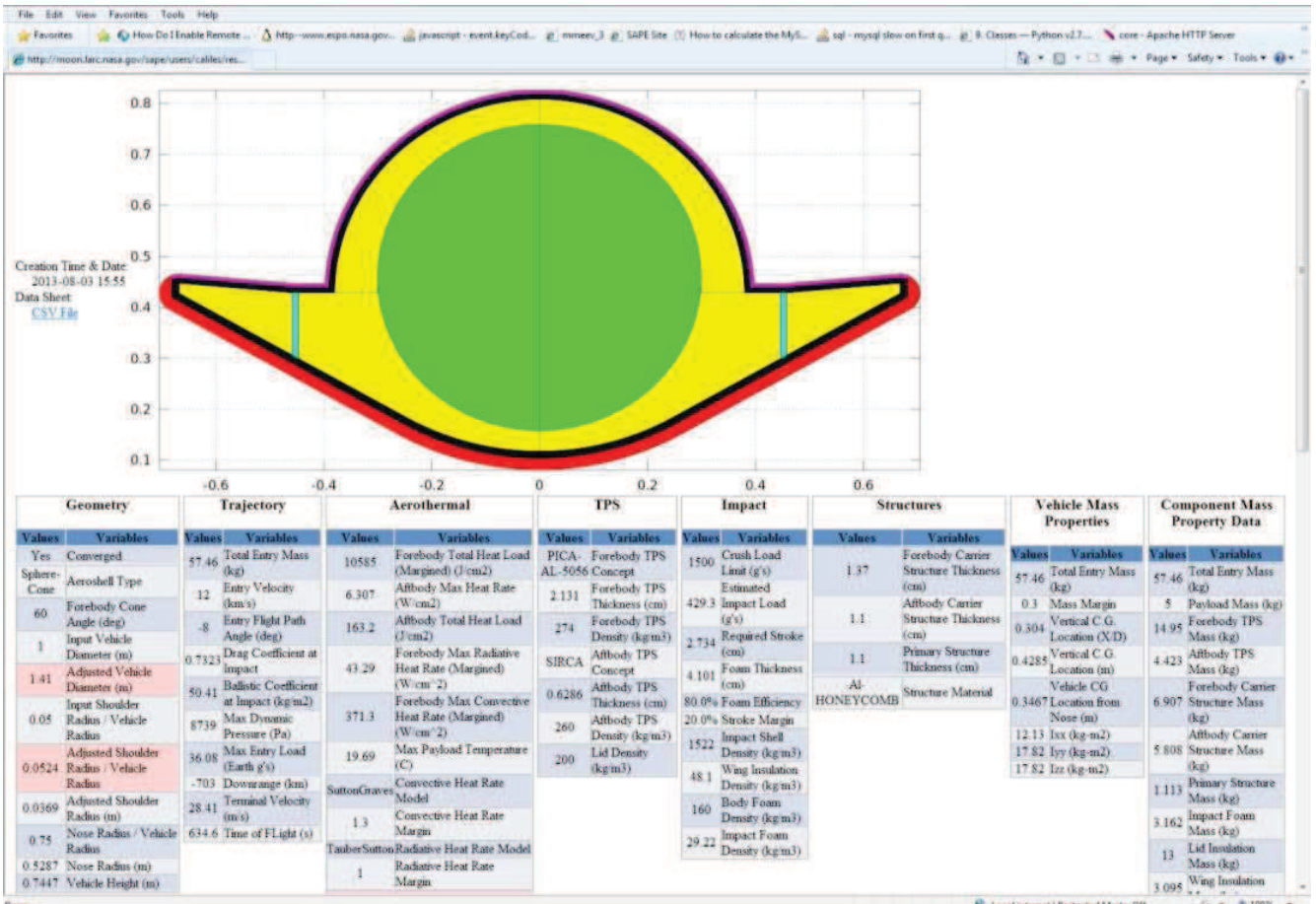


Figure 10. Screenshot of M-SAPE Sample Single Run Results

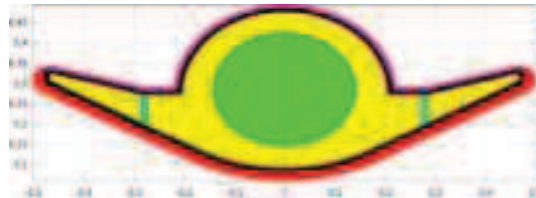
3.0 M-SAPE MODULES

The current M-SAPE software tool consists of five loosely coupled Python modules, POST, a MySQL Database, and a Web Portal. As of this writing, the completed modules are:

- 1) Parametric Vehicle Module
- 2) Flight Mechanics Module
- 3) Aerodynamics Module
- 4) Aerothermal Earth Entry Module
- 5) TPS Sizing Module
- 6) Thermal Soak Module

3.1 Parametric Vehicle Module

The parametric vehicle module is a MATLAB script that is used to create the vehicle geometry in 2-D, and then rotate the geometry 360° to generate a 3-D vehicle model from which mass properties are estimated. An MSR and a non-MSR concept have been implemented (see Figure 11). For the MSR concept, instead of simply setting the payload on top of impact foam sized to handle the stroke given an impact load requirement, an approach which encompasses the payload in both impact foam and an impact shell was also included. This design better approximates the MSR approach where increased reliability in off-nominal impact (e.g., backwards impact) is required.



a. Non-MSR Model



b. MSR Model

Figure 11. M-SAPE Vehicle Models

3.1.1 Inputs

The input parameters were selected to accommodate possible future trade space expansion and/or to provide some insight into vehicle sensitivities. The full list of inputs for the parameter vehicle model includes:

- MSR-mode designation (on or off)
- payload mass
- payload flag (payload diameter or density)
- payload size
- vehicle diameter
- ratio of vehicle nose radius to vehicle radius
- ratio of vehicle shoulder radius to vehicle radius
- vehicle mass margin (applied to all components except the payload)
- material selection (CP with ACC-6 or PICA with aluminum honeycomb)
- forebody TPS thickness
- vehicle terminal velocity
- maximum entry load

3.1.2 Rules and Constraints

In addition to input parameters, several rules and constraints were added to the vehicle model to assist with convergence process. Given the large number of inputs and associated geometric relationships, it was necessary to provide some realistic boundaries to the vehicle model to keep the iterative process from straying too far from the solution. In some cases, simple constraints (i.e., minimum and maximum allowed values) on such parameters as structure or TPS thickness were sufficient. However, in many other cases, the complex geometry required the enforcement of several other rules in order to ensure the vehicle model would converge to a feasible solution. These rules included such things as:

- Minimum vehicle diameter: Although the lower bound of the vehicle diameter in the mission trade space remained at 0.5 m, it is easy to see that given some payload mass and size inputs, a vehicle as small as 0.5 m would simply not close geometrically. In these cases, the vehicle diameter was gradually increased such that the minimum size vehicle was found that could accommodate the payload. In the cases where the input payload diameter was more than sufficient to accommodate the payload, no change was made.
- Shoulder radius: For all cases, the shoulder radius is kept fixed for the vehicle if at all possible. However, some cases may arise that would require a change in this parameter. In those cases where the slope of the aft-side of the vehicle wings is too steep (steeper than the forebody angle of 30° from horizontal), the shoulder radius is allowed to decrease. This is done in order to avoid those vehicles where the wing is thicker at the tips than at the wing base. This geometry is expected to be very difficult to accommodate in manufacturing as well as likely in aerodynamic flexing. In addition, for those cases where there is insufficient room in the shoulder to accommodate the required geometry (i.e., very thick forebody TPS), the shoulder radius is increased to the smallest value which would allow the shoulder geometry to close.

- Lid and attached structure placement: In closing the geometry during the iteration process in the parametric vehicle model, the most challenging aspect is the placement of the attached structure in relationship to the lid. In order to best ensure rearward aerodynamic instability (allow for self-righting prior to the heat pulse), it is best to keep the center of curvature of the lid at the vehicle CG. This makes the vehicle much less susceptible to variations or dispersions in the atmosphere and/or aerodynamics during rearward flight (since all normal forces on the lid would act through the vehicle CG and, thus, not result in a moment on the vehicle). Once the lid location is determined, the attached structure can be placed such that the lid is at most a hemisphere (can be less), and also provides the correct geometry for the wing (not shallower than 5° , but no steeper than 30°). This approach balances the need for a flexible geometry with the desire for rapid vehicle convergence. For the MSR-mode “On” cases, the lid was constrained to a full hemisphere in order to allow for reasonable access to the payload through the impact shell/sphere. For these cases, a constraint was applied that the payload center and the lid center of curvature must be coincident, and the attached structure must also be at the same height.

The vehicle module iterates until there are no geometry changes (e.g., vehicle diameter or shoulder radius change) and the vehicle CG and attached structure locations converge to within 0.1 mm. If a geometry change is flagged, then the vehicle is re-initialized with that change and the iterative processes starts over. A flowchart of parametric vehicle model is shown in Figure 12.

3.1.3 Validation

Once the parametric vehicle model was complete, it was critical to validate the results for both the final geometry and estimated mass properties. Because a parametric Pro/Engineer Wildfire 3.0 (ProE) was created with several of the more straightforward constraints and relationships described above, a setup already existed to generate a vehicle for a given set of inputs. A file interface was set up between MATLAB and ProE to provide the minimum number of inputs necessary to fully define the vehicle. This allowed for use of each piece of software to be used where it is strongest, i.e., MATLAB for the complex vehicle geometry iteration process and ProE in the design and mass properties calculations. This also allowed for continued use of the ProE model, integrated with M-SAPE, to provide CAD models in STEP or IGES format or other geometric data for other modules for such things as meshing. Several test cases were run for both MSR and MSR-modes. Input data was provided to ProE that generated an output file including geometric references (i.e., vehicle total height, attach structure location, etc.) as well as mass properties (CG and inertias) for both the total vehicle as well as the individual components. These were then compared against the MATLAB vehicle model output. In all cases, the geometry matched. For the mass properties, several different test cases were run to “tune” the MATLAB vehicle model (e.g., in the number of points which define a curve or the delta angle the vehicle is rotated at to generate the 3-D model) such that good comparisons could be made in the mass properties while also allowing the vehicle model to converge more quickly. In the end, all mass properties in the MATLAB model were within 5% of the ProE values, with total vehicle mass and CG location always better than 1%, and the mass inertias typically within 1–3%.

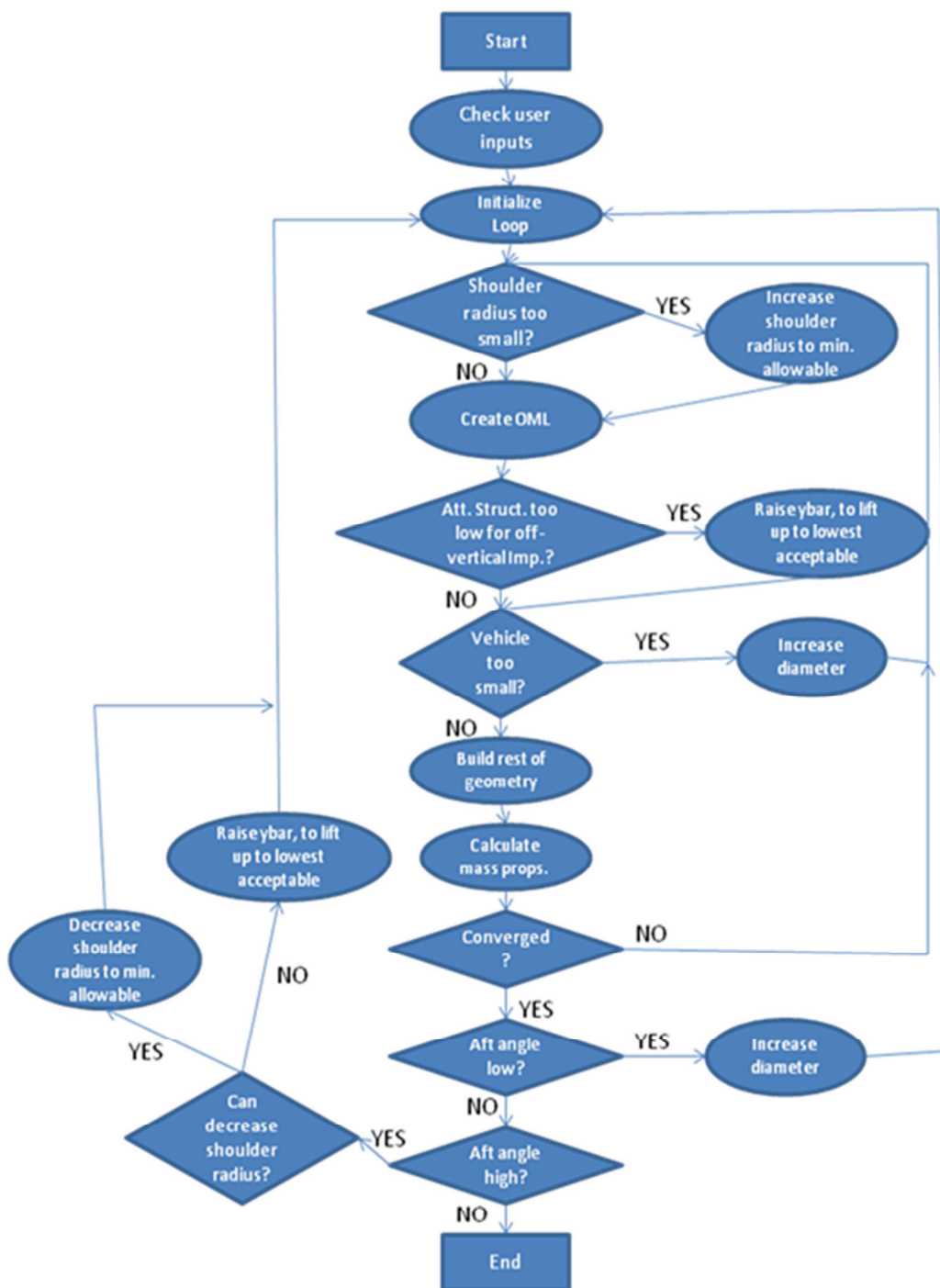


Figure 12. Flow Chart for Parametric Vehicle Model

The Parametric Vehicle Software Module consists of the following primary sub-components:

- Geometry and Mass Sizing
- Impact Analysis
- Structural Analysis

3.1.4 Geometry and Mass Sizing

Geometry requirements are outlined in Section 3.1.1-3.1.2. This section provides additional CAD related discussions. A parametric vehicle model representing a simplified MMEEV model was developed based on the MSR EEV design in ProE. The CAD model was constructed from a series of curves in a “skeleton” model that references a set of geometric relations defined within the trade space. This approach allows for automatic vehicle regeneration as input parameters are modified. This skeleton model was built around certain dimensional assumptions that serve as constants in the geometric relations.

Solid models of the MMEEV components were created from the curves defined within the skeleton file. Because the vehicle components reference these curves, they are recreated appropriately in response to changes in input parameters. Each component was assigned a user-defined density, allowing ProE to generate a new set of mass properties at the component and assembly level for each design. Analysis features were created to allow non-geometry properties such as ballistic coefficient to be defined as features in the model and thus be used as output for further analysis.

The result is a parametric vehicle model for the MMEEV trade space, covering a range of overall vehicle diameters and payload masses as inputs and the overall vehicle mass and axial center of gravity as outputs. For this trade space, the center of gravity is assumed to be axial with no lateral component.

From the parametric vehicle model, two generalized configurations can be created. The first is the “MSR” configuration, in which the payload is encapsulated within a foam-filled impact sphere as shown in Figures 13 and 15. The second is a “Non-MSR” configuration, in which the payload is nested in impact foam, with no surrounding impact sphere as shown in Figures 13 and 14.

Several geometric assumptions were made for these two parametric models. For both, the vehicle coordinate system (CSYS) is assumed to be at the virtual apex of the vehicle and the horizontal portion of the aftbody is 60 mm (Fig. 14). In the Non-MSR configuration, the distance between the payload and the lid structure is 50 mm (Fig. 15). In the MSR configuration, the impact shell is tangent to the FWD structure and the impact sphere is concentric with the payload.

The geometric input variables for the parametric model are illustrated in Figures 16-18 with the variable description shown in black text with the model variable name shown in red. The model will automatically be regenerated based on these user-defined values.

As part of MMEEV trade space studies, the user is able to vary several mass properties within the model. The CAD user-defined mass property input parameters and their respective ProE

variable names are shown in the Table 1. Based on these values, ProE can generate mass property output values such as the vehicle mass, vehicle CG, and moments of inertia.

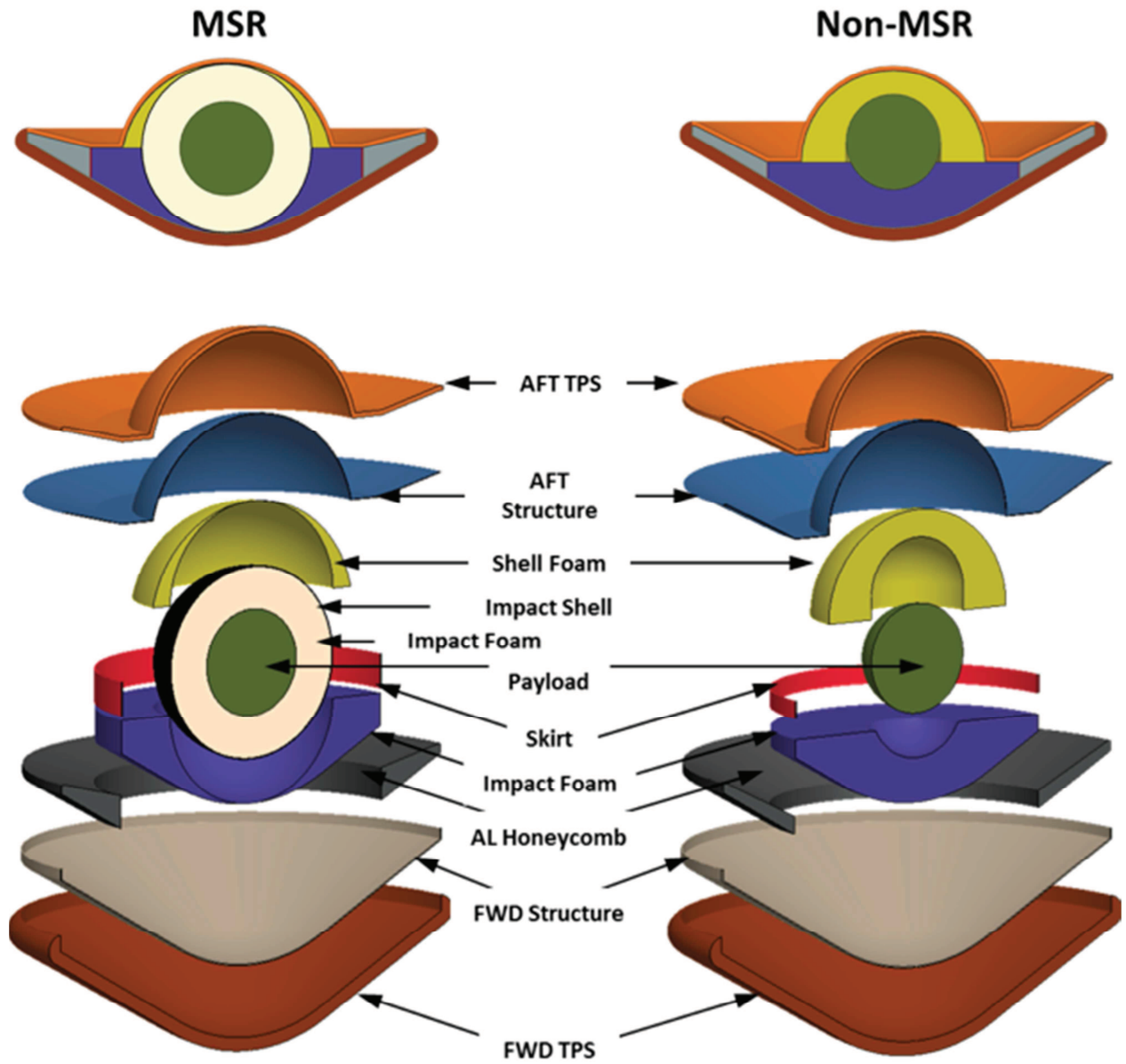


Figure 13. Geometry Models for MSR and Non-MSR Vehicles

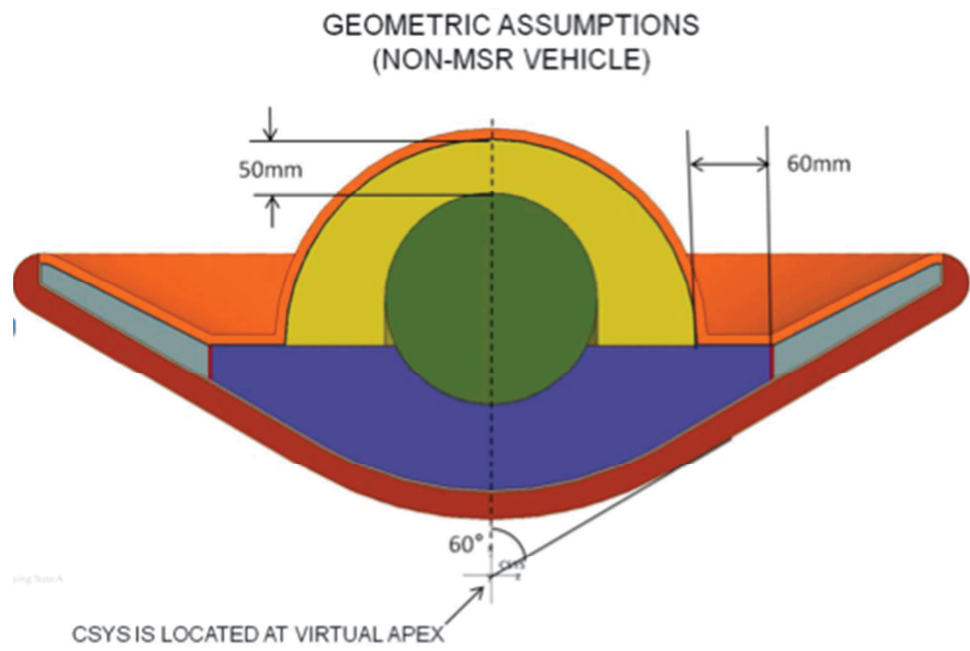


Figure 14. Non-MSR Vehicle Assumptions

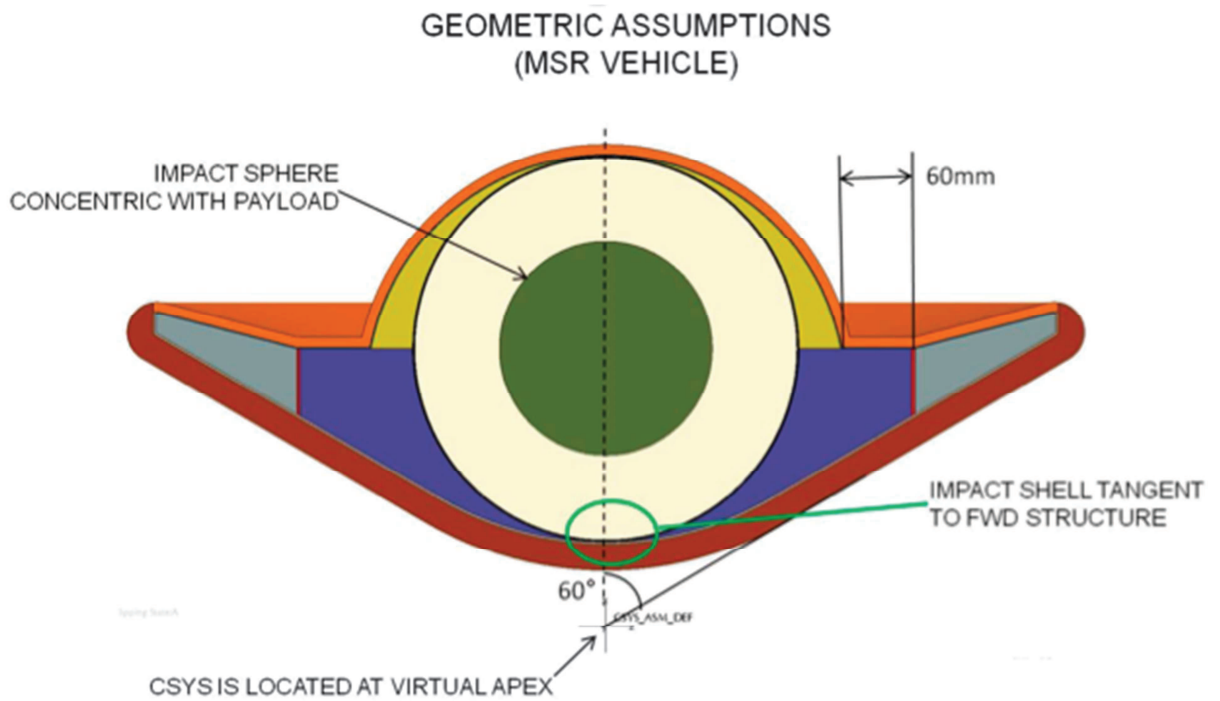


Figure 15. MSR Vehicle Assumptions

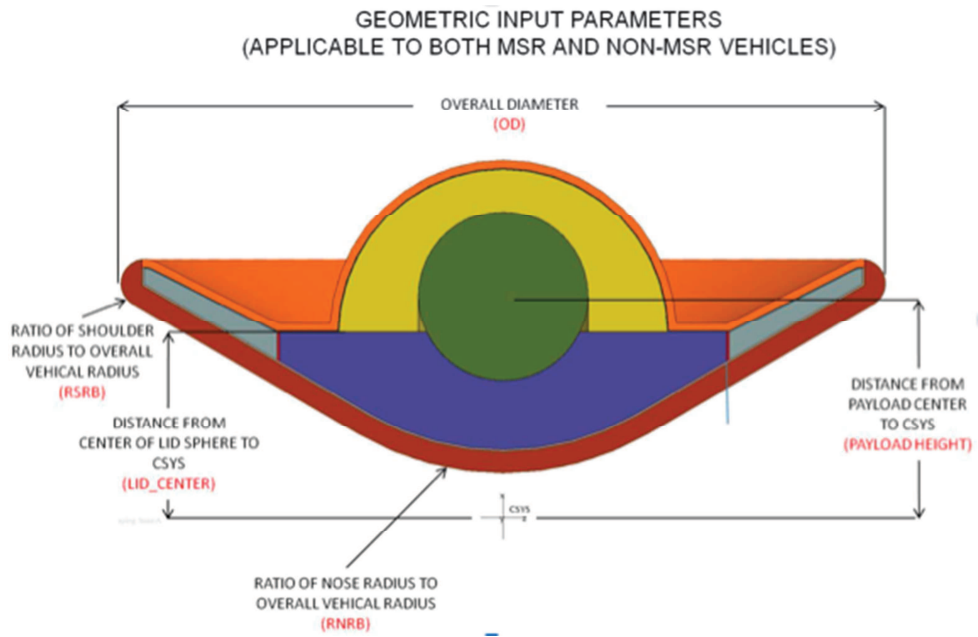


Figure 16. MSR and/or Non-MSR Vehicle Parameters

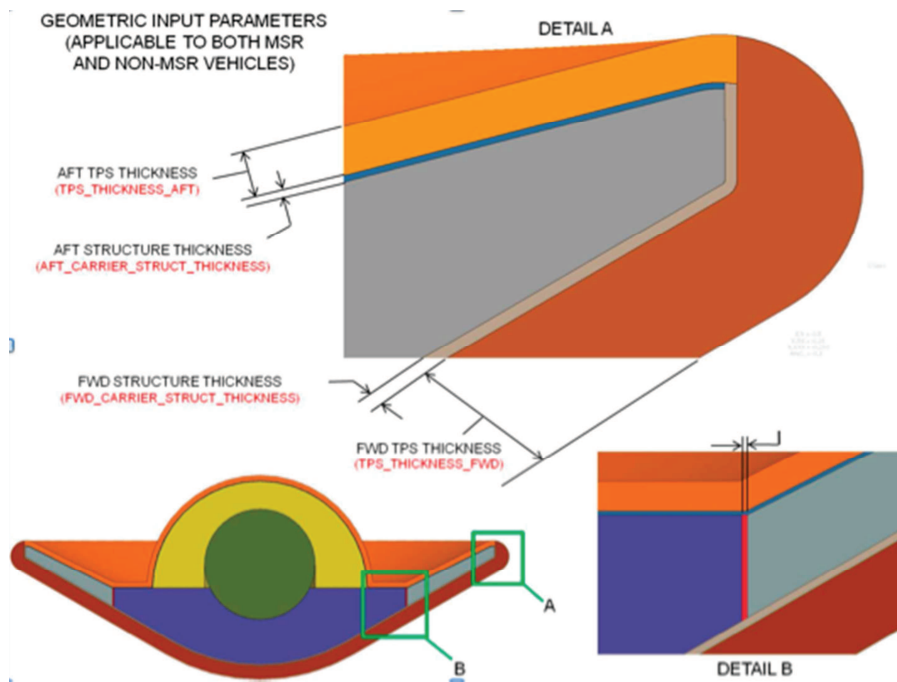


Figure 17. MSR and/or Non-MSR Vehicle Parameters (Close Up)

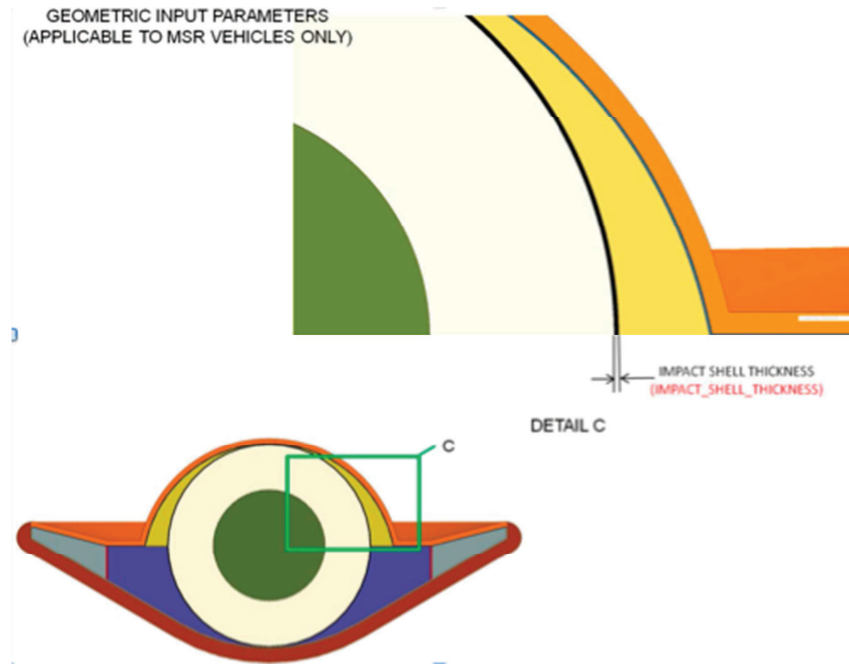


Figure 18. MSR Vehicle Parameters

Table 1. Mass Property Output Values

VARIABLE DESCRIPTION	MODEL VARIABLE NAME
AFT TPS Density	DENSITY_AFT_TPS_M
AFT Structure Density	DENSITY_AFT_STRUCT_M
Shell Foam Density	DENSITY_LID_INSUL_M
Payload Density	DENSITY_PAYLOAD_M
Skirt Density	DENSITY_PRIMARY_STRUCT_M
Impact Foam Density	DENSITY_IMPACT_FOAM_M
Aluminum Honeycomb Density	DENSITY_WIND_INSUL_M
Fwd Structure Density	DENSITY_FWD_STRUCT_M
FWD TPS Density	DENSITY_FWD_TPS_M
Impact Shell Density	DENSITY_IMPACT_SHELL_M
Body Foam Density	DENSITY_BODY_FOAM_M
Payload Mass	MASS_PAYLOAD
Mass Margin	MASS_MARGIN

3.1.5 Impact Analysis

Two approaches were used to develop the impact model, and both approaches assume a 1-D and perfectly vertical impact. The first approach assumes all impact energy is transferred from a perfectly rigid body and payload through ground penetration. During MSR EEV development, penetrometers were used to perform ground characterization tests at the UTTR (Fasanella 2001). These test data were then used to develop a simple empirical relationship that was used to determine peak deceleration of the EEV when penetrating the soft clay surface of UTTR:

$$G = \alpha \frac{D_n V_t^2}{M} \quad (1)$$

where G is the peak deceleration (Earth g 's), D_n is the nose diameter (m) of the penetrometer or vehicle, V_t is the impact velocity (m/s), M is the total mass (kg) of the penetrometer or vehicle, and α is an empirical constant determined from test data (α is found to be between 27 and 29 for UTTR soft clay). The penetrometer results show that peak deceleration is a function of nose diameter. It may be counter intuitive that peak deceleration is inversely proportional to mass, but one can think of the heavier masses penetrating deeper, therefore having a longer stroke that spreads out the impact acceleration pulse. For vehicles reaching terminal velocity before the impact, the vehicle terminal velocity can be expressed as:

$$\frac{1}{2} \rho C_D A V_t^2 = Mg \quad (2)$$

where parameters ρ , C_D , A , V_t , M , g are atmospheric density at impact, vehicle drag coefficient, drag area, terminal velocity, vehicle mass, and Earth gravity, respectively. Assuming the vehicle terminal velocity has been reached before or at impact, Eqs. 1 and 2 are combined into:

$$G = \alpha \left(\frac{8g}{\pi \rho C_D} \right) \left(\frac{D_n}{D} \right) \frac{1}{D} \quad (3)$$

where D is the vehicle overall diameter. Equation 3 shows that maximum acceleration is independent of mass and is inversely proportional to the overall diameter. This is only true for vehicles that have reached terminal velocity before impact. Figure 19 compares impact G 's results from Eq. 1 with over 17,000 M-SAPE runs calculated for a wide range of entry conditions, TPS types, vehicle concepts, and payload masses.

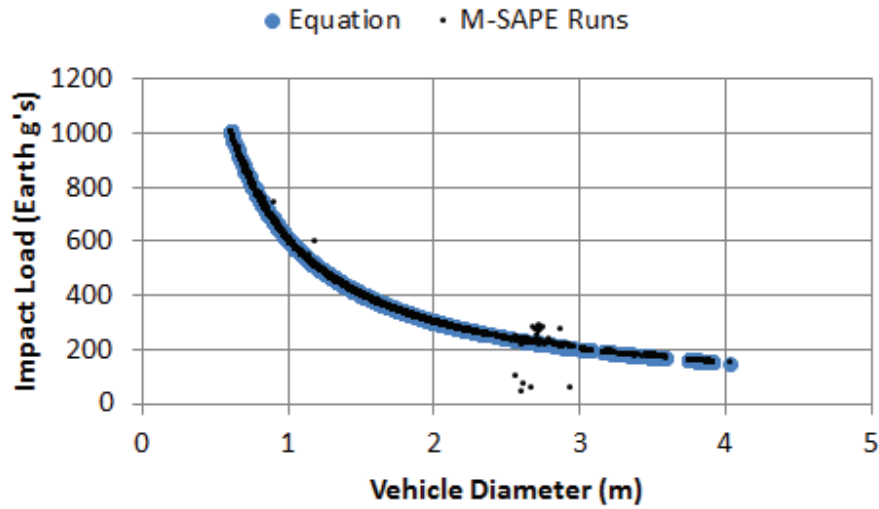


Figure 19. Impact G's Assuming Ground Penetration

The second approach uses a simplified energy balance approach to understand the impact of the MMEEV with a perfectly rigid surface. In this case, since penetration is not possible, the vehicle and/or payload must be allowed to decelerate over some distance, or stroke, while transferring the kinetic energy by crushing a material designed for this purpose. Because the payload is the only critical element of the MMEEV that needs to survive, the mass and size of the payload are used to determine the resulting payload stroke distance:

$$\text{Stroke} = \frac{V_i^2}{2 \times \bar{G} \times g} \quad (4)$$

where *Stroke* is payload stroke (m), \bar{G} is the design impact load (Earth g's), and g is Earth acceleration due to gravity (m/s^2). For MSR concepts, a triangular acceleration pulse is assumed, and stroke is multiplied by a factor of two. Combining Eqs. 2 and 4 results in:

$$\text{Stroke} = \frac{\beta}{\rho \bar{G}}, \beta = \frac{M}{C_D A} \quad (5)$$

This equation shows that stroke is linearly proportional to the vehicle ballistic coefficient (β) at impact. Figure 20 shows stroke calculated using Eq. 5 and M-SAPE run results for over 17,000 M-SAPE runs calculated for a wide range of entry conditions, TPS types, vehicle concepts, and payload masses. Equations 3 and 5 are accurate for estimating the impact loads and required stroke.

Once the stroke length is known, the compression strength, FS (Pa), of the foam is calculated as a function of the Stroke, payload mass (M_{PL}), and payload reference area (A_p).

$$(6) \quad FS = \frac{M_{PL} \times V_t^2}{2A_p \times \text{Stroke}}$$

With the stroke length and the stroke efficiency factor, the required foam thickness and compression strength can be calculated.

Combining the stroke and compression strength calculations causes the velocity term to drop out, making the compressive strength of the foam solely a function of payload mass.

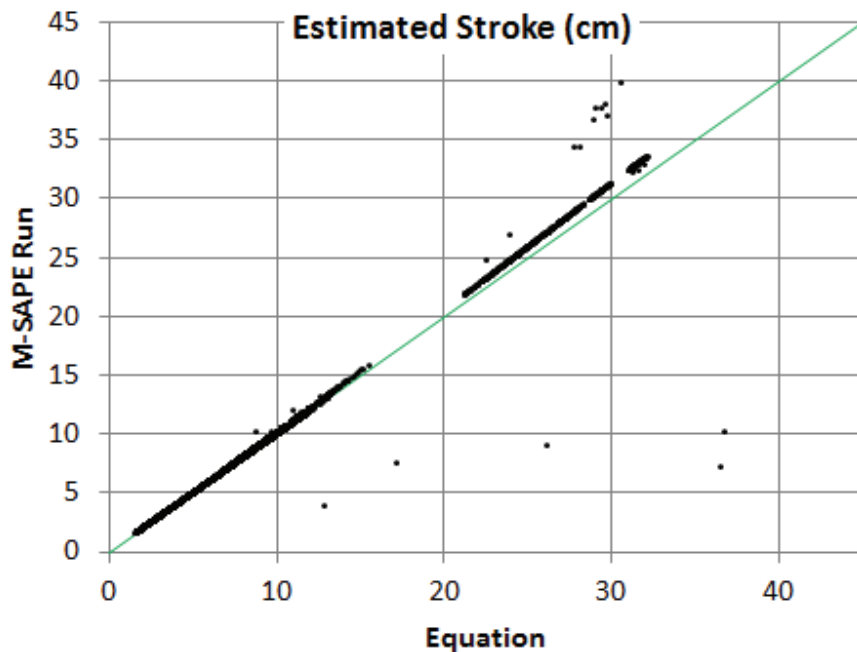


Figure 20. Required Stroke Comparison with Eq. 5

3.1.6 Structural Analysis

The structural analysis in this section is limited to EEV MSR concept as shown in Fig. 13. The EEV structural analysis was divided into two analysis modules: an impact module and a structural dynamics module. The EEV requires an impact absorbing sphere called an impact sphere (IS) to protect the payload during the severe collision with Earth. The IS shown in Fig. 21 is a lightweight high energy absorption structural system comprised of radially oriented interlocking hybrid fiber composite panels and crushable foam filled chambers. The features of the impact sphere allow the structure to be subjected to progressive crumpling failure rather than less efficient buckling failure. Numerical representation of the interactions between stiff and soft components under high-rate compressive loading is difficult and often fails to reproduce the

proper mechanics. To incorporate such intricacies, in this analysis methodology, complex structural interactions and a wide range of failure physics are uniquely addressed. Numerical models using the developed methodology were created and benchmarked against experimental tests conducted at the Impact Dynamics Research Facility at NASA Langley Research Center. The post impact structural damage assessment showed close correlation between simulation predictions and experimental results. Acceleration, velocity, displacement, damage modes, and failure mechanisms were all effectively captured.

Two fully parametric finite-element models were developed for the structural analysis of the EEV. The structure primarily responsible for the impact response of the EEV is the IS, which was the focus of the first analysis module. A biplane cross sectional view of the FE model for the first module is shown in Fig. 21, which different elements have been selectively hidden so that most components are visible. The key challenge in the developing the EEV is ensuring the containment and integrity of the samples contained within the IS. Thus when designing the EEV much effort was spent focusing on the IS and its ability to meet these requirements. More details can be found in Perino et al. 2013 and 2014.

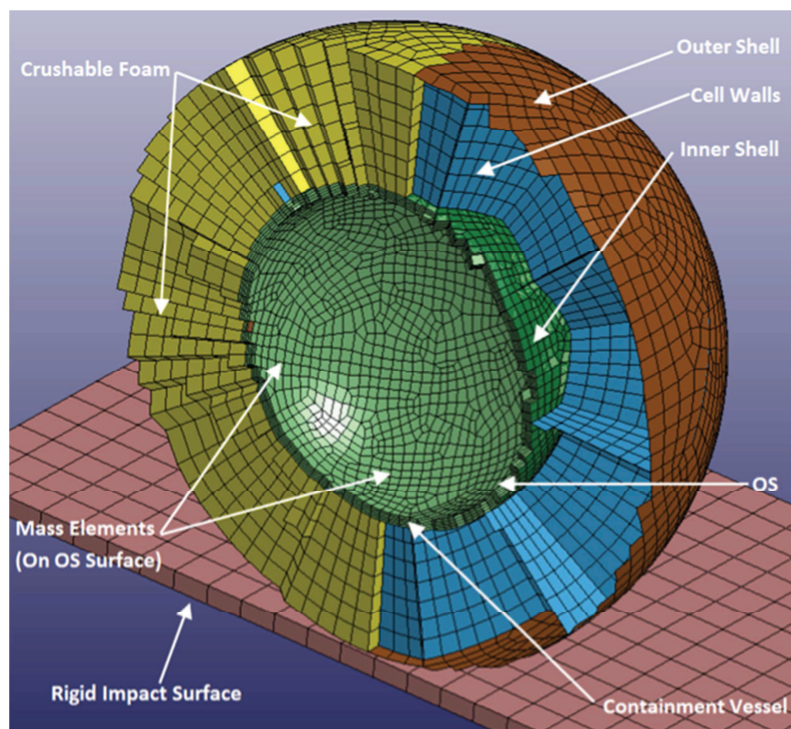


Figure 21. A Biplane Cross Section View of the Finite-Element Model of Impact Sphere

The second structural dynamics analysis module was developed for evaluating the quasi-static and dynamic structural response of the vehicle during launch and entry (see Fig. 22). During launch and reentry the EEV may experience large structural loads from multiple sources. In an effort to decrease development time and cost, a fully parametric and automated finite element

analysis methodology was developed. In contrast to the typical analysis method where models are built manually using a pre-processor GUI, the developed methodology uses a parametric technique to build EEV models. The parametric technique allows rapid modification of nearly all aspects of the model including: geometric dimensions, material properties, loads and boundary conditions, mesh properties, and analysis controls. Furthermore once model parameters are defined, all required analyses can be performed automatically. Given the proper computational resources, the developed methodology can be used to rapidly generate data for thousands of potential EEV configurations. A range of analyses including quasi-static inertial, structure born vibration frequency response, random acoustic, and aeroelastic analyses are automatically executed. Preliminary parametric analyses indicate that the quasi-static load cases induce the highest stresses near the structural attachment points. Cone angle and vehicle diameter have been identified as two parameters that have strong influence on vehicle mass and structural response. These investigations demonstrated that the two structural analysis modules have great potential in facilitating future planetary exploration missions. More details can be found in Perino et al. 2013 and 2014.

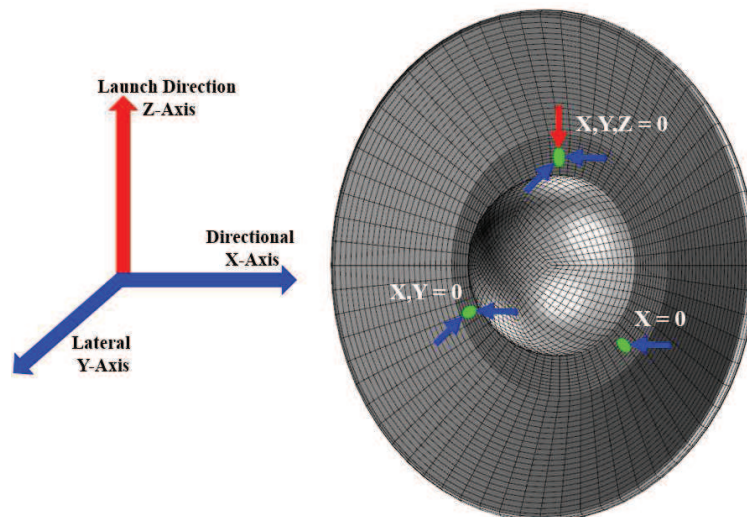


Figure 22. Finite-Element Model of EEV for Launch and Entry

3.2 Flight Mechanics Module

The POST2 software is a generalized point mass, discrete parameter targeting and optimization program. POST2 provides the capability to target and optimize point mass trajectories for multiple powered or unpowered vehicles near an arbitrary rotating, oblate planet. POST II has been used successfully to solve a wide variety of atmospheric ascent and reentry problems, as well as exoatmospheric orbital transfer problems. The generality of the program is evidenced by its multiple phase simulation capability which features generalized planet and vehicle models. This flexible simulation capability is augmented by an efficient discrete parameter optimization capability that includes equality and inequality constraints (Brauer et al, 1977 and Striepe et al. 2004). Some other projects that have used POST2 include the Mars Exploration Rover for EDL

analyses, Genesis, Stardust, X-43 (Hyper X), Huygens Probe, Mars Phoenix Lander, and many others. It has also been used on flight projects such as Mars Science Laboratory (MSL), Orion, Ares, Space Launch System (SLS), and Launch Abort System. Figure 23 gives a graphical representation of how MSL models are integrated into POST2.

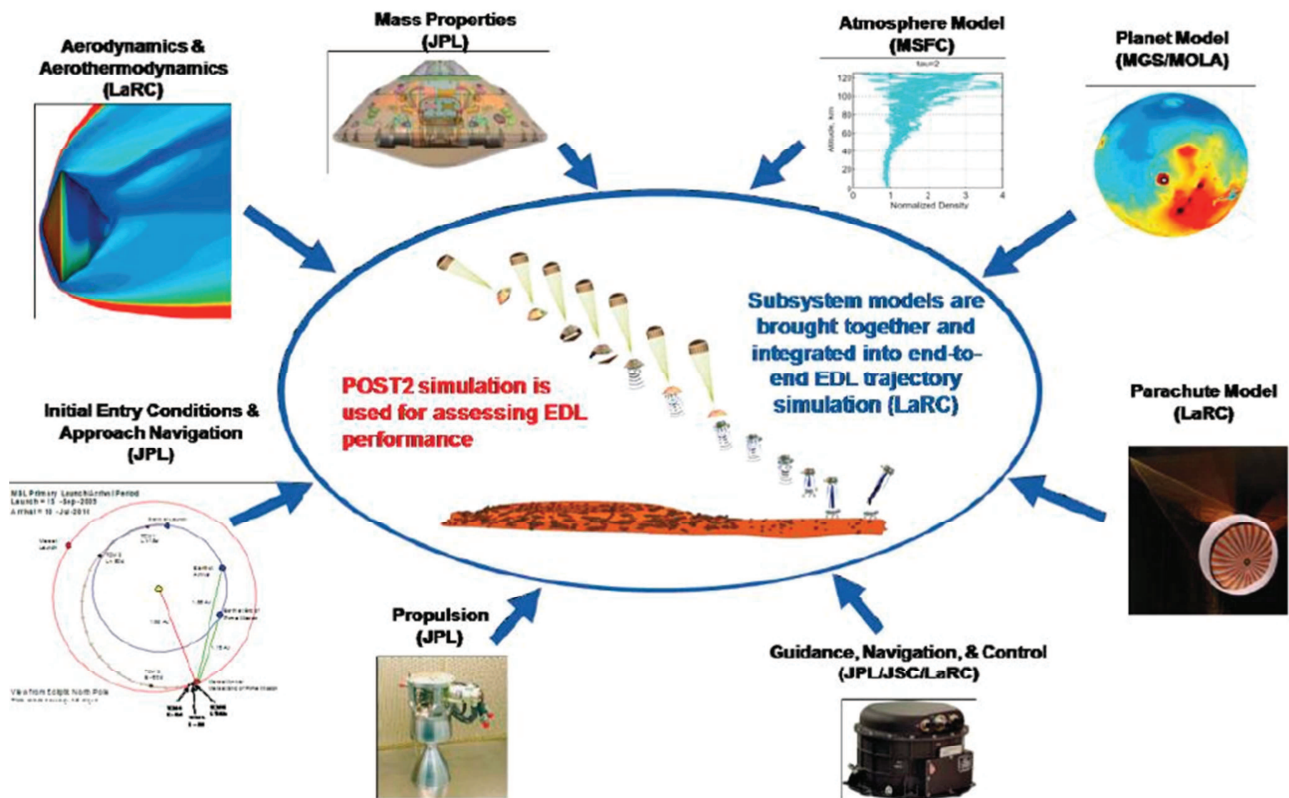


Figure 23. Model Integration into POST2, MSL Example

Many fewer models are required for the MMEEV application as the vehicle is unguided and ballistic. However, initial entry conditions, aerodynamic, aerothermodynamic, planet, atmosphere, and vehicle mass properties models are still required. The POST2 simulation uses a 4th order Runge-Kutta numerical integration method for the MMEEV application, although other methods can be chosen in POST2. Simulations may be run in either a 3-degree of freedom (DoF) or 6-DoF mode, where 3-DoF is the translational equations of motion and the rotational equations of motion are also integrated in the 6-DoF mode.

The planet model is an oblate planet based on the one adopted by the U.S. Air Force Satellite Control Facility from the 1960's forward, taken from Mercer, 1965. Table 2 contains a list of Earth gravitational moment coefficients, which are the dimensionless parameters describing the Earth's gravitational field. The listed values are the first three geopotential coefficients, J_2 - J_4 , for a non-spherical planet.

Table 2. Geopotential Coefficients

J ₂	1.0823x10 ⁻³
J ₃	0.0
J ₄	0.0

The corresponding rotation rate of the planet is 7.292115×10^{-5} rad/s, the gravitational constant (μ) is 3.986×10^{14} m³/s², the equatorial radius is 6378.1 km, and the polar radius is 6356.8 km.

Atmospheric interface is defined at a geodetic altitude of 125 km. The initial state is selected to be representative of the UTTR landing constraint. While not landing at UTTR, it was decided to direct the vehicle towards UTTR. The initial geodetic latitude used was 33.0° north and the initial longitude was 246.3833° (east longitude relative to the Prime Meridian). More in-depth studies may start at spacecraft separation to account for perturbations due to the separation event. The initial velocity and flight path angle were varied in the trade space. For 6-DoF mode, the attitude rates are initialized through body rates. The ideal would be zero pitch and yaw body rates and only a roll body rate. The roll body rate is used to provide gyroscopic stability to counter aerodynamic perturbations. This method has been used on many previous missions such as Stardust and Genesis at Earth (Mitcheltree et al. 1999). Perturbations from the spacecraft separation event must also be accounted here, usually in Monte Carlo simulations.

The atmospheric model used in the simulation is the 1976 U. S. Standard Atmosphere. Future iterations may use Global Reference Atmosphere Model (GRAM) (Justus et al. 1999, Justus et al. 2007, and Leslie et al. 2011) and/or a specific range reference atmosphere for the landing site. No winds are included for this current trade space study.

The vehicle aerodynamics is incorporated into the POST2 simulation as a FORTRAN routine. The moment reference center is defined at the virtual apex of the cone of the vehicle. Section 3.3 and 3.4 describe the aerodynamics and aerothermodynamic models, respectively.

The aerothermodynamics in the POST2 simulation are based on a Sutton-Graves (Sutton and Graves 1972) estimation of the convective heating and a Tauber-Sutton (Tauber and Sutton 1991) estimation of the radiative heating (Tauber 1991). The Sutton-Graves constant used was 1.74153×10^{-4} . Section 3.3 describes the comparison to computational fluid dynamics (CFD) in further detail. The nose radius, reference area, and reference lengths varied based on the overall vehicle diameter in the trade space.

The POST2 simulation event sequence is simple since this is a ballistic and unguided vehicle. For the trade space studies, only monitor events were used. These events monitor quantities like altitude, peak heating, peak entry deceleration, and touchdown. The events are used to pull information out from the results for compilation.

3.3 Aerodynamic Module

The MMEEV capsule will perform a stable, yet uncontrolled, atmospheric entry and deceleration through the hypersonic and supersonic regimes, and will reach subsonic velocity at a high altitude of approximately 25 km. A representative trajectory profile is shown in Figure 24. To better resolve the time scale of deceleration, only the first half of the entry duration is shown. The latter half (not shown) contains the remainder of subsonic flight over roughly 25 km of altitude (82,000 ft). Figure 24 illustrates the amount of time during entry that is spent at a low subsonic velocity, thus stressing the importance of characterization of subsonic aerodynamics.

The aerodynamics database of MMEEV uses a range of sources, including Direct Simulated Monte Carlo (DSMC), CFD, wind tunnels and ballistic range data. Aerodynamic performance in the rarefied atmosphere is described by collision-less calculation with DSMC Analysis Code (DAC) for angles of attack from zero to 180 degrees. Hypersonic aerodynamics is described by non-equilibrium calculation of Langley Aeroheating Upwind Relaxation Algorithm (LAURA) for high flight enthalpy, and perfect gas air wind tunnel data at low enthalpy. Rarefied and hypersonic continuum data are blended through the transitional region by interpolation on Knudsen number. The validity of this approach was confirmed by comparison with the full DSMC calculations. At low velocities, wind tunnel data is used.

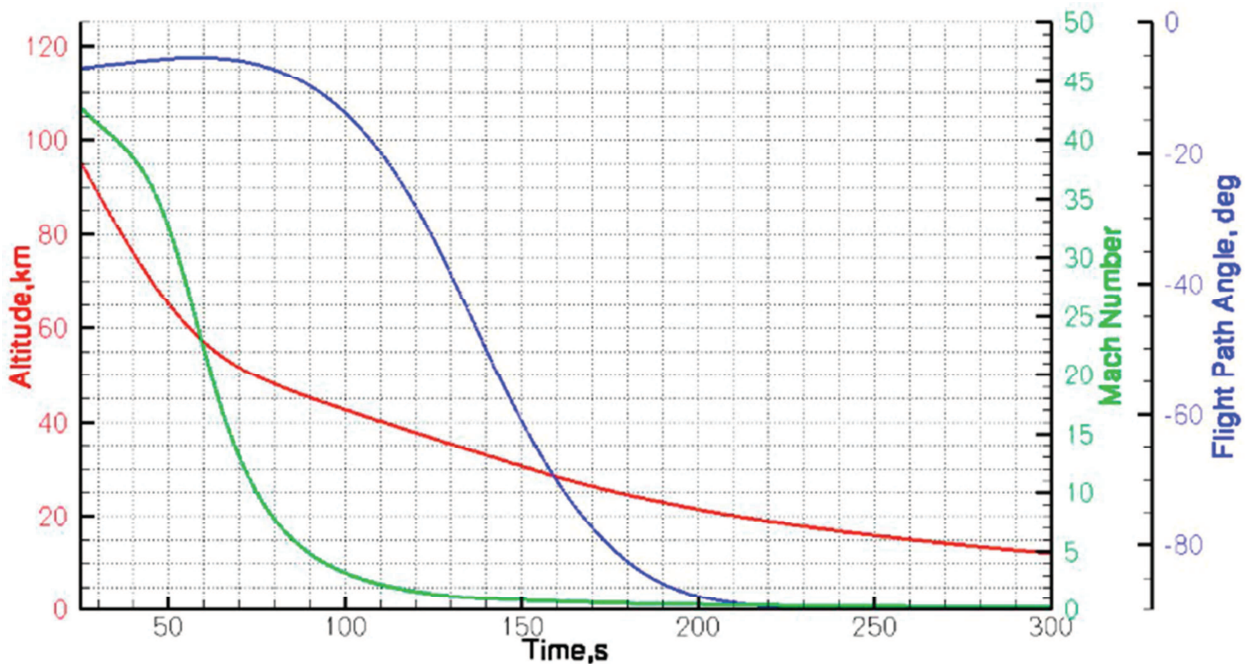


Figure 24. MMEEV Representative Trajectory

3.3.1 Summary of Data Sources

- Free-molecular static aerodynamics based on the collisionless DAC calculations.

- Hypersonic static aerodynamics are computed using LAURA code with the perfect gas air model (Cheatwood 1996)
- Low supersonic and high subsonic static aerodynamics were measured in the Ames 2x2 ft transonic wind tunnel by Marko 1968 and Walker et al. (1967).
- Low subsonic statics and dynamics obtained at NASA Langley in the Vertical Spin tunnel (VST) by Mitcheltree, Fremaux, and Yates (1999).
- Transonic and supersonic dynamics from Viking Project (Steinberg 1970)
- Collision-less DAC solutions on the updated shape. Consistency of trends between collision-less, DSMC and hypersonic continuum LAURA results were verified.
- Non-equilibrium LAURA results for high hypersonic regime to replace earlier perfect gas calculations.
- Walker and Weaver 1967 statics data for Mach 2.2 to 9.5 to blend high hypersonics to transonic data from Marko (1968) that is used in the database.

The moment reference point for static aerodynamics was shifted to the virtual nose of the vehicle. This point is the cone virtual apex point, and is generally a few centimeters ahead of the physical nose. It is chosen because the physical nose presents a challenge, when datasets come from different experiments with different values of nose bluntness.

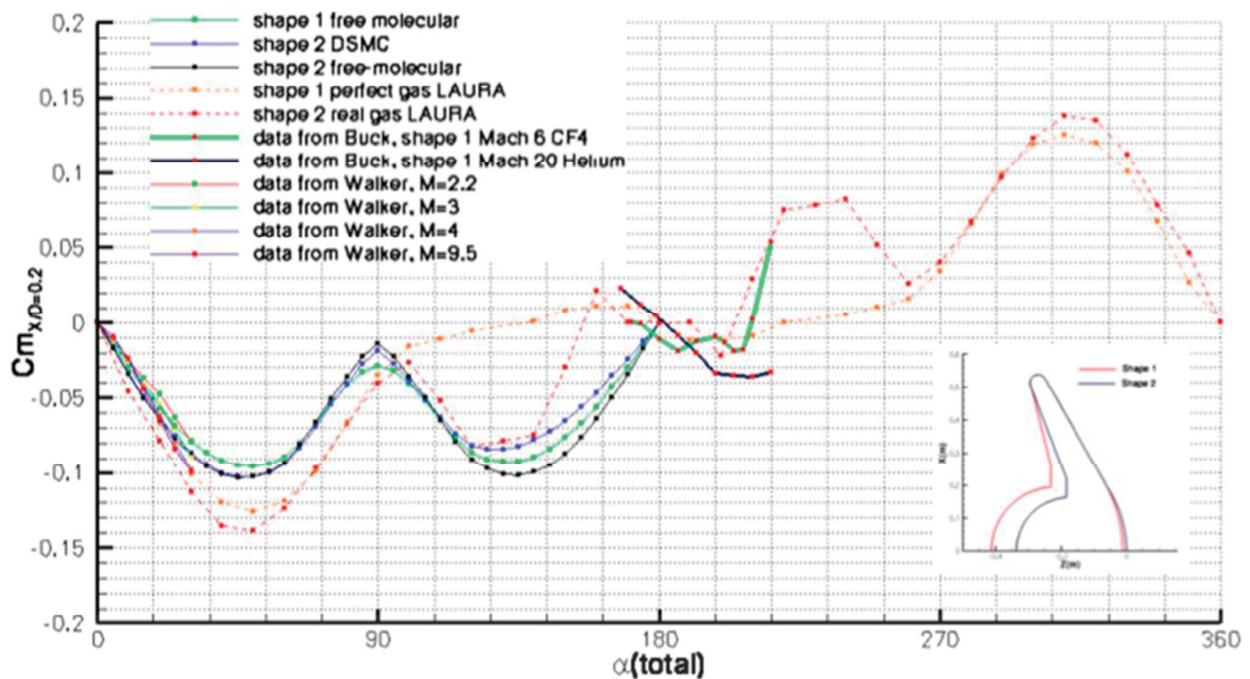


Figure 25. MMEEV Supersonic, Hypersonic, and Rarefied Flow Pitching Moment at 0.2D C_m

3.3.2 Rarefied and Hypersonic Aero Data

Substantial updates were made on the V_021 MMEEV aero database to address the area of pitch stability in the 2010 timeframe by Artem Dyakonov. Figure 25 is the summary of the high-speed aerodynamics pitching moment data that is available for use for the MMEEV.

In the free-molecular regime the differences between the previous calculation on the older iteration of the capsule's shape (shape 1) and the recent calculation on the shape from the family of the MMEEV contours (shape 2) is represented by the green and black curves in Figure 25. Some differences occur at near 40°, near 90° as well as near 140°. Near 90° the differences can be traced to the larger overhang of the center aftbody for the shape 1. In general, however, it is difficult to quantify these differences because the work on shape 1 was at least ten years old and the procedures used in these calculations could not be verified. It should be pointed out that in the free-molecular regime, under the assumption of the accommodation coefficient of unity, the body shape matters only so far as it affects the body outline in the direction of the incident velocity vector. The details within the outline do not matter.

Hypersonic pitch stability was described by perfect gas calculations in LAURA, which were performed on shape 1 (shown in orange through the entire range of incidence). Shown for comparison are the plots of real gas calculations on an updated shape, as well as in Walker 1967 low angle of attack data from the perfect gas wind tunnel. Walker's data is entered into the database for low Mach numbers, though not presently used. Prediction of hypersonic aerodynamics of a sphere-cone in air by CFD is considered reliable for nominal (nose forward) flight, and it is unlikely that experimental data will have to be used to fill the aero database in this regime. Transition between the hypersonic and supersonic datasets in the aero database is handled through interpolation on the free-stream Mach number.

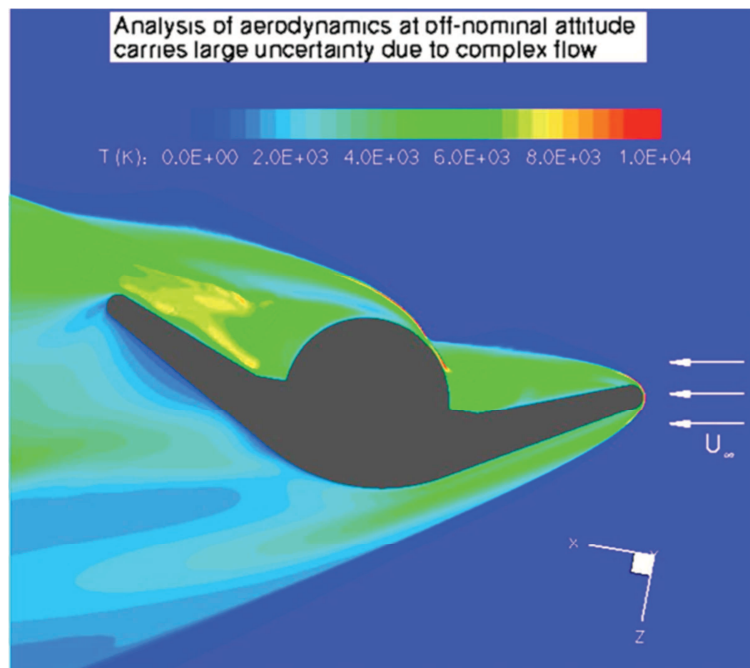


Figure 26. CFD Computed Flow Field at 100° Degrees Angle of Attack.

The potential, however small it may be, for the aftbody-forward entry does require some amount of analysis of the trim characteristics in this regime. In the free-molecular and transitional regime, the capsule will tend to right itself, as shown in the Figure 25. However, a previous investigation by Buck and Cheatwood (unpublished) has shown capsules of this shape stable in reverse orientation in the hypersonic continuum, as witnessed by the slope of the trim curve in

Figure 25 near 180° degrees angle of attack. Predictive capability of CFD is somewhat degraded for high angles of attack because of the flow complexity. Figure 26 shows the computed flow at 100° degrees angle of attack. As the figure indicates, there is potential for shock interaction and unsteadiness, and because of that, the high angle of attack aerodynamics are uncertain.

It is possible to address this problem in the future through one of the following venues:

- Various passive aerodynamic aides can be added to avoid hypersonic backward stability altogether. Impact of these aerodynamic aides on capsule mounting, TPS etc. should be assessed.
- Design of sufficiently conservative margin and demonstration of robustness to it.
- Comprehensive definition of conditions that would lead to a backward stable entry.
- Reassessment of the likelihood of backward conditions.

To demonstrate robustness for MMEEV, an analysis was carried out where a high fidelity, six degree-of-freedom trajectory tool, together with the existing aerodynamics aero database, was tested across a range of flight path angles, entry velocities and ballistic coefficients. The results, shown in Figure 27, indicate passive reorientation before the onset of continuum flow. Center of gravity (CG) placement was shown to be a significant driver. While these results indicate that reorientation is possible, they do not represent what could be a worst case scenario, i.e., a vehicle with a non-zero rotation rate. Preliminary simulations indicate that even for small pitch rates, on the order of one to two degrees per second, a vehicle could end up with a rearward entry if it entered the atmosphere at the wrong time. While the MMEEV vehicle is not expected to be rearward stable in the rarefied flow regime, the very low dynamic pressures that are acting on the vehicle during this period of flight would be unable to exert much force. It should be noted that further research and testing is needed in this area to achieve very high reliabilities.

The aerodynamic data are provided in Appendix A in Figures A1, A2, and A3, for the rarefied flow, Mach=24 and Mach =9.8, respectively. For these Figures, the moment reference center is the virtual nose apex of the vehicle.

3.3.3 Supersonic Aero Data

The supersonic aero data for the MMEEV is defined for M=3.98 and provided in Appendix A in Figure A4.

3.3.4 Transonic Aero Data

Transonic data in the database is derived from the experimental data obtained by Marco 1968 on models with a nose radius 15% of the base diameter. It was previously shown that for small angles of attack the nose radius is not a major driver, but this area will need to be revisited.

The transonic Mach data were defined for $M=1.3, 1.15, 0.85$ and 0.75 and aerodynamic data are provided in Appendix A Figures A5, A6, A7, and A8, respectively.

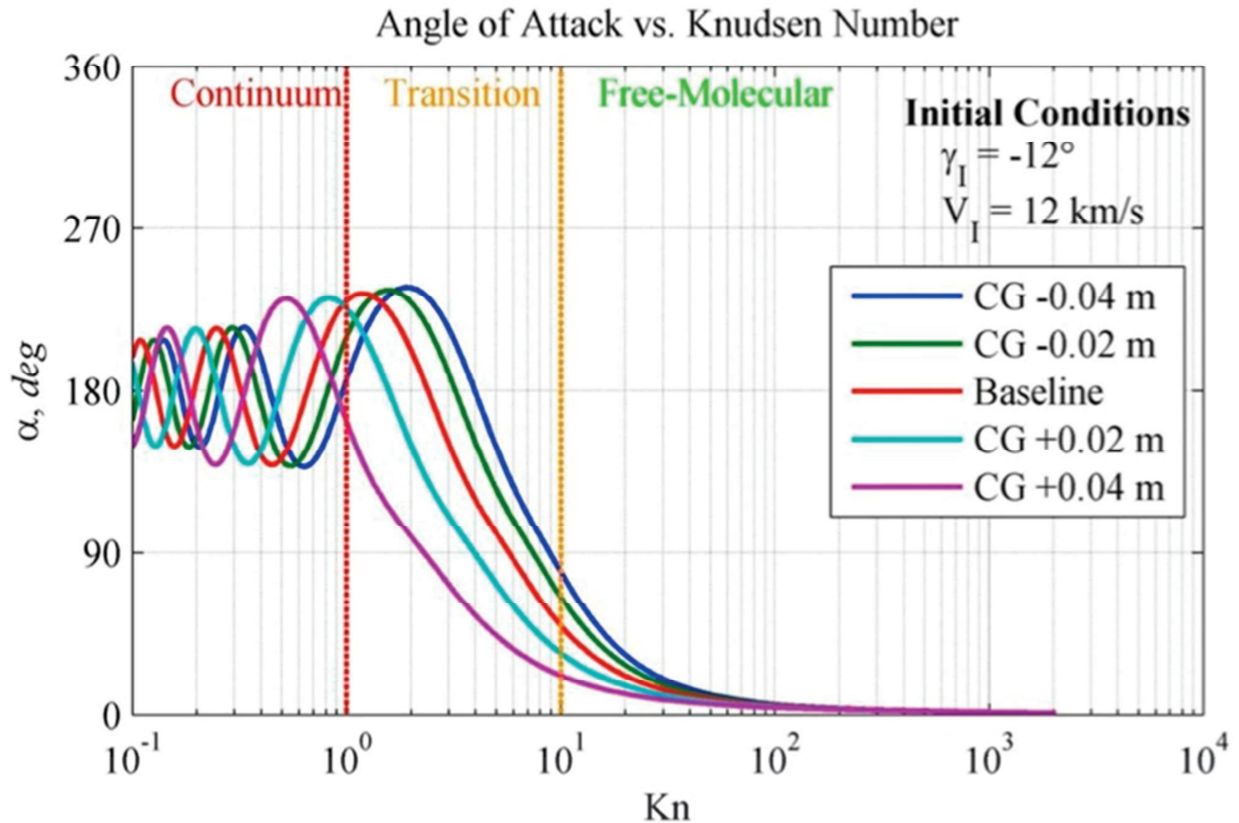


Figure 27. Time History Data for Several Trajectories with Different CGs (Cms).
Baseline CG = 0.2D

3.3.5 Subsonic Aero Data

Low subsonic static and dynamic characteristics were obtained by Mitcheltree as a result of experiments in the Langley Vertical Spin Tunnel (VST) (Mitcheltree, Fremaux, & Yates 1999). This data is in the form of curve fits, and some assumptions are made about applicability across the range of the Reynolds number. No work has been done to assess those assumptions in the context of MMEEV. Data is used as is, with the intent to revisit it in later analyses. Aerodynamic data for Mach numbers of 0.6 and 0.5 and provided in Figures A9 and A10.

3.3.6 Summary of all Static Data across the Mach Number Range

This section provides summary plots for all of the Mach numbers in the V-021 aero database. Providing the data in this format provides the ability to evaluate Mach effects as they are currently modeled. Figures 28 and 29 provide a summary of the static aerodynamic data for all Mach numbers. From these Figures it can be seen that there are high levels of C_N , C_M , and C_A for rarefied flow conditions. These levels decrease for $M=24$ and then continue to decrease through

the Mach number range down to M=0.6. However, between Mach numbers of 0.5 to 0.6, there is a large increase in C_N , C_M , and C_A which is not expected.

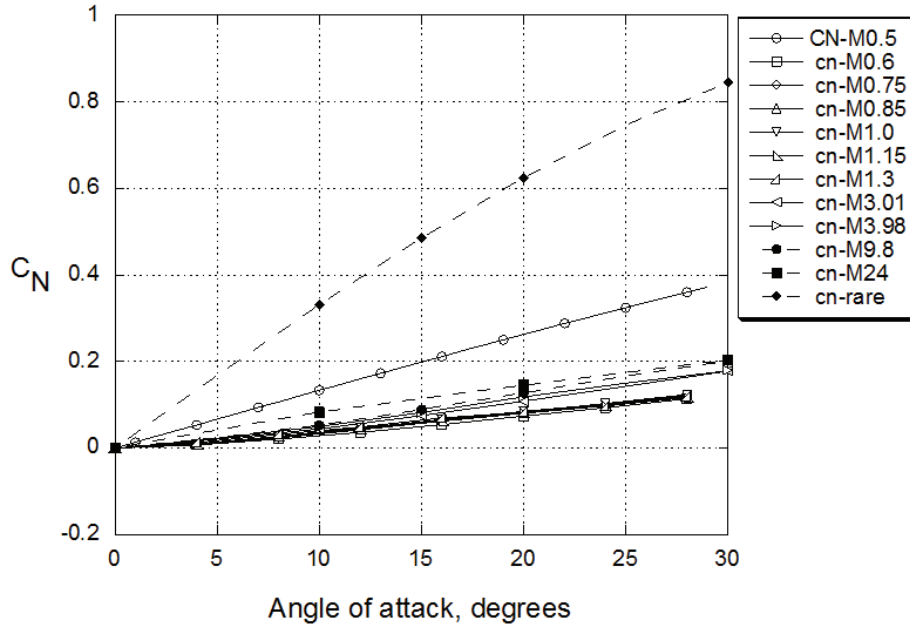


Figure 28. MMEEV Normal Force Coefficient for All Mach Numbers

3.3.7 MMEEV Dynamic Data

The MMEEV dynamic aero database is composed primarily of Viking data and some data from the LaRC 20-FT wind tunnel (for Mach numbers below 0.5). Figure 28 provides the MMEEV dynamic damping data. Viking damping data covers Mach numbers from 2.1 down to 0.7. For a Mach number of 0.5, pitch damping is provided from the equation provided below. Above 10° degrees angle of attack, the Viking vehicle is indicated to have nearly constant pitch damping as shown by the relatively constant negative values of C_{mq} over this range of angle of attack. Below 10° degrees, there is a strong decrease in pitch damping and some unstable damping for Mach numbers above M=0.9. Bottom of Figure 30 also provides an expanded view of the Viking data below 10° degrees angle of attack. As can be seen from Figure 30, the low-speed subsonic damping data for M=0.5 is significantly different from the data at the next highest Mach number (0.7). More work is needed to define the damping data for the MMEEV across the speed range, especially in the low-speed area where it is likely to be the most critical.

The subsonic pitch damping is provided by the following equation:

$$C_{m_q} = C_{m_q \text{ limit}} \times C_{m_q \text{ epsi}} \div (C_{m_q \text{ epsi}} + \alpha) \times C_{m_{q^*}} + C_{m_{q^*}} + C_{L\alpha} \times r^2_{\text{gyration}} \quad (7)$$

where:

$$C_{m_q \text{ limit}} = -1.7$$

$$C_{m_{q\text{epsi}}} = 0.05$$

α = angle of attack in radians

$$C_{m_{q*}} = -0.0468$$

$$r^2_{gyration} = 0.25$$

$$C_{L\alpha} = (C_{N\alpha} - C_A) \times \cos(\alpha) - (C_N + C_{A\alpha}) \times \sin(\alpha)$$

$$C_{N\alpha} = 0.749 \times \cos(\alpha)$$

$$C_A = 0.654 - 0.5 \times \sin(\alpha)^2$$

$$C_N = 0.749 \times \cos(\alpha)$$

$$C_{A\alpha} = -\sin(\alpha) \times \cos(\alpha)$$

The V_021 database includes several blending functions involving the dynamic data. Below $M=0.5$, the subsonic damping data as defined above is used. Between Mach numbers of 0.5 and 1.5 a blending of the subsonic and Viking data are used. The Viking damping data are used up through hypersonic Mach numbers. At Knudsen numbers greater than 0.001, a blending of the Viking data with zero damping is performed up to Knudsen number of 10.0. For Knudsen numbers greater than 10, zero pitch damping is assumed.

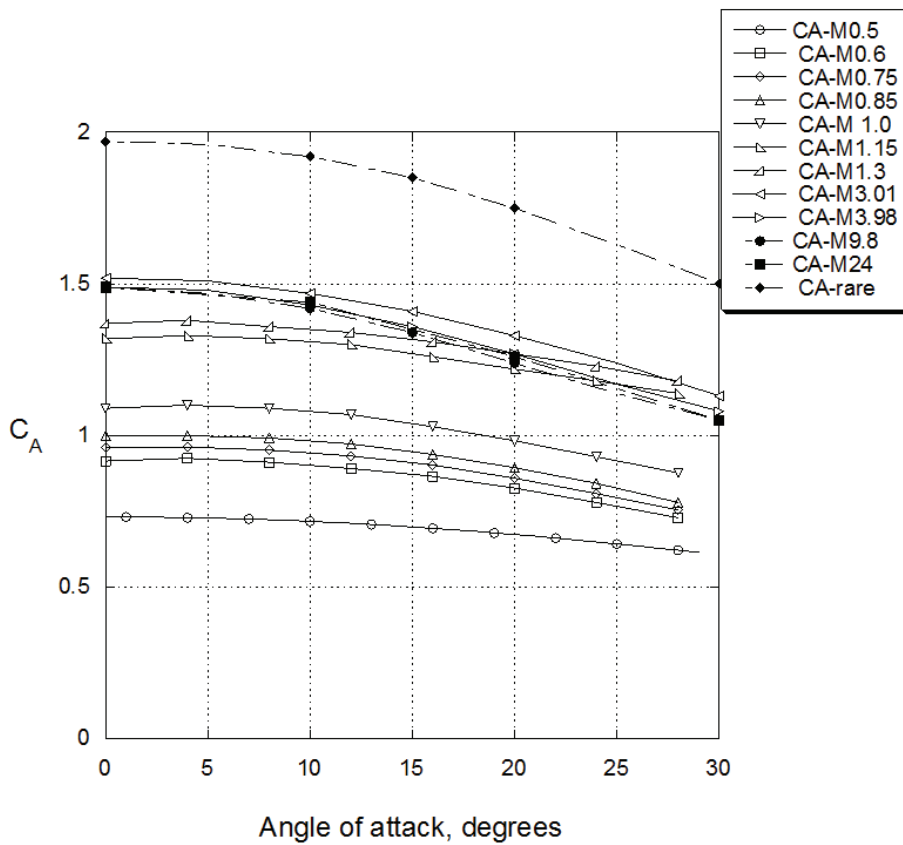
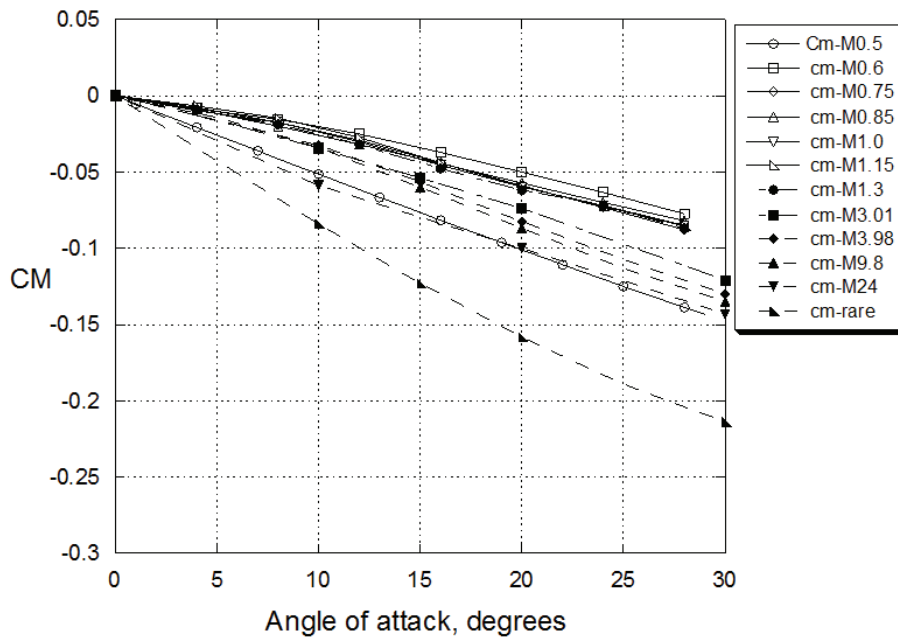


Figure 29. MMEEV Pitching Moment and Axial Force Coefficients for All Mach Numbers

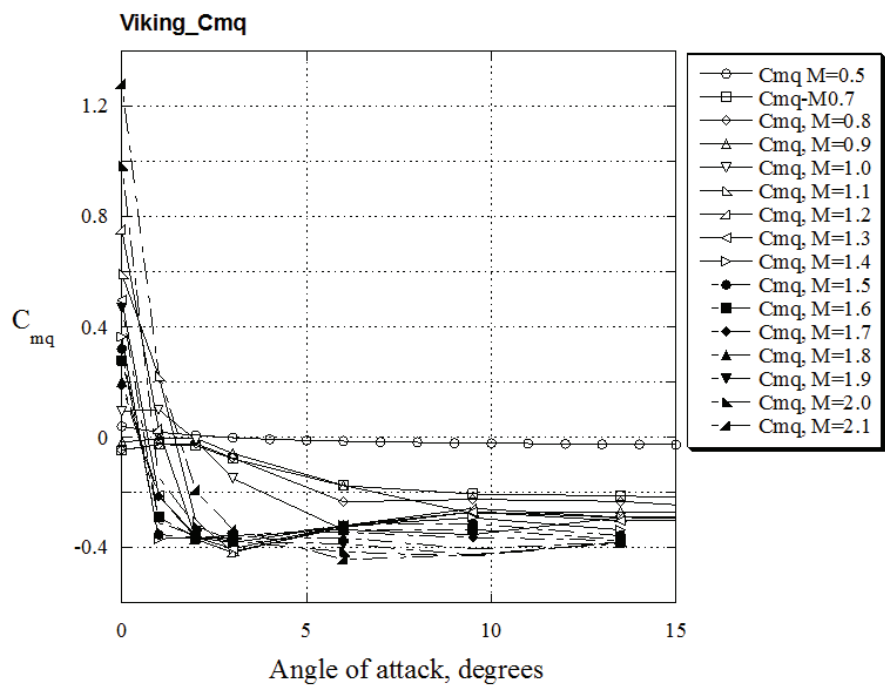
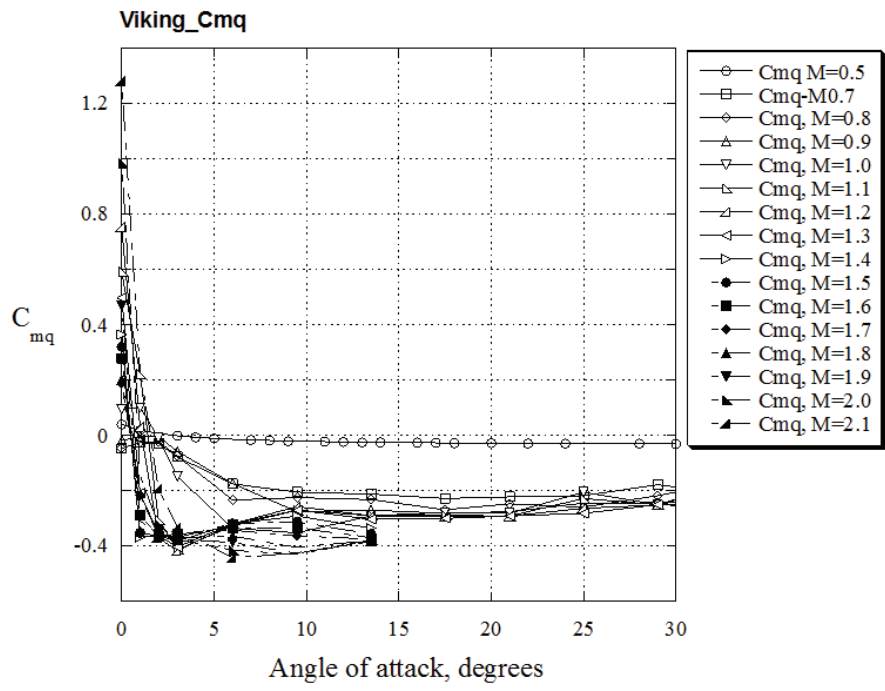


Figure 30. MMEEV Pitch Damping Data from M=0.5 to 2.1

3.4 Aerothermal Module

This section describes the computational fluid dynamic (CFD) aerothermal analyses for the M-SAPE application. The goal for this analysis is to provide heating estimates for the probe surface that could be further used for thermal soak analysis (Agrawal and Sepka, et al. 2012) and to establish correlation coefficients for aerodynamic heating based on the Sutton-Graves (Sutton and Graves 1972) equation for the vehicle that could be used for rapid design trades. An additional outcome was to study the effect of varying the shoulder radius while keeping the nose radius and vehicle diameter constant.

The concept vehicle's TPS model must be designed for a large matrix of entry velocities (10 to 16 km/s), ballistic coefficients (42 to 129 kg/m²) and entry flight path angles (−5 to −25 degrees). An aerothermal database is necessary to understand the environments the vehicle could experience. The parametric space consists of too many cases for a high-fidelity CFD code to perform affordable characterization of the heating. An engineering approach which is CFD anchored was established to quickly characterize quantities pertinent to TPS design, such as heat flux, heat load, and surface pressure. The engineering approach uses outputs from POST II and Data Parallel Line Relaxation (DPLR) CFD code based correlations to find surface quantities. For addition details, readers are referred to Aliaga-Caro, Zarchi, and Sepka 2013.

3.4.1 Vehicle Geometries

Three capsule geometries—version 1 (v1), version 2 (v2), and version 3 (v3)—have been considered and are shown in Figure 31. Table 3 lists the configurations' defining geometric dimensions.

A series of CFD simulations were conducted to determine how CFD compared with the Sutton-Graves correlation for all geometries.

A parametric study was conducted for the v3 geometry to assess the affect of shoulder radius on maximum shoulder heating. Shoulder radius was varied at one Mach number to determine change in shoulder heating versus the shoulder radius non-dimensionalized with vehicle radius, R_s/R_b . Additionally, one trajectory was run for two different shoulder radii (0.0234 and 0.0384 meters) to determine the change, if any, of the fraction of maximum shoulder heating over stagnation point heating as a function of Mach number. For the Sutton-Graves comparison, all simulations of the v3 geometry were performed on the smallest shoulder radius as the highest heating is expected to occur at the shoulder for this radius. For this set of analyses, only the forebody of the v3 geometry was considered.

Table 3. Geometry Configurations

	v1	v2	v3
Nose Radius [m]	0.35	0.132	0.352
Vehicle Diameter [m]	1.08	1.057	0.900
Shoulder Radius [m]	0.025	0.048	0.02340-0.0495

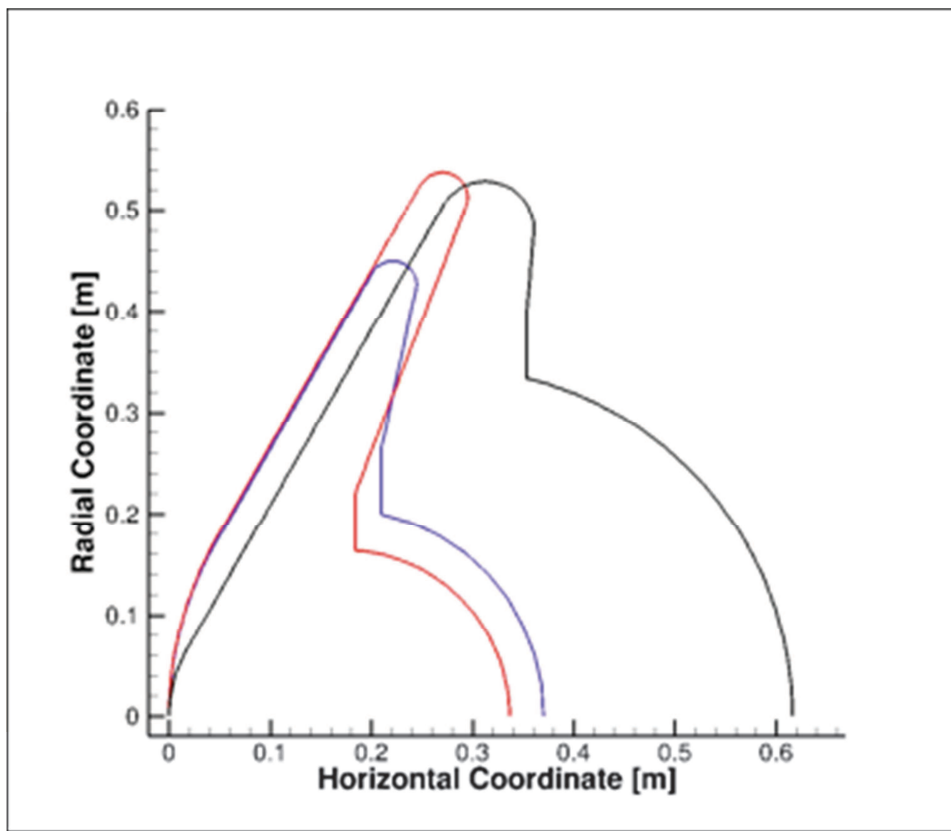


Figure 31. Geometries are Superimposed (v1 = red, v2 = black, v3 = blue). Only the Fore-body (from the nose of the vehicle to the apex at the shoulder) of v3 is used for CFD Simulations

3.4.2 CFD Methodology

The DPLR v. 4.02 CFD code was used for all the analyses (Wright et al. 2009). It is a parallel, structured multi-block, finite volume code that solves the reacting Navier-Stokes equations for continuum flow, including finite rate chemistry and thermal non-equilibrium. In the present study, the Euler fluxes are computed using modified Steger-Warming flux vector splitting (MacCormack and Candler 1989) with third-order spatial accuracy via Monotone Upstream-centered Schemes for Conservation Laws (MUSCL) extrapolation coupled with a min-mod limiter (Yee 1989). The viscous fluxes are computed to second-order spatial accuracy with a central difference approach.

The surface of the vehicle was modeled using the radiative equilibrium wall boundary condition with a constant emissivity of 0.85. The flow field was assumed laminar throughout the entire trajectories and was modeled using an 11-species finite-rate air chemistry model. Transport properties are computed using Yos mixing rule and multi-species diffusion coefficients are computed using consistent effective binary diffusion. At least ten points were chosen along each

trajectory to capture the heat pulse. Three grid adaptations were performed for each location along the trajectory.

3.4.3 CFD Results

Convective Heating: 1.33 Factor

A common engineering relation for convective heating is the Sutton-Graves (Sutton and Graves 1972). The Sutton-Graves correlation is defined as:

$$q_w = C \sqrt{\frac{\rho_\infty V_\infty^3}{R_n}} \quad (8)$$

where q_w is heat flux (W/cm^2) at the stagnation point, C is a constant with value of 1.74153×10^{-4} for Earth, R_n is the nose radius (m) and ρ_∞ and V_∞ are the freestream density (kg/m^3) and freestream velocity (m/s), respectively.

The first parametric trade space for the v1 geometry is made up of 840 trajectories ranging in entry velocities (V_∞) from 10 to 16 km/s, ballistic coefficients (β) of 42 to 129 kg/m^2 and entry flight path angles (γ) of -5 to -25 degrees. A number of DPLR cases were performed on the v1 geometry that spanned the parameter space (Table 4). Figure 32 shows a representative Mach contour at $V_\infty=14$ km/s, $\gamma=-7$ deg, and $\beta=63.4$ kg/m^2 for this geometry. By holding two parameters (entry velocity, flight path angle or ballistic coefficient) constant and varying the third, a correction factor to stagnation point heat flux was found to bring the Sutton-Graves correlation closer to the DPLR heat flux. All CFD simulations were run at peak heating. The correction factor to Sutton-Graves for the stagnation point was found to be 1.33. Figures 33, 34, and 35 show the correction factor agrees well with DPLR predictions.

Table 4. CFD Trade Space for v1 Geometry

CFD Cases					
Ballistic Coefficient (kg/m ³)		Flight Path Angle (degrees)		Entry Velocity (km/s)	
V=10, $\gamma=5$	50.5794	V=10, $\beta=50.57$	5	$\gamma=10, \beta=50.57$	10
	41.9481		10		11
	66.6691		15		12
	82.2981		20		13
	54.2618		25		14
	97.8409	V=10, $\beta=42.40$	5	15	
	113.3129		10	16	
	128.7391		15		
	42.401		20		
			25		
V=13, $\gamma=25$	50.5794				
	42.401				
	82.2981				
	48.7736				
	51.7517				
	113.3129				
	128.7391				
71.4557					

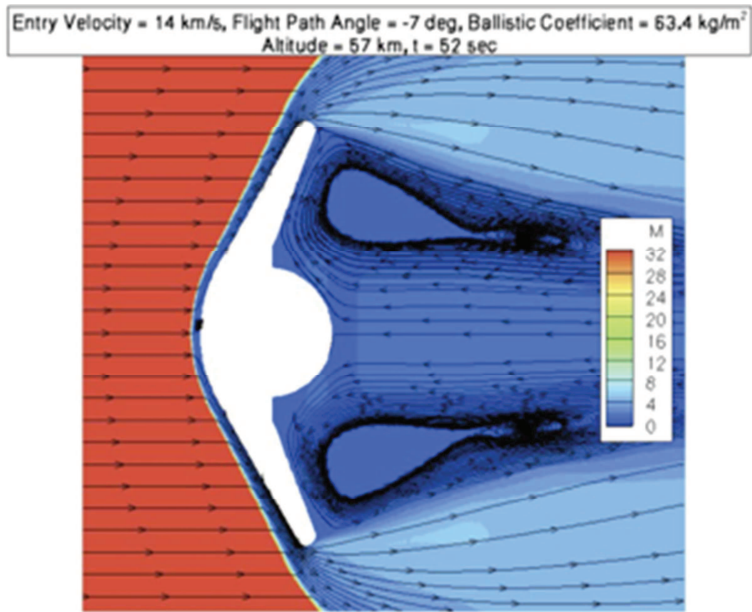


Figure 32. Mach Contour for the v1 Geometry

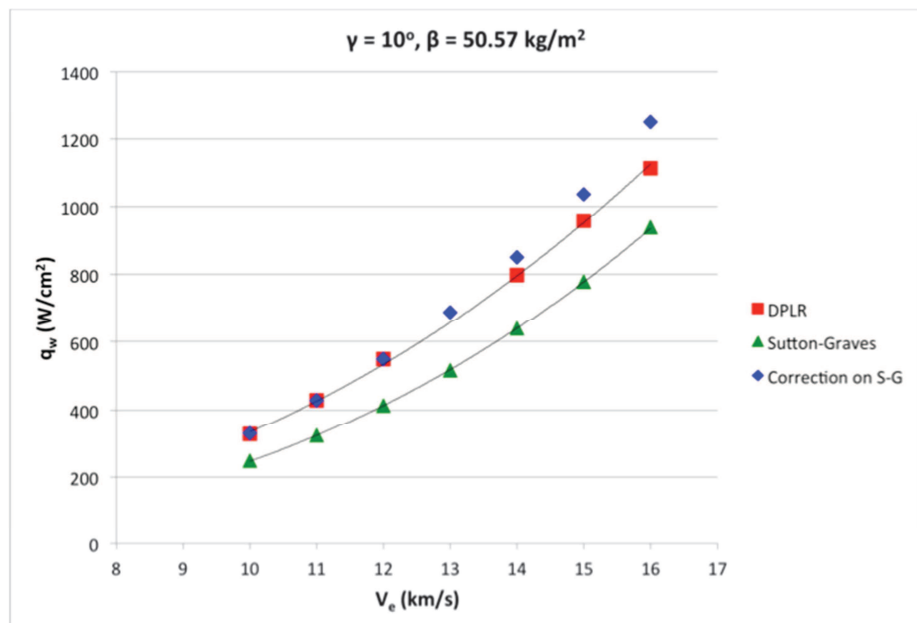


Figure 33. Correlated Heat Flux with Varying Velocity as Compared to DPLR and Sutton-Graves

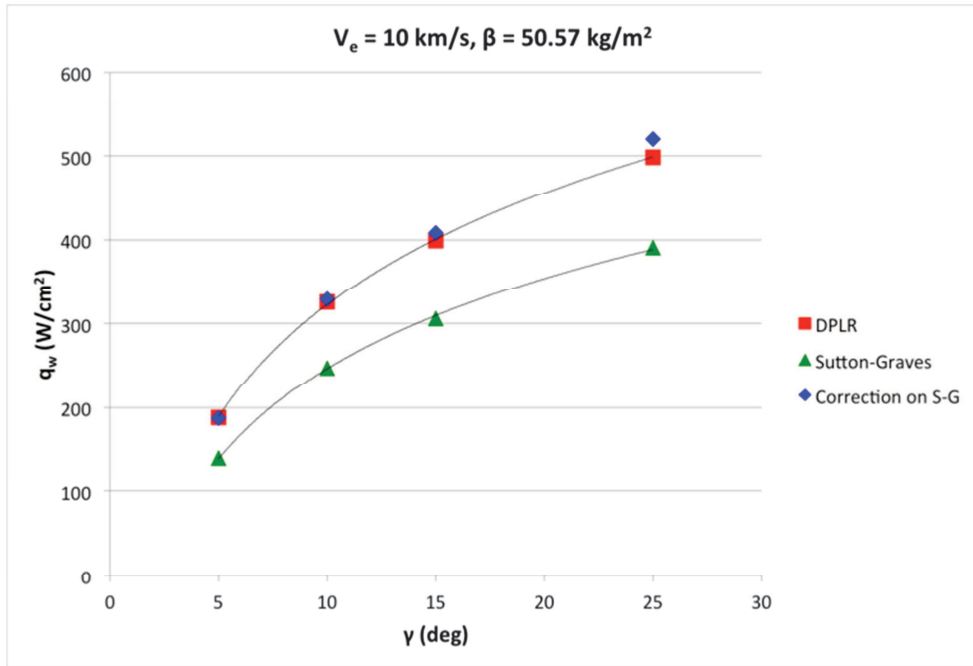


Figure 34. Correlated Heat Flux with Varying Entry Flight Path Angles as Compared to DPLR and Sutton-Graves

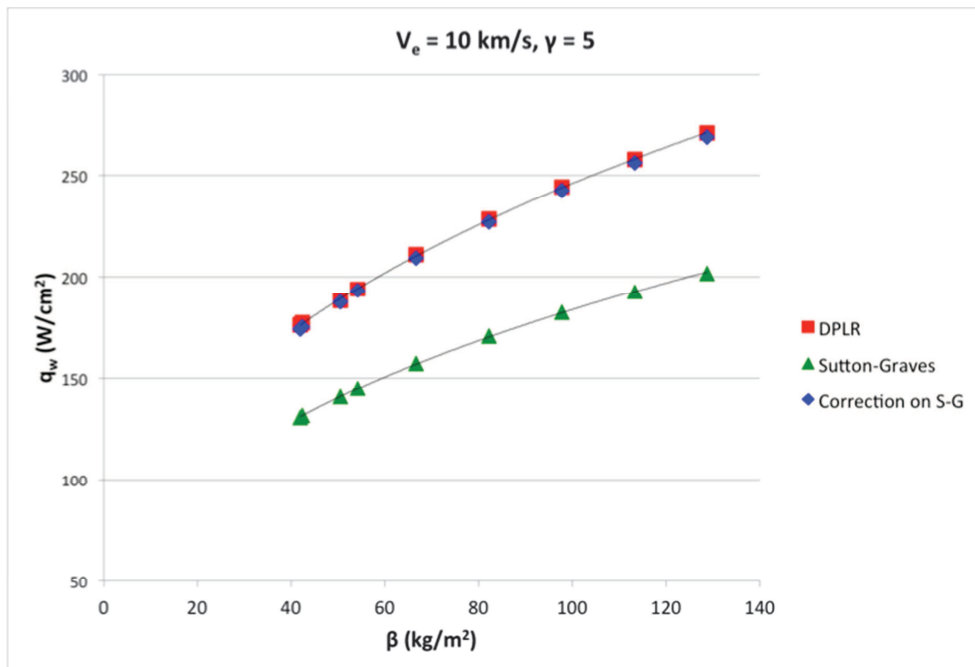


Figure 35. Correlated Heat Flux with Varying Ballistic Coefficient as Compared to DPLR and Sutton-Graves

The second set of trajectories for the v2 and v3 geometries consisted of over 2700 cases each. Entry velocities for these trajectories range from 10 to 16 km/s. The range of ballistic coefficients is from 42 to 129 kg/m² and the range of entry flight path angles is from -5° to -25° degrees. From these, a representative set of trajectories for the CFD analyses was selected based on the statistical average and standard deviations of peak heating and heat load. The aim of the CFD simulations of the v2 and v3 geometry was to confirm the 1.33 correction factor derived from a different geometry and trajectory space. Figures 36 and 37 show the DPLR stagnation point heat fluxes for one trajectory for each of the v2 and v3 geometries respectively. CFD results lie within the 1.33 correction indicating the correction factor is conservative. Figures 38 and 39 show Mach contours after the grids were aligned with the shock.

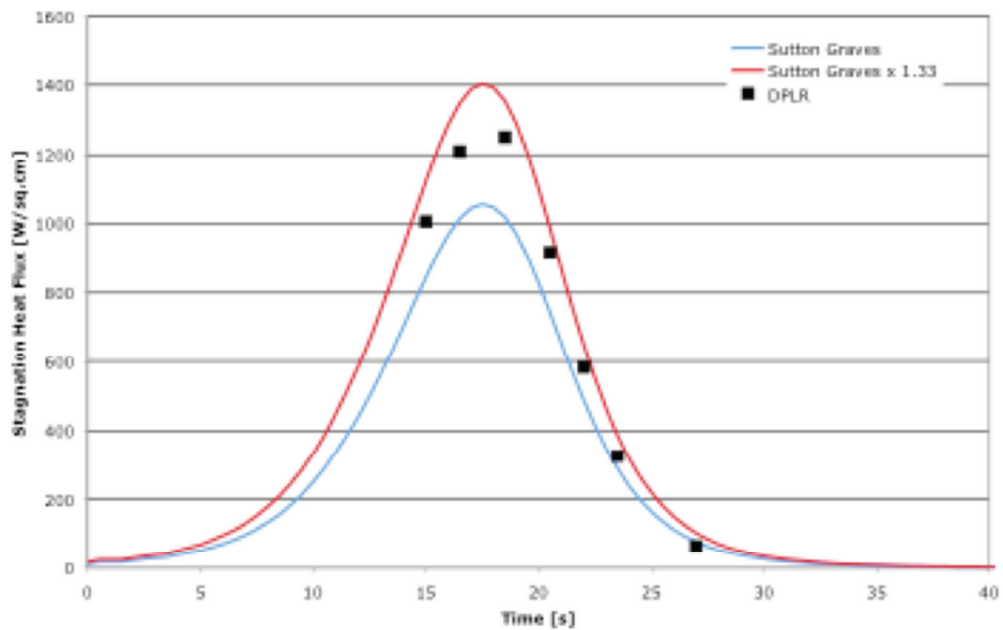


Figure 36. Stagnation Point Heat Flux Along a Trajectory for the v2 Geometry.

$$V_{\infty} = 14.0 \text{ km/s}, \gamma = -15^{\circ} \text{ degrees}, \beta = 15 \text{ kg/m}^2.$$

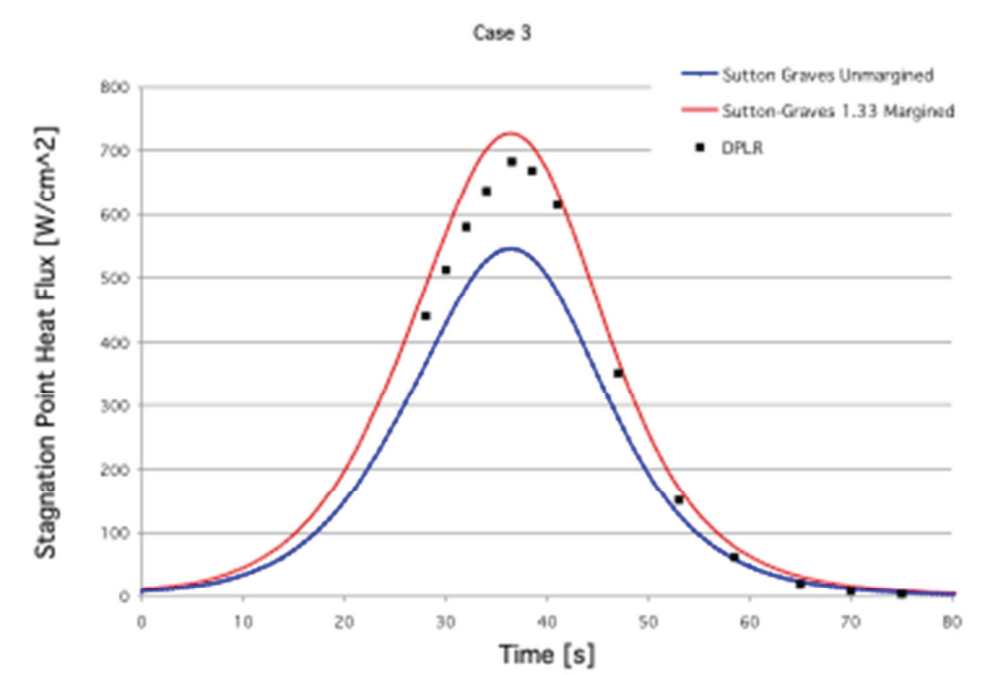


Figure 37. Stagnation Point Heat Flux Along a Trajectory for the v3 Geometry.
 $V_\infty = 14.0$ km/s, $\gamma = -8^\circ$ degrees, $\beta = 25.67$ kg/m².

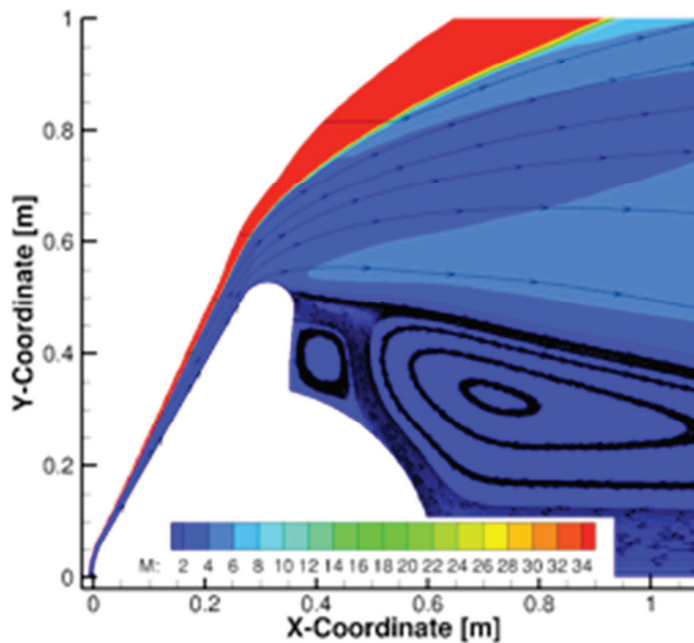


Figure 38. Mach Contour after Grid Adaptation for the v2 Geometry,
 $V_\infty = 14.0$ km/s, $\gamma = -15^\circ$ degrees, $\beta = 15$ kg/m².

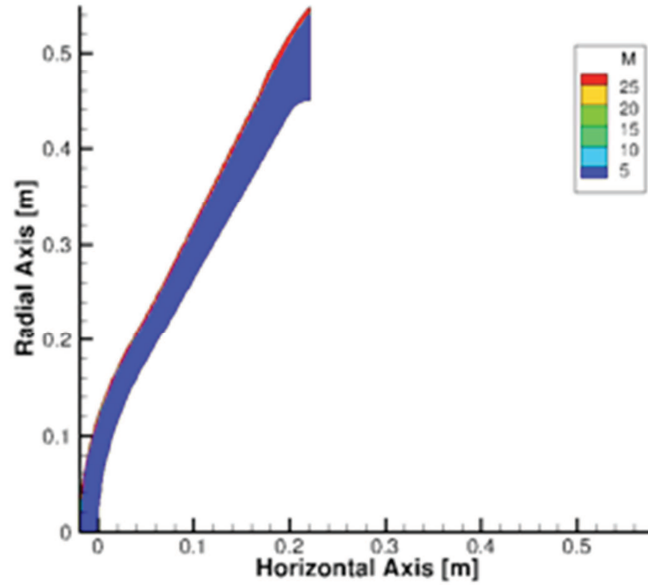


Figure 39. Mach Contour after Grid Adaption for the v3 Geometry,
 $V_{\infty} = 14.0$ km/s, $\gamma = -8^{\circ}$ degrees, $\beta = 25.67$ kg/m².

Pressure

For the v1 geometry, the stagnation point surface pressure was found with a curve fit of DPLR pressure values to the Newtonian relationship:

$$p = C\rho^m V^n \quad (9)$$

where $C = 0.792$, $m = 1.00357$ and $n = 2.02529$. The pressure fit is well characterized as seen in Figure 40 where the correlation goes directly through all of the DPLR data points.

Figure 41 shows the same equation applied to the prediction on the v3 geometry. The pressure fit again goes through all the DPLR data points. Also plotted in these graphs are the M-SAPE values for pressure. M-SAPE uses the equation:

$$C_p = C_{P_{\max}} \sin^2 \theta \quad (10)$$

$$C_{P_{\max}} = \frac{2}{\gamma M_{\infty}^2} \left(\left[\frac{(\gamma+1)^2 M_{\infty}^2}{4\gamma M_{\infty}^2 - 2(\gamma-1)} \right]^{\gamma/(\gamma-1)} \left[\frac{1-\gamma+2\gamma M_{\infty}^2}{\gamma+1} \right] - 1 \right) \quad (11)$$

$$p - p_{\infty} = C_{P_{\max}} \frac{1}{2} \rho_{\infty} V_{\infty}^2 \quad (12)$$

where $\theta = 90$ degrees, $C_{P_{\max}}$ is the stagnation point pressure coefficient, γ is the ratio of specific heats and M_{∞} is the freestream Mach. In the limits as $M_{\infty} \rightarrow \infty$ and $\gamma=1$, $C_{P_{\max}} = 2$. So the stagnation pressure becomes two times the freestream dynamic pressure. The M-SAPE values for pressure are conservative against the DPLR values.

Affect of Shoulder Radius

A parametric study using the v3 geometry was conducted at the peak heating point of one trajectory, at Mach 30, to see the shoulder radius effect on maximum shoulder heating. Nose radius and vehicle diameter were kept constant while the shoulder radius was varied. Figure 42 shows non-dimensionalized shoulder heat flux as a function of Mach number for the v3 geometry. A power law correlation between the maximum shoulder heat flux and non-dimensional shoulder radius was established, with decreasing heat flux corresponding to increasing shoulder radius.

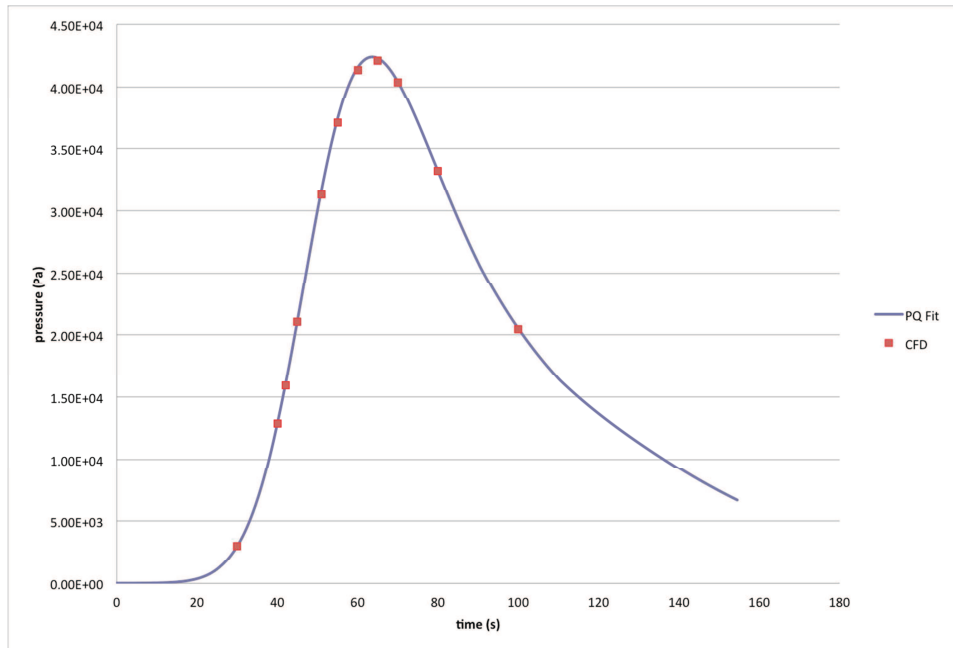


**Figure 40. Stagnation Pressure for the v1 Geometry,
 $V_{\infty} = 14.5$ km/s, $\gamma = -7^{\circ}$ degrees, $\beta = 50.5$ kg/m².**

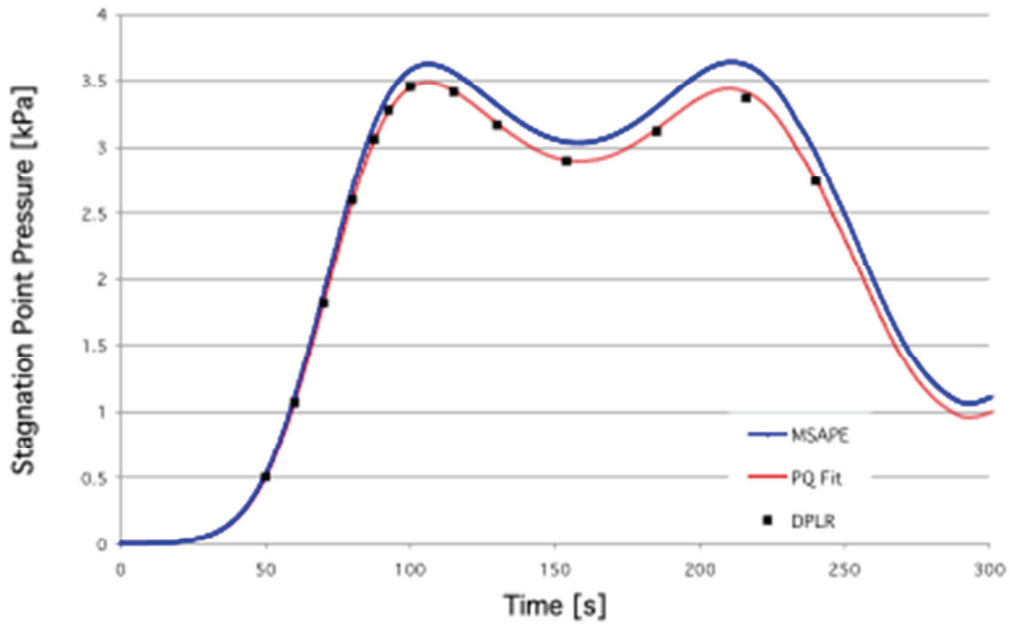


Figure 41. Stagnation Pressure for the v3 Geometry,
 $V_{\infty} = 11.0$ km/s, $\gamma = -5^{\circ}$ degrees, $\beta = 30.75$ kg/m².

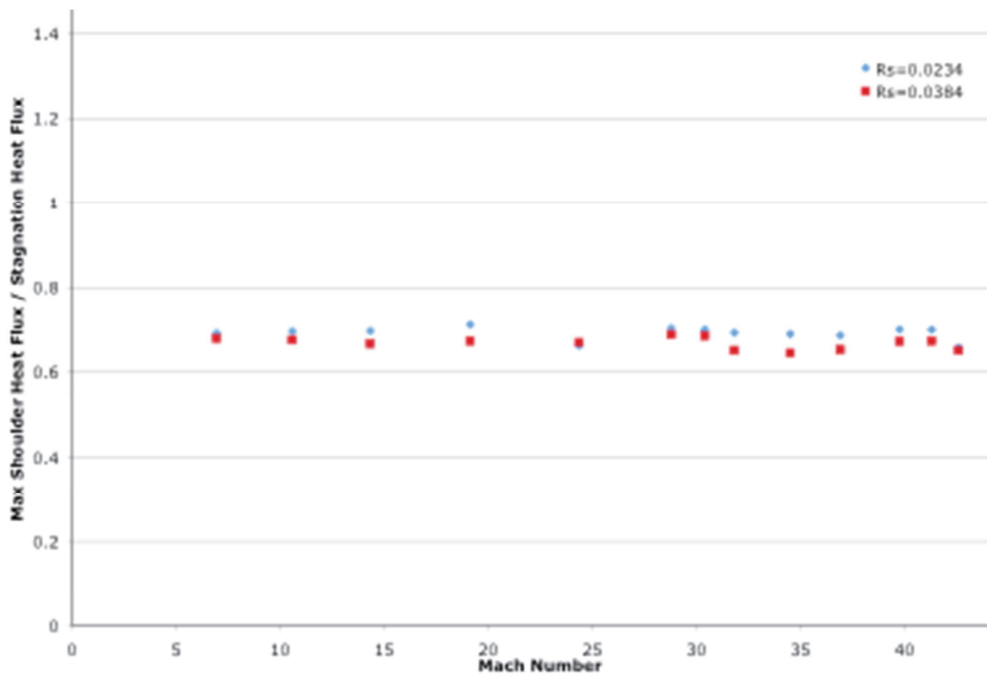


Figure 42. Non-dimensionalized Shoulder Heat Flux as a Function of Mach Number for the v3 Geometry,
 $V_{\infty} = 12.0$ km/s, $\gamma = -30^{\circ}$ degrees, $\beta = 70.73$ kg/m².

Turbulence

Turbulent simulations were performed for all cases of the v3 geometry. The turbulent model used was the Baldwin-Lomax model. This model assumes a fully turbulent flow everywhere along the surface of heat-shield. Figures 43 and 44 show turbulent solutions plotted against the laminar solutions for two instances along one of the trajectories.

Transition from laminar to turbulent flow is characterized by the value of the momentum thickness Reynold's number, Re_θ . Experimental data has found transition to turbulence occurs at Re_θ of 200 to 300 (Hollis 2012). Figure 45 shows the time history of the maximum value of Re_θ for all trajectories—this occurs in the vicinity of the shoulder region as seen in Figure 42. For the majority of the cases considered here, Re_θ remains below 200 indicating laminar flow. It is only for Case 4 and Case 5 that Re_θ gains a value above 200, but below 300, indicating transitional flow. Figure 45 shows the calculated Re_θ along the probe for Case 5 corresponding to the solutions of Figure 43 and 44, respectively.

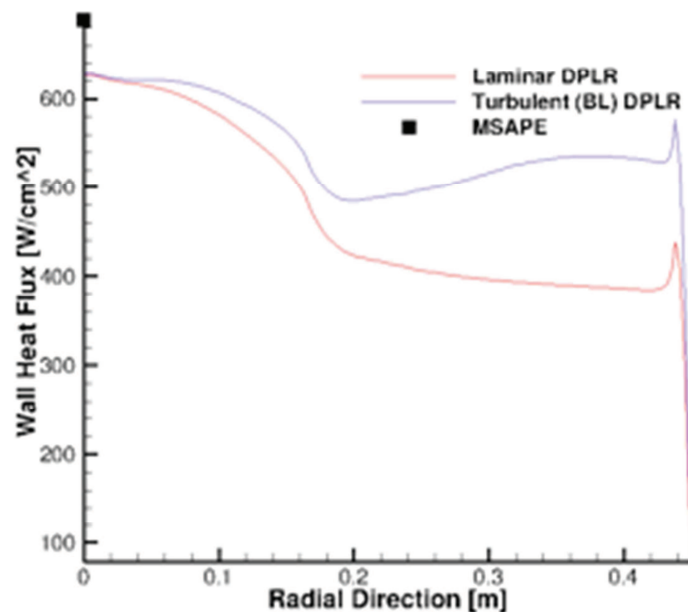


Figure 43. Heat Flux Comparison between Laminar and Fully Turbulent Solutions at an Early Point in the Trajectory

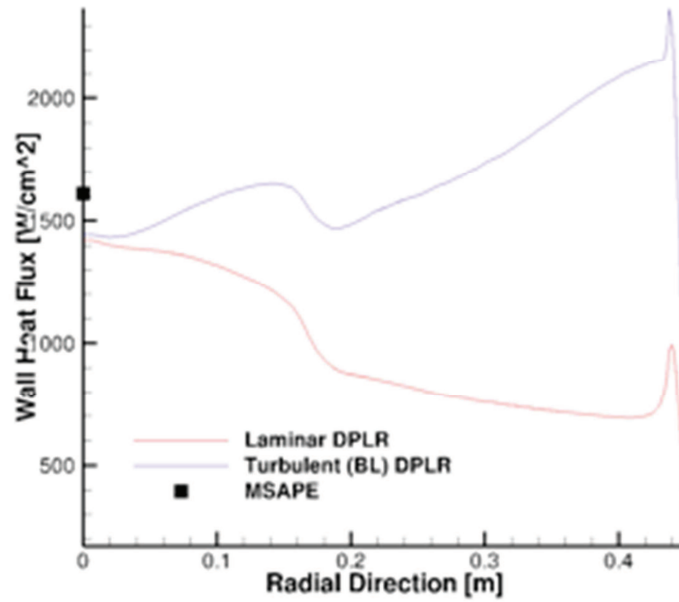


Figure 44. Heat Flux Comparison between Laminar and Fully Turbulent Solutions at Peak Heating Along the Trajectory

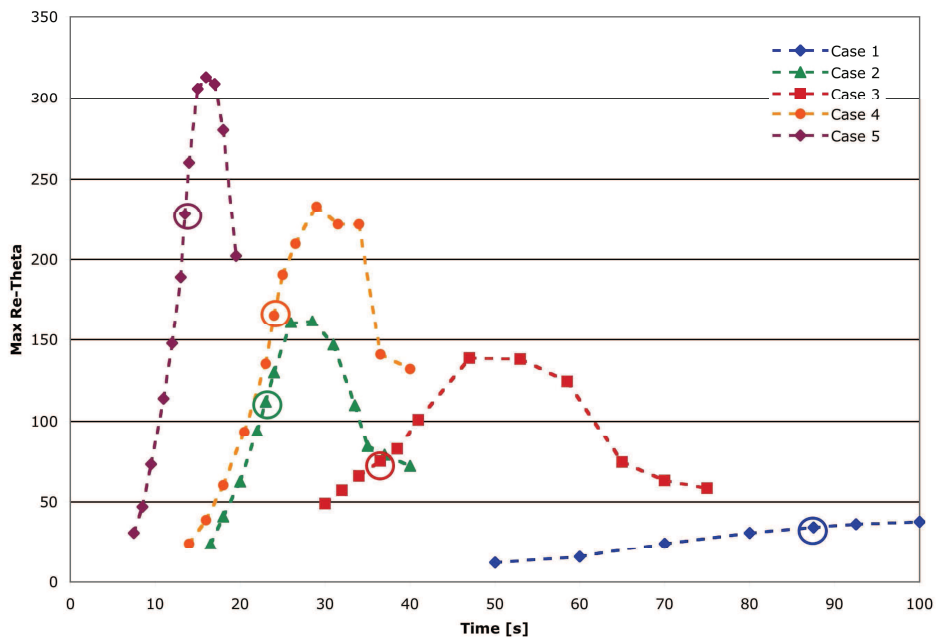


Figure 45. Time History of the Maximum Value of Momentum Thickness Reynolds Number for the v3 Geometry. (Circled values correspond to peak heating for each trajectory.)

3.5 TPS Sizing Module

Mass estimating relationships (MERs) were formulated to determine a vehicle's Thermal Protection System (TPS) required thickness for safe Earth entry. The objective of this study was to develop MERs using simple correlations that were non-ITAR and matched as accurately as possible NASA's high-fidelity ablation modeling tool, the Fully Implicit Ablation and Thermal Analysis Program (FIAT) (Chen and Milos 1999). These MERs would be a first-estimate for feasibility studies; it is understood that higher-fidelity modeling like FIAT would be necessary once a proposed trajectory was down-selected. The trajectory space for these MERs consisted of 840 different trajectories, and a material's heating limit was the main constraint for an allowable trajectory. MERs for the vehicle forebody included the ablating materials Phenolic Impregnated Carbon Ablator (PICA) and Carbon Phenolic atop Advanced Carbon-Carbon. For the backshell the materials were Silicone Impregnated Reusable Ceramic Ablator (SIRCA), Acusil II, SLA-561V, and LI-900. The MER/FIAT ratio indicates MERs are accurate to within 14% (at one standard deviation) of FIAT prediction, and the most any MER can under-predict TPS thickness is 19% of FIAT prediction. MERs resulting from these analyses are used to determine the pre-flight mass of the vehicle TPS.

3.5.1 Background

A typical re-entry problem requires computational aerothermodynamics to understand the flow conditions around the vehicle and to determine the convective and radiative heating to its surface. Once the surface heating is known, appropriate TPS materials can be chosen. A TPS material response model would then be used to determine the amount of heat shield material required to keep its bond line temperature below a specified value and to know the amount of surface recession. The traditional approach for this coupled problem would be to first use a high fidelity computational fluid dynamics code such as DPLR or LAURA for the aerothermal component and then FIAT (Chen and Milos 1999), CMA (Curry 1965) or STAB (Moyers and Rindal 1968), for the TPS response. However, this coupled approach usually had a very slow turnaround time and was highly dependent upon analyst availability. To circumvent these issues, M-SAPE employs correlations to bypass these codes with as minimal a loss in accuracy as possible.

To determine the aerothermal environment, M-SAPE uses the Sutton-Graves (Sutton and Graves 1972) correlation for the convective heating and Tauber-Sutton (Sutton and Graves 1972) for radiative heating. To date, however, no correlations based on high-fidelity FIAT modeling have been determined. The current work was to develop MERs using FIAT-based correlations with as high accuracy to FIAT prediction as possible. Toward that end, six MERs have been developed. For the vehicle forebody, the ablators were Phenolic Impregnated Carbon Ablator (Hui and et al. 1996) (PICA) and Carbon Phenolic (Clements and Ward 1966) atop Advanced Carbon-Carbon. For the vehicle backshell, the materials were Silicone Impregnated Reusable Ceramic Ablator (Tran 1996) (SIRCA), Acusil II (Edquist 2009), SLA-561V, and LI-900 because the aerothermal environment was so mild that ablation did not take place. As will be shown, the MERs were accurate to FIAT prediction within 14% at one standard deviation.

Using these MERs, the M-SAPE tool can now be used to perform trade studies involving entry velocity, ballistic coefficient, vehicle geometry, entry flight path angle, etc. and include TPS thickness as an output variable. Design turnaround times for a possible Earth entry configuration have been reduced from weeks to minutes for a set of proposed flight conditions. For these MERs, no margins were added to the calculated TPS thickness requirement.

3.5.2 MER Model Development

Applications of MERs

The MERs presented in this paper are statistical correlations developed to predict FIAT output. Each MER has a listed accuracy to FIAT prediction that was found by taking the standard deviation of the MER/FIAT value for all the trajectories. These correlations are only valid up to the TPS material limits (see Table 7) with respect to the total (convective and radiative) heat flux. If the trajectory were to predict a heating greater than allowed by the material capabilities, the analysis should be discarded. It is emphasized that the MER TPS predicated thickness is not the manufacturing limit of the material's thickness.

Finally, as for any statistical analysis, there are some trajectories for which the ratio of MER/FIAT prediction can exceed the listed MER accuracy at one SD. It is for this reason that full datasets are presented in Appendix B showing MER/FIAT data with FIAT predicted thickness. The most any MER can under predict FIAT is by 19%. M-SAPE utilizes these MERs as a “rough approximation” to determine flight trajectories of interest, but always maintains that a true high-fidelity analysis would be a requirement as proposed sample return missions move forward in development.

The flight trajectory range that was considered for MERs model development study is shown in Table 5.

Table 5. Flight Trajectory Space Considered for the MERs

Flight Trajectory Parameter	Range of Values	Resolution
Entry Velocity [km/s]	10-16	1
Entry Flight Path Angle [abs. deg.]	5°-25°	5°
Ballistic Coefficient [kg/m ²]	41.95 – 128.74	15.5 (max)
Total number of trajectories	840	-

FIAT Modeling Constraints

FIAT was run for each trajectory with the following constraints common for each developed MER:

- Maximum temperature at bondline was 250°C.
- Adiabatic back face of the material stack up.

- Surrounding environment temperature of 21.3°C (for radiation from the spacecraft surface).
- 1D planar geometry
- FIAT v3

It should be noted that FIAT, being a 1D code, was most applicable for regions on the heat shield that did not change shape quickly, such as at the stagnation point, along the flank or any other acreage location. For regions that do change shape quickly, like the shoulder, the material response code TITAN (Milos and Chen 2008)] would be more appropriate because it includes 2D effects. In addition, PICA's heat conduction was orthotropic, which also necessitates the use of TITAN along regions of the heat shield that change shape quickly. The range of heating rates, heat loads, and surface pressure that were found from the FIAT analysis of the 840 flight trajectories are shown in Table 6. The back shell aerothermal environment was estimated to be 5% of the fore body stagnation point heating and 50% of the surface pressure.

Table 6. Surface Heating and Pressure Ranges Found by Running FIAT over the 840 Trajectories

	Forebody	Backshell
Maximum heat flux, cold wall [W/cm ²]	130 – 7900	5% of forebody
Heat Load, cold wall [J/cm ²]	3175 – 39943	5% of forebody
Maximum pressure, atm	0.005 – 3.288	50% of forebody

Sensitivity studies were conducted by plotting required TPS thickness against a variable of interest and looking to see if any correlation existed. Variables of interest included: peak heat flux, peak surface pressure, heat load, ballistic coefficient, entry velocity, and entry flight path angle. Of these, heat load and entry velocity showed the greatest sensitivity to required TPS thickness and were chosen as the variables to use in a power-law correlation. A power-law fit (Eq. 13) or quadratic equation (Eq. 14) were used to approximate the TPS thickness and are given in the form:

$$TH = a \left(\frac{HL}{V^2} \right)^b \quad (13)$$

$$TH = a \left(\frac{HL}{V^2} \right)^2 + b \left(\frac{HL}{V^2} \right) + c \quad (14)$$

Table 7. Summary of MERs Model Development Data

	PICA	CP/ACC	SIRCA	Acusil II	LI-900	SLA-561V
Recession [cm]	0.60 – 1.15	0.0002 – 0.141	none	none	LI-900 none	SLA-561V none
Accuracy to FIAT (one SD)	6.3%	7.3%	8.5%	7.6%	14.0%	8.5%
Largest possible under prediction (% of FIAT)	11.7	16.6	15.6	15.1	18.7	15.7
Minimum thickness [cm]	3.27	2.27	0.518	0.614	0.686	0.454
Max allowable heat flux, CW [W/cm ²]	1200	30000	100	100	75	100
Thickness [cm]	$1.8696 \left(\frac{HL}{V^2} \right)^{0.1873}$	$1.1959 \left(\frac{HL}{V^2} \right)^{0.2102}$	$0.5281 \left(\frac{HL}{V^2} \right)^{0.5416}$	$0.623 \left(\frac{HL}{V^2} \right)^{0.5697}$	$q_{cw} \leq 10 \text{ W/cm}^2$ $0.6961 \left(\frac{HL}{V^2} \right)^{0.656}$ $q_{cw} > 10 \text{ W/cm}^2$ $-0.0306 \left(\frac{HL}{V^2} \right)^2 + 0.5896 \left(\frac{HL}{V^2} \right) + 0.6739$	$0.0064 \left(\frac{HL}{V^2} \right)^2 + 0.0961 \left(\frac{HL}{V^2} \right) + 0.3322$

HL = heat load, cold-wall, J/cm²
V = entry velocity, km/s
CW = cold-wall

Table 8. Summary of Arcjet, Galileo, Pathfinder, and MSL Materials Test Data (Acusil is missing)

Name	Max Heat Flux (W/cm ²)	Max Heat Rate for Short Duration Heat Pulse (W/cm ²)	Short Duration (s)	Max Pressure, (atm)	Minimum Thickness (cm)	Maximum Thickness (cm)
PICA *	1,200	1,200	N/A	1.5	0.5	15
CP**	30,000	30,000	N/A	7.5	0.5	N/A
SLA-561V!	100	125	15	0.25	0.5	3
LI-900 (uncoated)	75	100	15	2	0.5	15
SIRCA	100	125	30	1	0.5	15
Acusil II	100	125	20	1	0.25	10

* Based on test data. The material performance may be better than this.

** Based on Galileo entry.

!Based on Pathfinder and MSL test data

MERs have been presented for the vehicle forebody ablators PICA and Carbon Phenolic atop ACC, and for the backshell materials SIRCA, Acusil II, SLA-561V, and LI-900. Applications include quick estimates of TPS mass during early stages of vehicle design. These MERs have been integrated into M-SAPE and will be used with FIAT as an initial estimate of required material thickness to speed sizing estimates. When using these MERs, care needs to be taken so that sizing environments, such as peak heating, are within the capabilities of the material.

3.6 Thermal Soak Module

The survival of the entry vehicle and successful payload recovery are key to the success of sample return missions. Mission requirements for outer-space samples could be very stringent. For example, MSR requires maintaining temperature control below 20⁰ C. Thus, knowledge of payload temperature history and peak payload temperature is critical for mission success. During the entry into Earth’s atmosphere, vehicles are subjected to severe thermal and mechanical loading due to aerothermal heating followed by the impact of landing. Figure 46 shows a schematic of different phases of the entry vehicle. In order to protect vehicles from atmospheric heating, a layer of ablative and/or insulative Thermal Protection System (TPS) materials is used on the fore and aft body. The relatively lower conductivity of thermal protection materials causes a slow absorption of thermal energy into the interior of these vehicles. In addition, low density porous foams are used surrounding the payload container to absorb the kinetic energy during the impact of landing. Thus, it could take several minutes to hours before the interiors (impact foam

and shell) and payload of the vehicle start to show a rise in temperature. Because the retrieval process for the vehicle could take several hours, thermal soak analysis becomes very important to predict the survivability of the payload (Agrawal et al. 2012).

In the past, a preliminary thermal analysis of a nominal MSR entry vehicle for a given trajectory, including predictions of payload temperature, was performed by researchers at NASA Langley (Amundsen et al. 2000). The present work, designed as a thermal soak module for inclusion into the M-SAPE tool, has a broader objective. The objective is to build a parametric thermal soak model such that analysts could predict the peak payload temperature of a sample return vehicle for any given trajectory by entering the vehicle diameter and trajectory parameters, such as peak stagnation heat flux and heat load.

To serve this objective, multiple thermal soak analyses were performed in a simplified parametric MSR-EEV-type geometry. To build the model, analyses were performed on trajectories with varying heat loads ranging from 3000 J/cm^2 to $38,000 \text{ J/cm}^2$ and heat fluxes varying from 100 W/cm^2 to 1500 W/cm^2 . In addition, the vehicle model was scaled from 0.8 meter in diameter to 1.4 meters in diameter thereby including vehicle diameter as a variable in the parametric soak model.

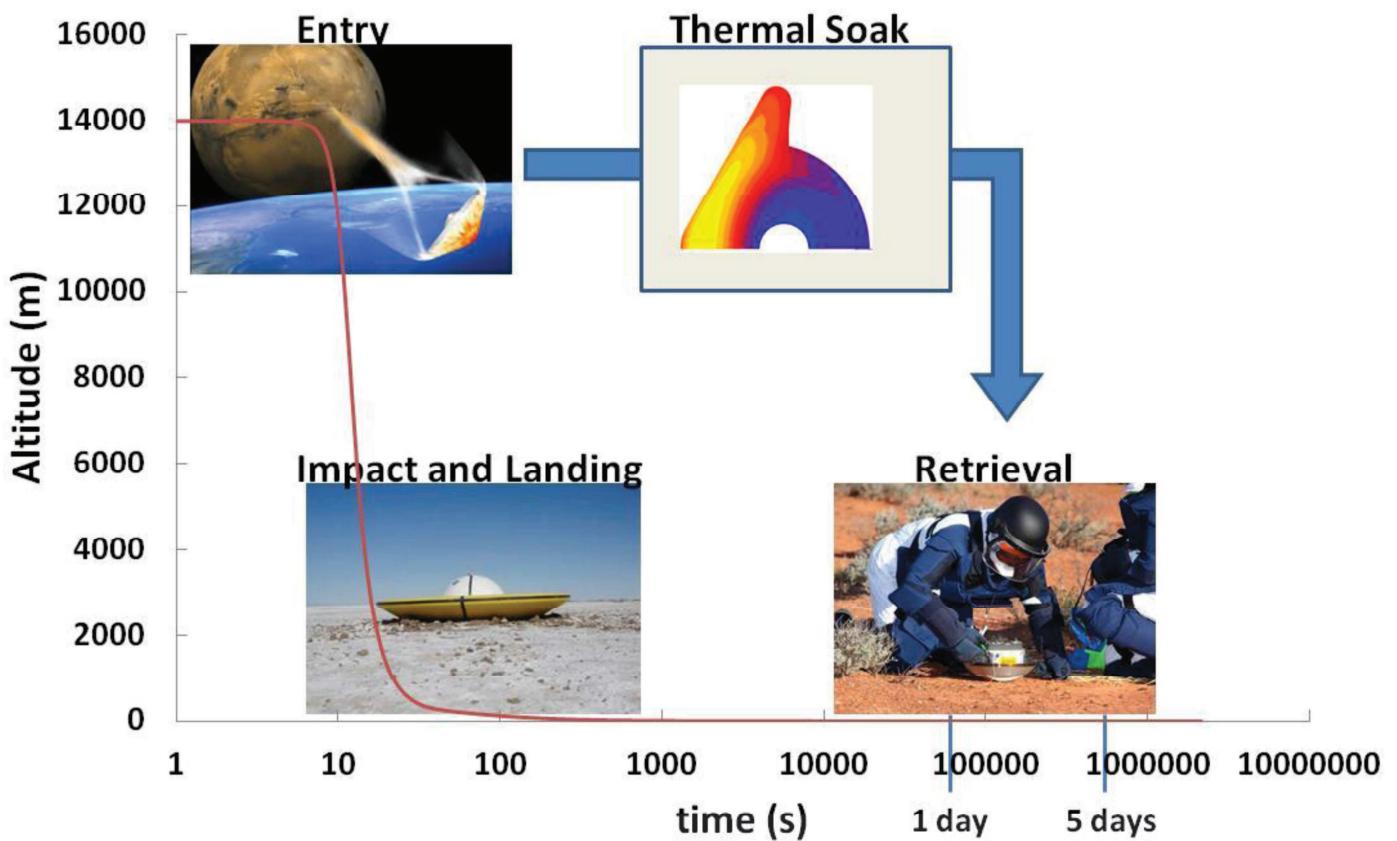


Figure 46. Different Phases of Earth Entry Vehicle and Time Span for Thermal Soak Inside the Vehicle

Although the design foundation is based on MSR, the end result is a thermal soak module that could be used for other mission architectures, as well. The spatially and time varying aerothermal environments on both forebody and aftbody are applied to the present model as boundary conditions resulting in accurate representation of thermal energy input.

The next section describes in detail the components, materials and finite element modeling approach for thermal soak model development.

3.6.1 Finite Element Model Development

To conduct finite element modeling, the CAD geometry of the vehicle design that was developed for the M-SAPE tool was imported into a commercial finite element software package, Marc-Mentat, developed by MSC Corporation. MSC Marc supports fully transient, non-linear, thermal Finite Element Analysis (FEA). It includes an integrated user interface, Mentat, for pre- and post-processing. A two dimensional cross-section of the nominal 1.05m diameter geometry that was developed for simple parametric MMEEV model is shown in Figure 47. The various sub-components of the vehicle and their thickness along the centerline vertical position for nominal geometry are listed in Table 9. This geometry was scaled to vary the diameter from 0.8 meter to 1.4 meters.

The FE model was created based on this simplified MMEEV geometry and assumed to be 2-D axisymmetric for several reasons. It takes the solver significantly less time to analyze an axisymmetric geometry compared to a three dimensional geometry, which could be very time efficient when conducting thermal soak analysis for a wide spectrum of trajectories and sensitivity analyses for various parameters. In addition, it is significantly easier to impose the thermal boundary conditions like heat-flux distribution from 2-D axisymmetric Computation Fluid Dynamics (CFD) models and temperature distribution from thermal response models.

The model was meshed in such a way that each of the main sub-components was represented as a separate element set. These sets include forward and aft-TPS, substructures, impact and body foam, wing and lid insulation, impact shell, and payload. The inclusion of various element sets will allow for flexibility in implementing different sets of materials properties when needed, shape changes after impact etc. The model was meshed using linear quad elements as shown in Figure 48. The average element size was about 1.8 mm which led to total 51,200 elements and 51,700 nodes.

The payload was assumed to be kept inside a hollow aluminum container. At this time, the focus of the thermal soak analysis is to provide the temperature history of the payload container and the impact foam so that it can meet the thermal requirements of sample return missions.

The following materials were considered for the development of the parametric model:

- Carbon phenolic (CP) and Phenolic Impregnated Carbon Ablator (PICA) for forebody TPS. Separate models were developed for both TPS materials.
- PICA for aft TPS

- Advanced carbon-carbon for substructure as well impact shell
- Rohacell for all the foams and insulations
- Aluminum 6061 T6 alloy for payload container

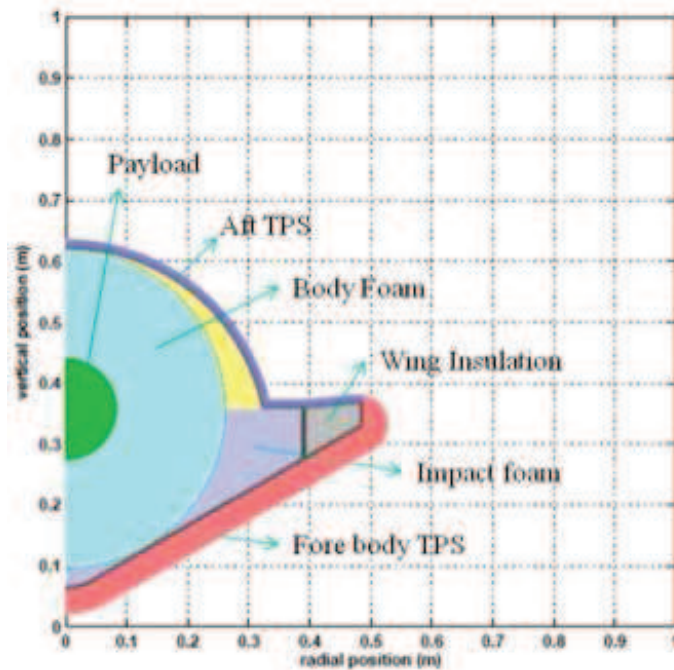


Figure 47. MMEEV Thermal Soak Model Geometry

Table 9. Thickness of the Subcomponents along the Vertical Centerline for MMEEV Vehicle

Component	Thickness (m)
payload	0.1684
forebody TPS	0.0402
aft TPS	0.01
fwd carrier structure	0.0068
aft carrier structure	0.0055
primary structure	0.0081
impact shell	0.002
impact foam	0.1767
body foam	0.0275
lid insulation	0.0583
wing insulation	0.0759

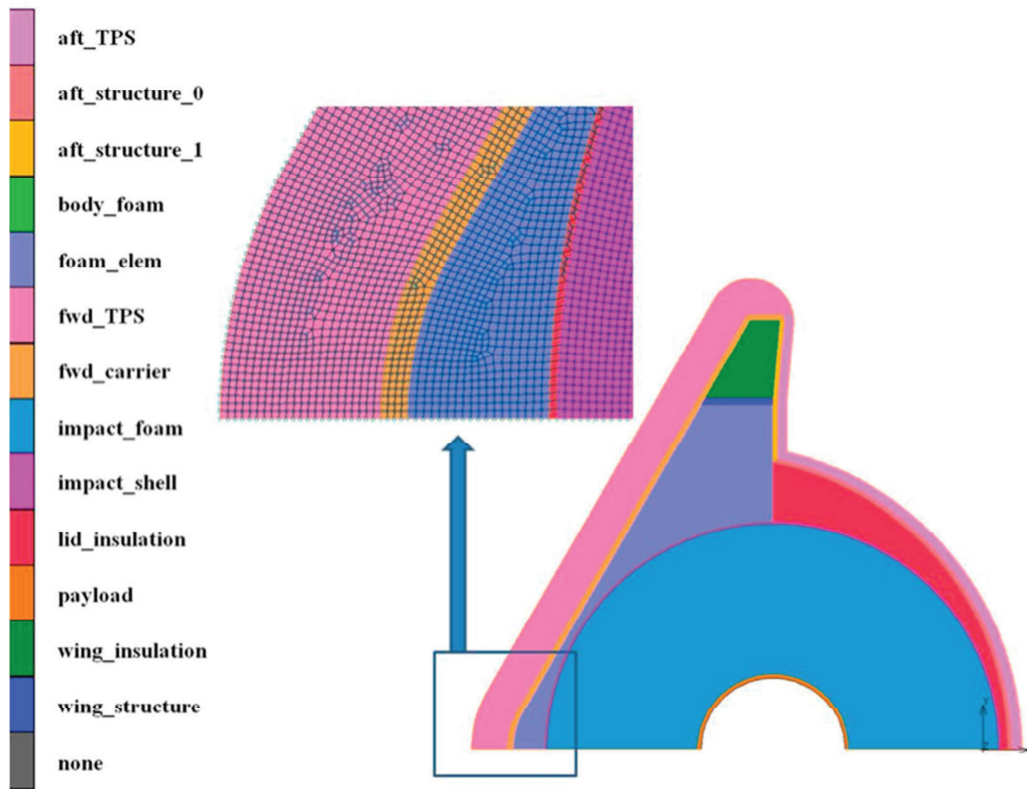


Figure 48. Finite Element Mesh with Component Sets

The materials map of the FE model is shown in Figure 49. Temperature-dependent thermal properties were considered for each of the materials. The TPS and substructure materials were assumed to be transverse isotropic with thickness along the x -axis. The material properties for the first three thermal protection materials on the list were obtained from Configuration Managed (CM) database developed during the time of the Crew Exploration Vehicle (CEV) TPS advanced development program (Feldman et al. 2010 and Britt 2006). The properties for Rohacell foam were obtained from communications with the manufacturer and Langley Research Center and are listed in Tables 10 and 11. Aluminum 6061 values for the payload container were obtained from the MIL handbook.

The heat flux values derived from CFD were input as surface boundary condition for the model. The next section provides a detailed discussion on aerothermal environment for various trajectories. Thermal conduction, surface re-radiation to ambient environment, and internal cavity re-radiation, and ablation was not modeled at this time. In general, absence of ablation should lead to higher peak temperature predictions as more energy will get absorbed by the system. The heating due to applied heat flux during re-entry as well as thermal soak during the cool down period after re-entry were analyzed. An adaptive time step based on the change in temperature was used for the solver to make the computations more efficient. One of the major events after re-entry is the touchdown, when the entry vehicle is subjected to severe impact that

causes significant deformation and compression of impact foams. The foam compression causes an increase in density, which in turn,

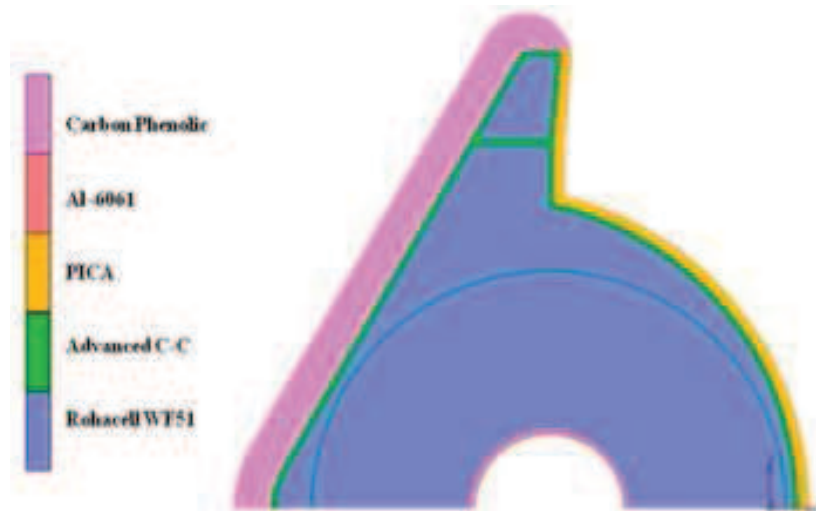


Figure 49. Materials Map for the Baseline Thermal Analysis

Table 10. Specific Heat Capacity of Rohacell-51

Temperature	Specific Heat Capacity (Cp)
(K)	(J/kg-K)
T < 302.56	2399.04
320.56	2399.04
340.33	2687.93
360.33	2394.85
380.33	1896.62
400.33	1565.86
420.33	1423.51
440.33	1394.20
460.33	1193.24
666.67	1193.24

Table 11. Thermal Conductivity of Rohacell-51

Temperature	Thermal Conductivity
(K)	(W/m-K)
95.83	0.0127
134.94	0.0171
154.72	0.0190
174.44	0.0208
228.89	0.0272
288.33	0.0360
367.22	0.0567
479.44	0.0848
666.67	0.0848

changes the thermal properties of the foam. The touchdown and impact event would also cause changes in thermal pathways. For the present set of analyses, the changes to the model caused by impact have been ignored.

3.6.2 Entry Environments and Boundary Conditions

The entry environment for the MMEEV program encompasses a fairly large mission trade space that includes entry velocities ranging from 10-16 km/s, ballistic coefficients of 42-129 kg/m², and entry flight path angles ranging from -5° deg to -25° deg. These translate to a wide spectrum of trajectories, heat loads, and peak heat fluxes. One of the main objectives for thermal soak analyses is to be able to identify the important parameters and to develop correlation coefficients so that, for a given heat load and trajectory, one can estimate the peak payload temperature, the time to arrive at peak temperature, and the temperature histories of the interior components of the vehicle such as the impact foam and payload. For the first set of analyses a nominal trajectory for MSR with a very high heat load at the stagnation point was considered. Subsequently a trajectory space consisting of over 2700 cases was created from which a representative set of trajectories for the thermal soak analyses were selected based on statistical average and standard deviation. These trajectories have flight path angles ranging from -25° to -10° degrees and entry velocities of 10 to 14 km/s. Figure 50 shows the representative trajectory space, where maximum heat flux at the stagnation point of the probe is plotted against the corresponding heat load for each trajectory. The high heat load, nominal MSR trajectory is also included in this plot. The high heat load trajectory was selected because thermal soak analysis began with this trajectory and the geometry was developed for this trajectory.

When the lower heat load trajectory space was generated, the initial, high heat load trajectory was retained for comparison as it provided a bounding high value to compare with other trajectories and could show the influence of heat load on thermal soak and peak payload container temperature.

The representative trajectories selected for FE thermal soak analyses and development of parametric soak models are shown in red. The results from the highest heat load and one of the low heat load trajectories are highlighted in Section 3.5.

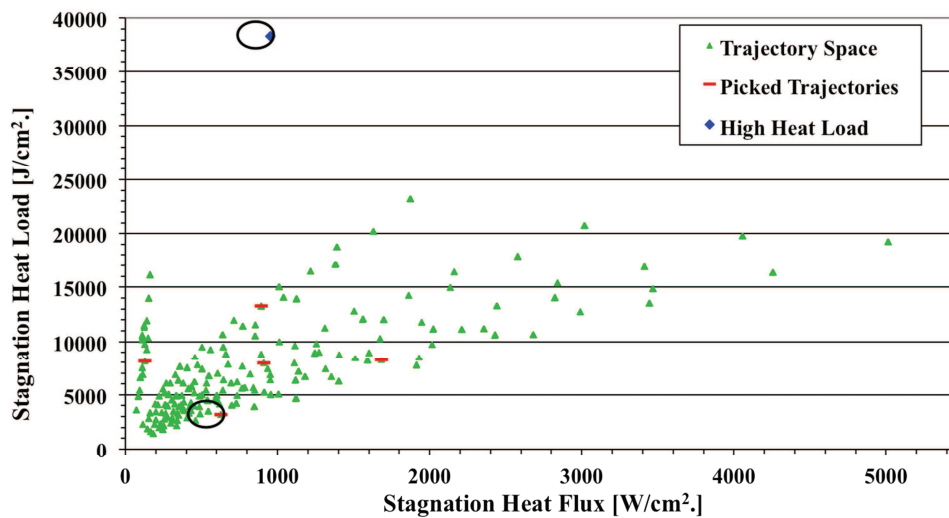


Figure 50. Trajectory Space with Selected Trajectories

The flow field was computed using the CFD code DPLR (Wright et al. 2009) (as described in Section 3.4) to generate spatially varying heat-flux values along entry trajectory. The MMEEV geometry was represented as a two-dimensional axisymmetric body. The surface of the vehicle was made up of 256 body points.

Appendix C, Figure C1, presents CFD outputs showing the surface of the vehicle and every tenth body point plotted along the surface. The body point “zero” corresponds to the nose stagnation point of the vehicle where the highest heating occurs. The incoming flow is from left to right.

The heat flux distribution at peak heating along the vehicle for both the high heat load and low heat load trajectories are plotted in Appendix C, Figure C2. For the high heat load trajectory, peak heating occurred between 60 and 70 seconds. The highest CFD value obtained was close to 1000 W/cm^2 at 66 seconds. For the low heat load trajectory, peak heating of 692 W/cm^2 occurred at 10.5 seconds.

The full time history of the aerothermal environment was obtained by curve fitting the CFD solutions. The interpolation function is a power-law fit using free stream velocity and density as the independent variables. In this manner a continuous time-history was obtained for each body point along the vehicle. In Figure C3, the heat flux distributions of ten discrete CFD solutions

and the interpolated curves are plotted against both body location and time for the low heat load trajectory (red circles). These are the solutions which are interpolated in time. The curve fits make it possible to estimate the integrated heat load at all 256 locations along the vehicle. The integrated heat load for the stagnation point was $38,000 \text{ J/cm}^2$ and 3000 J/cm^2 for the high and low heat load trajectories respectively. The FE software had in-built subroutine to apply the discrete heat flux values on 256 body points on the full outer mold line of the probe.

The spatially and temporally varying heat flux values for the trajectories were used as a surface boundary condition for the FE model. Three dimensional data tables were generated to apply the heat flux values as a boundary condition to the model. At the payload interface the heat was re-radiated due to hollow container. This would give a more conservative estimate of container heating. The next section describes the thermal modeling and results from the analyses from selected high and low heat load trajectories.

3.6.3 Temperature Predictions in Entry Vehicle Design

Transient thermal analyses were performed with two dimensional axisymmetric elements. The initial and ambient temperatures were assumed to be 290° K (17° C). The initial temperature is an important parameter and simulations will be performed in future to investigate the effects of initial temperature. The outer surface was modeled to be re-radiating to a sink temperature of 290° K (17° C) during the entry and cool-down periods. The start time for analysis coincided with atmospheric entry. During re-entry the vehicle experiences a very steep temperature gradient on the forebody due to high heat flux. Figure C4 in Appendix C shows the temperature contours on the vehicle at the end of the heat pulse during the re-entry and right before the touchdown to the ground. While the surface temperatures are very high exceeding, 1000° C during re-entry and exceeding 700° C during touch down on the forebody TPS, the interior of the vehicle (including the body foam and payload container) remains at the room temperature. Thermal analysis on the identical vehicle configuration (with same TPS thickness) was also performed for the low heat load trajectory discussed in previous section. Figure C5 shows the temperature contour plot at the end of the heat pulse and right before touchdown for this trajectory. As expected the in-depth temperature rise in the forebody TPS is significantly smaller compared to the high heat load trajectory, and a large portion of TPS and all of the interior stay at room temperature during the re-entry. The touchdown time (when altitude is close to zero) for this trajectory occurs at 2000 s, and by that time the whole vehicle shows temperature below 250° C .

Thermal soak is slow due to low conductivity of the impact and body foam, and the interiors take several hours to show a temperature rise. Figure C6 shows the temperature contours after several hours for both trajectories. For the high heat load trajectory, the body foam shows a temperature rise of 200° C , and the payload container reaches 55° C after several hours. In contrast, for the low heat load trajectory the body and impact foams stay under 120° C and payload container stays below 25° C .

The peak foam temperature comparisons are shown in Figure C7. For the high heat load trajectory, the peak foam temperature reaches 300° C , whereas for the low heat load trajectory, the foam temperature stays below 100° C through the entire thermal soak period. One point to be noted here is that these analyses do not consider foam compression due to ground impact. These

numbers may increase to a higher value if foam compression is taken into account. FE models that would include foam compression after impact are proposed as a future MMEEV task that will be performed after the parametric studies with the present configuration.

The present simulations were performed for 45 hours of cool-down period as the payload recovery operations could take more than a day. The temperature rise in the payload container for all the trajectories is shown in Figure C8 for PICA and CP TPS materials. PICA with low thermal conductivity acts as a good insulator, and for all the trajectories, the peak payload temperature stays below 30⁰C. For CP TPS, for the low heat load trajectory the payload container temperature stays below 25⁰C. This meets the science requirements of keeping the payload below 25⁰C. In contrast, the payload temperature for high heat load trajectory eventually rises beyond 50⁰C that could cause concerns if the payload recovery is not fast. These analyses lead to conclusion that while a thicker forebody TPS may seem very conservative for re-entry heating, it may be required to protect the interiors and payload from rising to very high temperature during the cool down period. Alternatively, a different architecture such as dual-layer TPS approach may be needed. The data suggests that for the same TPS thickness the choice of TPS material affects the peak container temperature. In addition, for a given TPS material, the heat load magnitude is one of the key contributors for payload temperature rise. Therefore, selecting among different trajectories, it may be useful to keep in mind that a trajectory with lower heat load value can be more desirable from thermal soak perspective even if it meant a higher stagnation point heat flux value. The next section describes some of the analyses that were performed to generate a parametric thermal soak model for M-SAPE.

3.6.4 Parametric Thermal Soak Model Development for M-SAPE

One of the goals for FE thermal analysis is to identify key factors that affect the peak payload and foam temperatures and to develop simple correlations based on these factors that could lead to a parametric thermal soak model for M-SAPE. To accomplish this objective, several parametric studies have been performed for five selected trajectories by varying heat flux magnitude, vehicle diameter TPS materials etc. This section describes those analyses.

The heat flux was varied by scaling the magnitude throughout the surface for the entire heating cycle for the high heat load and the low heat load trajectories. The magnitudes were scaled between 0.25 (25%) to 1.5 (150%) times the nominal heat flux values for the trajectory. The results from parametric studies for both a high and a low heat load trajectories are shown in Figure C9 and C10 respectively. In both the cases, the peak payload container temperature rose as the heat flux magnitude increased. For the heat flux range considered for parametric models, a linear relationship between the scaled heat flux magnitude and peak payload container temperature can be established for any given trajectory as shown in Appendix C, Figures C9b and C10b. For the nominal vehicle diameter of 1.05 meter, several simulations were run using PICA and CP TPS for various trajectories.

The next step was to investigate the influence of vehicle diameter. To perform these parametric studies, the whole vehicle (FE model) was scaled to a smaller or a larger diameter, while the input heat flux magnitude was kept constant to see for a given heat flux magnitude and distribution how changes in size affected the peak heating. As expected, for a smaller diameter vehicle the peak payload temperature was significantly higher compared to a larger diameter vehicle, information that could be useful for determining the vehicle geometry for a given

Temperature	Specific Heat Capacity (Cp)
(K)	(J/kg-K)
0.00	2399.04
320.56	2399.04
340.33	2687.93
360.33	2394.85
380.33	1896.62
400.33	1565.86
420.33	1423.51
440.33	1394.20
460.33	1193.24
666.67	1193.24

Temperature	Thermal Conductivity
(K)	(W/m-K)
95.83	0.0127
134.94	0.0171
154.72	0.0190
174.44	0.0208
228.89	0.0272
288.33	0.0360
367.22	0.0567
479.44	0.0848
666.67	0.0848

Table 12. For PICA TPS

a	0.0924541
b	-3.07762
c	44.0988662
d	7.83638822
e	-0.052928722
f	0.153994158
g	-0.47774583

Table 13. For CP TPS

a	0.012455
b	0.129143
c	14.15728
d	3.166053
e	-0.05195
f	0.302888
g	-0.95476

The goodness of fit for established correlations for peak payload container temperature for both PICA and Carbon Phenolic TPS are shown in Figure C12. The results were quite promising for this simplified architecture.

3.6.5 Summary and Future work

A finite element thermal soak model was developed for an MSR-based geometry. Preliminary thermal soak analyses were performed for different trajectories to study the temperature rise inside the vehicle. CFD analysis was conducted to generate an aerothermal environment for the entire vehicle including fore- and aftbodies for several high and low heat load trajectories. The temperature histories on the foam and payload were obtained by conducting FE thermal analysis for these trajectories and compared with each other. The data show that the magnitude of total heat load to the vehicle significantly influences the peak payload temperature, and thus it will be useful to include thermal soak requirement when sizing the TPS thickness for the vehicle to ensure low payload temperature after the touchdown.

Parametric studies were performed by varying heat flux magnitude, vehicle diameter, and TPS materials. The results suggest that correlations can be established to develop a surrogate thermal soak model. There are some limitations to present parametric soak model that will be addressed in the future work:

1. The TPS thickness in this model was not varied for various trajectories and kept out of the parametric model. Analyses are in progress for geometries with different TPS thicknesses to investigate the influence of TPS thickness in the prediction of peak payload temperature. In future, the model will include the TPS thickness variable.
2. Ablation, which may have led to more conservative estimations of peak payload temperature as more energy would be soaked in the system, was not considered in the present analyses. In the future, for high-fidelity thermal soak models, ablation, when necessary and prominent, will be accounted for in the model by coupling the temperature maps from the thermal response model, FIAT (Chen and Milos 1999) to the finite element model. This approach will be investigated for final point designs for missions like MSR and other sample return missions.
3. Post-impact crushed vehicle shape was not considered in the model. The change of foam density as well as deformation will affect the thermal soak. In the future studies, the analysis will be performed in two steps: 1) re-entry and time elapsed before impact and 2) cooling after impact. The geometric changes due to impact will be incorporated through significant mesh deformation, while the temperatures will be mapped from one model to the other model, keeping the same node and element numbers. The temperature distribution from the last time step of first analysis will be imposed as initial condition for the second analysis, and thermal soak will carry on.

4.0 SAMPLE RESULTS

The results for two sample test cases are presented in this section. Previous EEV baseline models and results (Dillman and Corliss 2008) were used to verify the integrated analysis tool. Figure 13 shows the nominal MSR model, and Table 14 shows the list of input parameters for the baseline model. The payload mass includes mass of sample return material, as well as the orbiting canister mass. The results shown in Table 15 compare well with results of Dillman and Corliss 2008.

Figure 51 shows the results for various entry velocities and flight path angles for three diameters. The EEV mass ranges from 34-62 kg. The entry load is a strong function of flight path angles and can vary from 75 to 230 Earth g's. The maximum heat rate is primarily a function of the entry velocity, and it varies between 1000-3000 W/cm².

The second case is the Galahad model, which is an asteroid sample return mission proposal response to the NASA New Frontiers solicitation. The mission goal is to return a sample from the binary C-asteroid 1996 FG3 and to make extensive orbital measurements. The plan is to return 60 g of samples to Earth. Figure 52 shows the Galahad EEV concept. Table 16 shows sample results for the Galahad EEV. The results are very similar: the total mass is within 4% of Maddock et al. 2010.

Table 14. Input Parameters for Case 1

Diameter, m	1.3
Payload mass, kg	12.5
Payload density, kg/m ³	4000
Nose radius/base radius	.25
Shoulder radius/base radius	.07
Mass margin, %	30

Table 15. M-SAPE Results Compared with Dillman and Corliss 2008

Parameters	circa 2008	M-SAPE
Diameter, m	0.9	0.9
Mass, kg	44	45.7
Entry velocity, km/s	11.56	11.5
Peak heating, w/cm ²	1500*	1302
Peak deceleration g's	130	134
Terminal velocity, m/s	41	39.8

*Peak entry heating limit

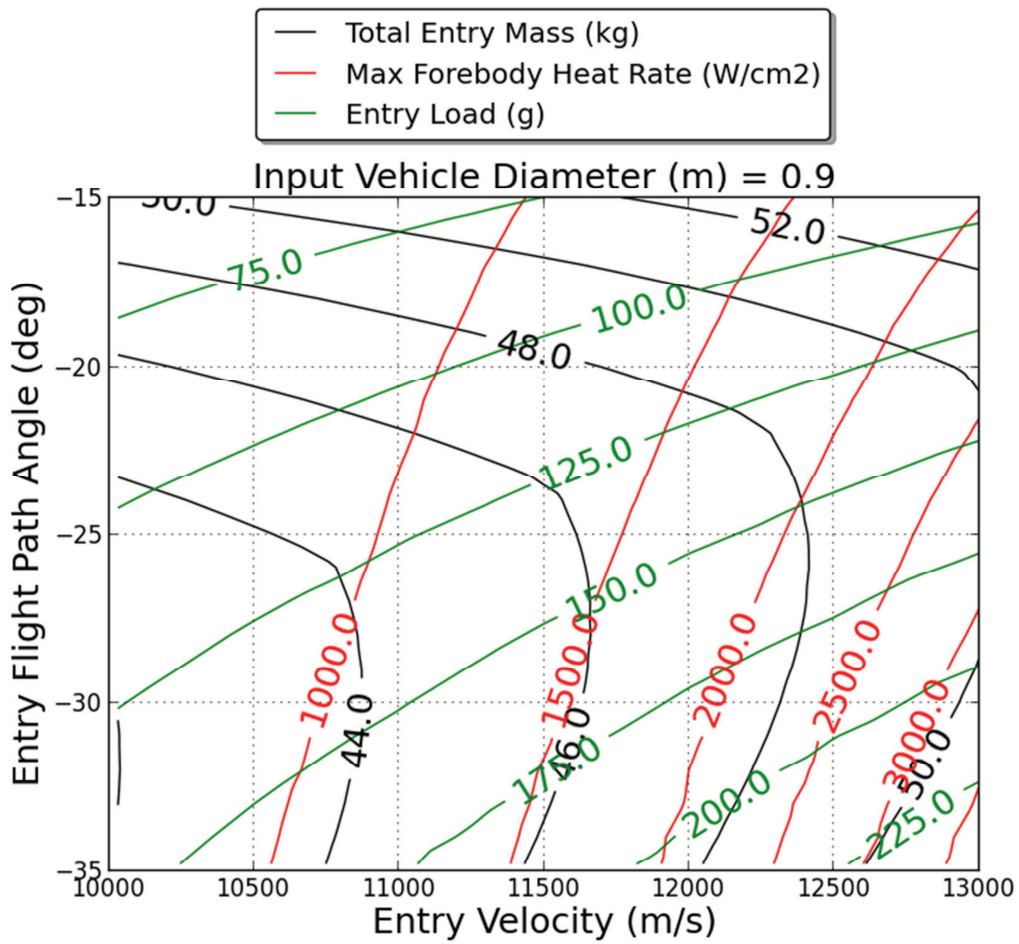


Figure 51. Sample M-SAPE Trade Space for MSR Model



Figure 52. Galahad EEV Concept Maddock et al. 2010

Table 16. M-SAPE Results Compared with Maddock et al. 2010

Parameters	circa 2010	M-SAPE
Total mass, kg	32.1	31.9
Maximum entry load, g's	33.9	34.7
Total peak heat rate, W/cm ²	400	441
Total heat load, kJ/cm ²	11.2	12.0
PICA thickness, cm	2.3	2.21
Time of flight, sec	595	673
Impact velocity, m/s	31	26.7
Impact load, g's	470	456
Impact stroke, cm	3.4	2.4

5.0 CONCLUSION

M-SAPE is an integrated system analysis tool for planetary entry. The current version of M-SAPE can perform system analysis of Earth entry vehicle for sample return missions. The system includes geometry, mass sizing, impact analysis, structural analysis, flight mechanics, TPS, and a web portal for user access.

M-SAPE enables rapid and consistent analyses for single runs, what if scenarios (e.g., change in payload mass), and technology evaluation (e.g., TPS concepts) in minutes verses weeks for traditional analyses. It also can provide system sensitivity analysis and system trade space analysis in hours verses months for traditional analyses. The system is design with uncertainty propagation and Monte Carlo analysis in mind. However, these capabilities have not been fully implemented yet.

The system was used to generate a large database of 80,000 unique designs. Users can either run a single design or explore the existing designs through the web portal, which is located within Langley's firewall.

M-SAPE is still in development. A prototype system was completed in fiscal year 2012 and version 1 was completed in fiscal year 2013. The effort in fiscal year 2014 will be focused on adding Venus, Saturn, and Uranus. In addition, the plan is to extend M-SAPE to include advanced TPS concepts and various vehicle shapes.

6.0 FUTURE DEVELOPMENT AND OPPORTUNITIES FOR COLLABORATION

The Multi-Mission System Analysis for Planetary Entry (M-SAPE) tool has been developed to facilitate the design and analysis of a family of Earth Entry Vehicles (EEVs). M-SAPE is a system analysis tool developed for use by EEV designers to provide enhanced information early in the design process to take advantage of design freedom existing at the initial stages of a vehicle design process. As a result, it is believed that use of M-SAPE will improve the probability of mission success through improved decision making and more effective use of resources early in the design process. M-SAPE provides the user the capability to perform rapid low-fidelity analysis, trades, and design optimization. M-SAPE also provides the potential for technology developers to define requirements for new technologies as well as determine their overall system benefit facilitating technology infusion.

The NASA In-Space Propulsion Technology (ISPT) Program has funded the development of the M-SAPE tool and the Multi-Mission Earth Entry Vehicle (MMEEV) design trade space for the past several years with the intent to release for use. NASA's software release policy will be employed to define authorized users. While M-SAPE is being provided to users at no cost it is recommended that users establish a collaborative arrangement with NASA for effective use the tool. Collaborative arrangements could include focused design and trade-space analysis, technology requirements and benefits development, updates or revisions to existing models, or the development of completely new models and capabilities. Currently M-SAPE is designed to address EEV design. However plans include evolving M-SAPE to include designs of probes to other planets as well as inclusion of new and emerging highly-promising technologies in support of technology development and infusion. In this context M-SAPE is being viewed more as a collaborative environment for EEVs and future planetary probe designs as well as supporting technology development and infusion aspects. Potential costs for collaboration would include only the costs for specific applications with the cost of prior development provided by NASA's investment in M-SAPE. Potential cost-sharing collaborations would also be possible with appropriate support from NASA programs if the application had benefits to both the users and NASA.

For collaborative use, please contact:

- 1) Jamshid Samareh at LaRC (757) 864-5776, jamshid.a.samareh@nasa.gov
- 2) Lou Glaab at LaRC (757)864-1159, louis.j.glaab@nasa.gov
- 3) Parul Agrawal at ARC (650)604-3764, parul.agrawal-1@nasa.gov

7.0 REFERENCES

- Agrawal, P., Prabhu, D.K., and Chen Y-K, *Thermal Analysis of Small Re-entry Probes*, AIAA paper 2012-0219, Jan. 2012.
- Agrawal, P., Sepka, S. A., Aliaga, J.F., Venkatapathy, E., and Samareh, J.A. 2012, *Thermal Soak Analysis of Earth Entry Vehicles, proceedings*, 43rd AIAA Thermophysics Conference, New Orleans, Louisiana, June 2012, AIAA 2012-3010.
- Aliaga-Caro, A. Zarchi, K., and Sepka, S. A., *Entry Vehicle Technology: Aerothermal Analysis of Trajectory Environments II*, 10th International Planetary Probe Workshop, 2013.
- Amundsen, R.M., Dec, J.A., Mitcheltree, R.A., Lindell, M.C., and Dillman R.A., *Preliminary Analysis of a Mars Sample Return Earth Entry Vehicle*, AIAA paper 2000-2584, June 2000.
- Bauer, G.L., Cornick, D.E., and Stevenson, R., *Capabilities and Applications of the Program to Optimize Simulated Trajectories (POST)*, NASA CR-2770, February 1977.
- Britt S., *Mechanical and Thermal Testing of ENKA Rayon Based MX4926 Carbon Cloth Phenolic*, Southern Research Institute Report. SRI-ENG-06-37-11610.01, August 2006.
- Cheatwood, F. McNeil, *User's Manual for the Langley Aerothermodynamic Upwind Relaxation Algorithm (LAURA)*, NASA TM-4674, 1996.
- Chen, y.-K., and Milos, F.S., *Fully Implicit Ablation and Thermal Analysis program (FIAT)*, Journal of Spacecraft and Rockets, Vol. 36, No. 3, pp 475-483, May-June 1999.
- Clements, H.R. and Ward, G.T., *Fabrication of Ablative Liners for Large Solid Booster Nozzles*, Journal of Spacecraft and Rockets, Vol. 3, No. 4, April, 1966.
- Curry, D. M., "An Analysis of a Charring Ablation Thermal Protection System, NASA TN D-3150, November 1, 1965.
- Dillman, R., Corliss, J., *Overview of the Mars Sample Return Earth Entry Vehicle*, Sixth International Planetary Probe Workshop, Atlanta, Georgia, USA, June 2008.
- Edquist, Karl T., Dyakonov, Artem A., Wright, Michael J., and Tang, Chun Y., *Aerothermodynamic Design of the Mars Science Laboratory Backshell and Parachute Cone*, AIAA Paper 2009-4078, presented at 41st AIAA Thermophysics Conference, San Antonio, Texas, USA, June 22-25, 2009.
- Fasanella, E. L., Jones, Y., Knight, N. F., and Kellas, S., "Low Velocity Earth-Penetration Test and Analysis," AIAA-2001-1388.
- Feldman J. et al., *Material Properties of PICA*, NASA TM-2010-216399, June 2010.
- Hollis, B.R., *Blunt-Body Entry Vehicle Aerothermodynamics: Transition and Turbulent Heating*, Journal of Spacecraft and Rockets, Vol.49, No. 3, May-June 2012.
- Hui, T., Johnson, C., Rasky, D., Hui, F., Hsu, M., Chen, Y-K., *Phenolic Impregnated Carbon Ablators (PICA) For Discovery Class Mission*, NASA Tech Briefs, AIAA paper 1996-1911, presented at 31st AIAA Thermophysics Conference, New Orleans, LA, June, 1996.
- Justus, C.G. and Johnson, D.L., *The NASA/MSFC Global Reference Atmospheric Model: 1999 Version (GRAM-99)*, NASA TM-1999-209630.
- Justus, C.G. and Leslie, F.W., *Earth Global Reference Atmospheric Model (GRAM99): Short Course*, Denver, CO., August 7, 2007.
- Leslie, F.W. and Justus, C.G., *The NASA Marshall Space Flight Center Earth Global Reference Atmospheric Model*, 2010 Version. June, 2011, NASA TM-2011-216467.
- MacCormack, R.W. and Candler, G.V., *The solution of the Navier-Stokes Equations Using Gauss-Seidel Line Relaxation*, Computers and Fluids, Vol.17, pp. 135-150, Nov. 1, 1989.
- Maddock, R. W., et al., *Multi Mission Earth Entry Vehicle Design Trade Space and Concept Development Status*, proceedings, 7th International Planetary Probe Workshop, Barcelona, Spain, June 2010.
- Maddock, R. W., et al., *Sample Return Challenges Multi-Mission Earth Entry Vehicle Design Trade Space and Concept Development Strategy*, proceedings, 6th International Planetary Probe Workshop, Atlanta, Georgia, USA, June 2008.
- Maddock, R.W., *Multi-Mission Earth Entry Vehicle Design Trade Space and Concept Status (Version 2.0)*, 8th International Planetary Probe Workshop, Portsmouth, VA, USA, 2011.
- Marko, Wayne J., *Static Aerodynamic Characteristics of the Three Blunted Sixty-Degree Half-Angle Cones at Mach Numbers from 0.6 to 1.3*, NASA JPL-TR-32-1298. July 1968.
- Mattingly, R., and May, L., *Mars Sample Returns as a Campaign*, proceedings, 2011 IEEE Aerospace Conference, Big Sky, Montana, USA, 2011.

- Mercer, R.J., *Physical Constants for Satellite Calculations*, Aerospace Corporation Report, TOR-469(5110-02)-2, El Segundo, CA, January 1965.
- Milos, F.S., and Chen, Y.-K., *Two-Dimensional Ablation, Thermal Response, and Sizing Program for Pyrolyzing Ablators*, AIAA paper 2008-1223, 46th AIAA Aerospace Sciences Meeting and Exhibit, January 7 - 10, 2008, Reno, Nevada, USA.
- Mitcheltree, R. A., Fremaux, C. M., and Yates, L. A., *Subsonic Static and Dynamic Aerodynamics of Blunt Entry Vehicles*, AIAA 99-1020.
- Mitcheltree, R.A., Kellas, S., Dorsey, J.T., Desai, P.N., and Martin, C.J., *A Passive earth-Entry Capsule for Mars Sample Return*, AIAA paper 1998-2851.
- Mitcheltree, R.A., Wilmoth, R.G., Cheatwood, F.M., Brauckmann, G.J., Greene, F.A., *Aerodynamics of Stardust Sample Return Capsule*, AIAA Journal of Spacecraft and Rockets, Vol. 36, No. 3, May - June 1999.
- Moyer, C. B., and Rindal, R. A., *An Analysis of the Coupled Chemically Reacting Boundary Layer and Charring Ablator Part II. Finite Difference Solution for the In-Depth Response of Charring Materials Considering Surface Chemical and Energy Balances*, NASA CR-1061, 1968.
- Perino, S.V., Bayandor, J., and Siddens, A., *A Comprehensive Structural Dynamic Analysis Approach for Multi Mission Earth Entry Vehicle (MMEEV) Development*, June 2013, NASA/CR-2013-218003.
- Perino, S.V., Bayandor, J., Samareh, J.A., and Armand, S.C., *Numerical Impact Analysis of a Novel Spherical Impact Absorber for Mars Sample Return*, in preparation for publication in International Journal of Impact engineering (2013).
- Samareh J.A., Maddock R. W. and Winski R.G., *An Integrated Tool for System Analysis of Sample Return Vehicle*, proceedings, 2012 IEEE Aerospace Conference, Big Sky, Montana, March 3-10, 2012.
- Samareh, A., *A Multidisciplinary Tool for Systems Analysis of Planetary Entry, Descent, and Landing (SAPE)*, NASA-TM--2009-215950.
- Squire, T., Milos, F., Agrawal, P., *Analytical Predictions of Thermal Stress in the Stardust PICA Heatshield Under Reentry Flight Conditions*, National Space and Missile Materials Symposium, 28 Jun. - 1 Jul. 2009, Scottsdale, AZ, USA.
- Steinberg, S., *Experimental Pitch Damping Derivative for Candidate Viking Entry Configurations at Mach Numbers from 0.6 thru 3.0*, June 1970, Martin Marietta Corporation.
- Striepe, S. A., Powell, R. W., Desai, P. N., Queen, E. M., Brauer, G. L., Cornick, D. E., Olson, D. W., Peterson, F. M., Stevenson, R., Engel, M. C., Marsh, S.M., and Gromko, A.M., *Program To Optimize Simulated Trajectories (POST II): Utilization Manual*, Vol. 2, 2004.
- Sutton, K., Graves, R.A., *A General Stagnation-Point Convective Heating Equation for Arbitrary Gas Mixtures*, NASA TR R-376, November 1972.
- Tauber, M., Sutton, K., *Stagnation-Point Radiative Heating Relations for Earth and Mars Entries*, AIAA Journal of Spacecraft, Vol. 28, No. 1, pp. 40-42, Jan-Feb 1991.
- Tran, H., Johnson, C., Rasky, D., and Hui, F., *Silicone Impregnated Reusable Ceramic Ablators for Mars Follow-on Missions*, AIAA Paper 96-1819, June 1996.
- U.S. Standard Atmosphere, 1976, National Oceanic and Atmospheric Administration, National Aeronautics and Space Administration, United States Air Force, NOAA-S/T 76-1562, Oct. 1976, Washington, D.C.
- Walker, B., Weaver, R.W., *Static Aerodynamics Characteristics of Blunted Cones in the Mach-Number Range from 2.2 to 9.5*, December, 1967, NASA TR 32-1213.
- Wright, M.W., White, T., and Mangini, N., *Data Parallel Line Relaxation (DPLR) Code User Manual*, Acadia Version 4.01.1, NASA TM-2009-215388, October 2009
- Yee, H.C., *A Class of High-Resolution Explicit and Implicit Shock Capturing Methods*, NASA TM-101088, Feb. 1989.

APPENDIX A

AERODYNAMICS SUPPLEMENTAL DATA

Aerodynamic Data for Rarefied and Hypersonic Flow Conditions

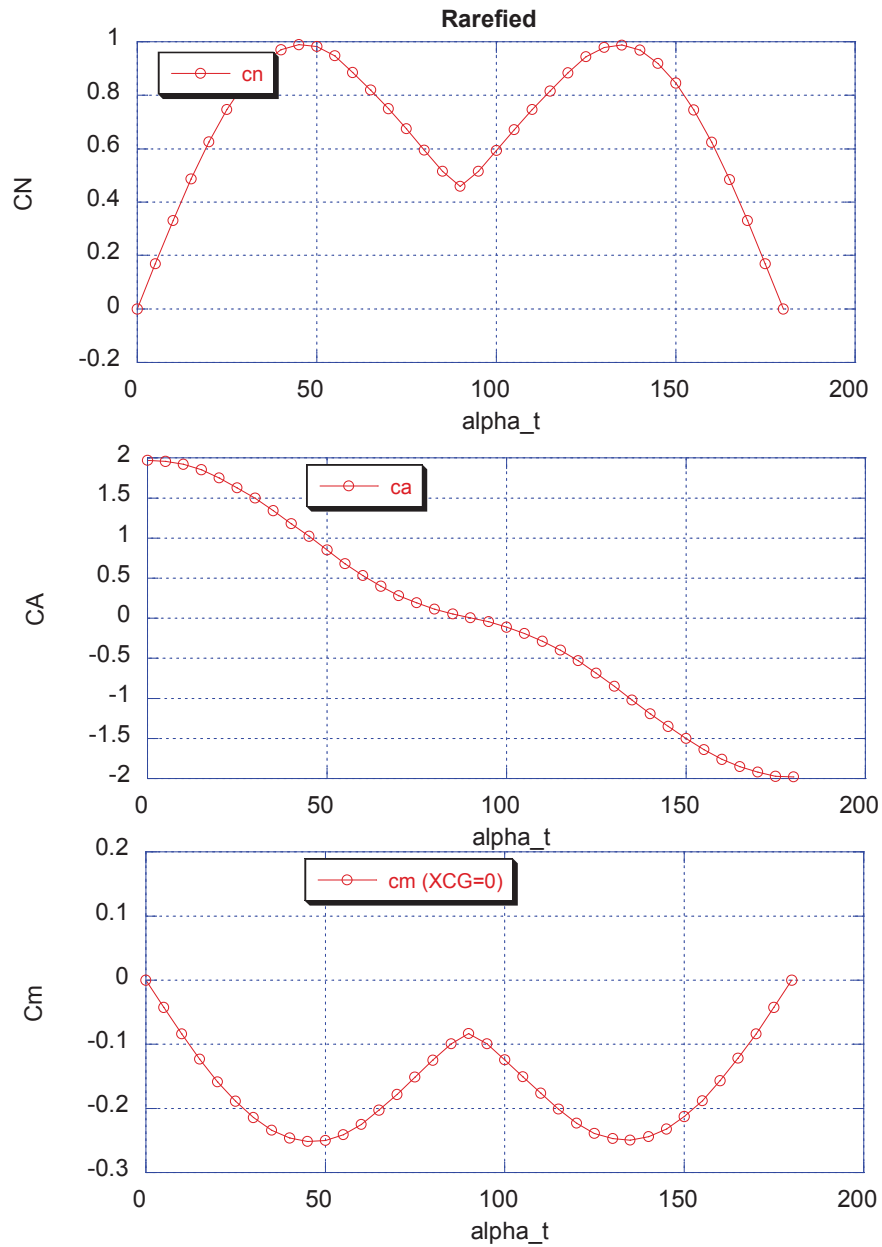


Figure A1 - MMEEV Aero Database for Rarefied Flow Conditions. Moment Reference Point is the Vehicle Virtual Nose Apex.

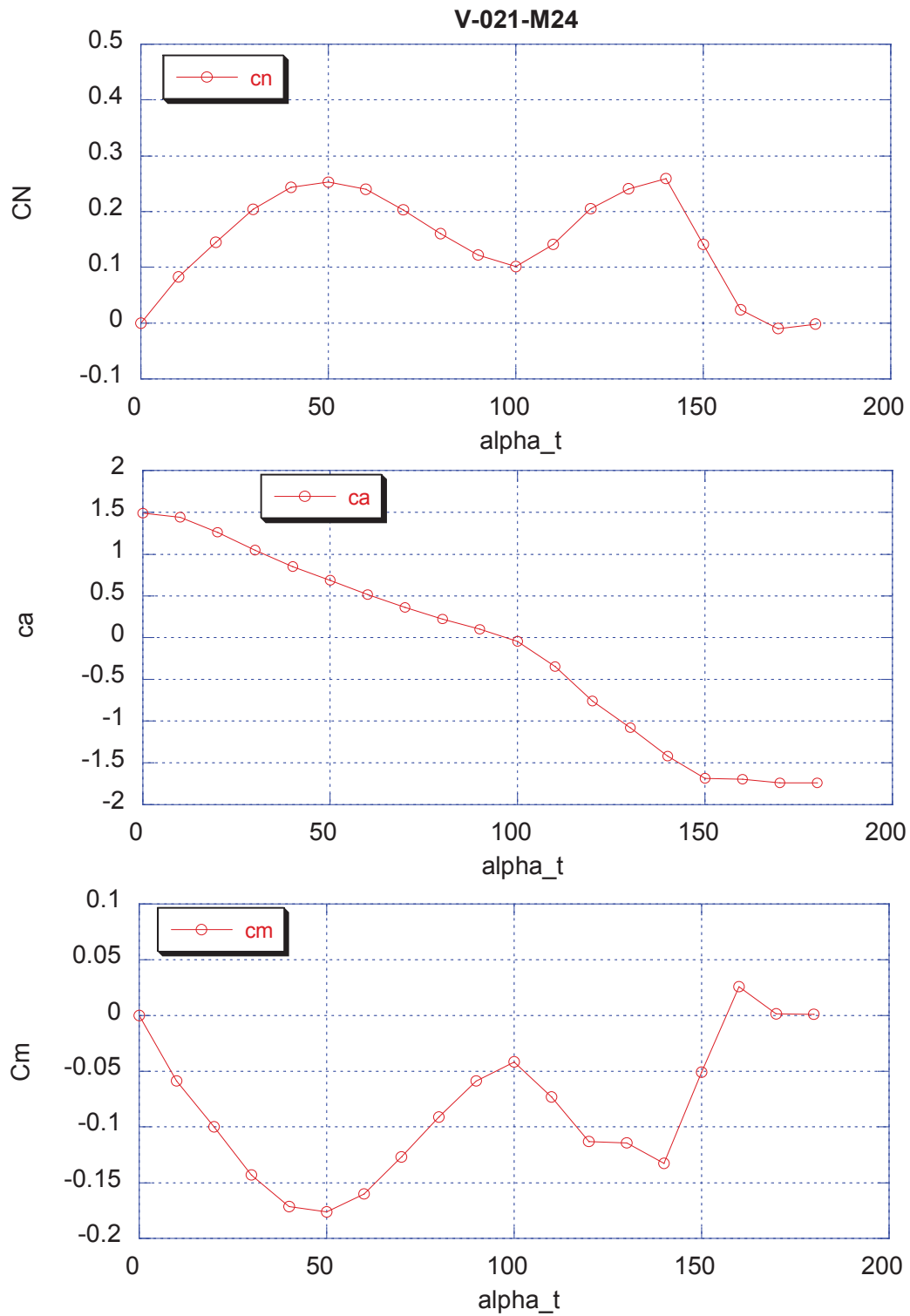


Figure A2 - MMEEV Aero Database for M=24. Moment Reference Point is the Vehicle Virtual Nose Apex.

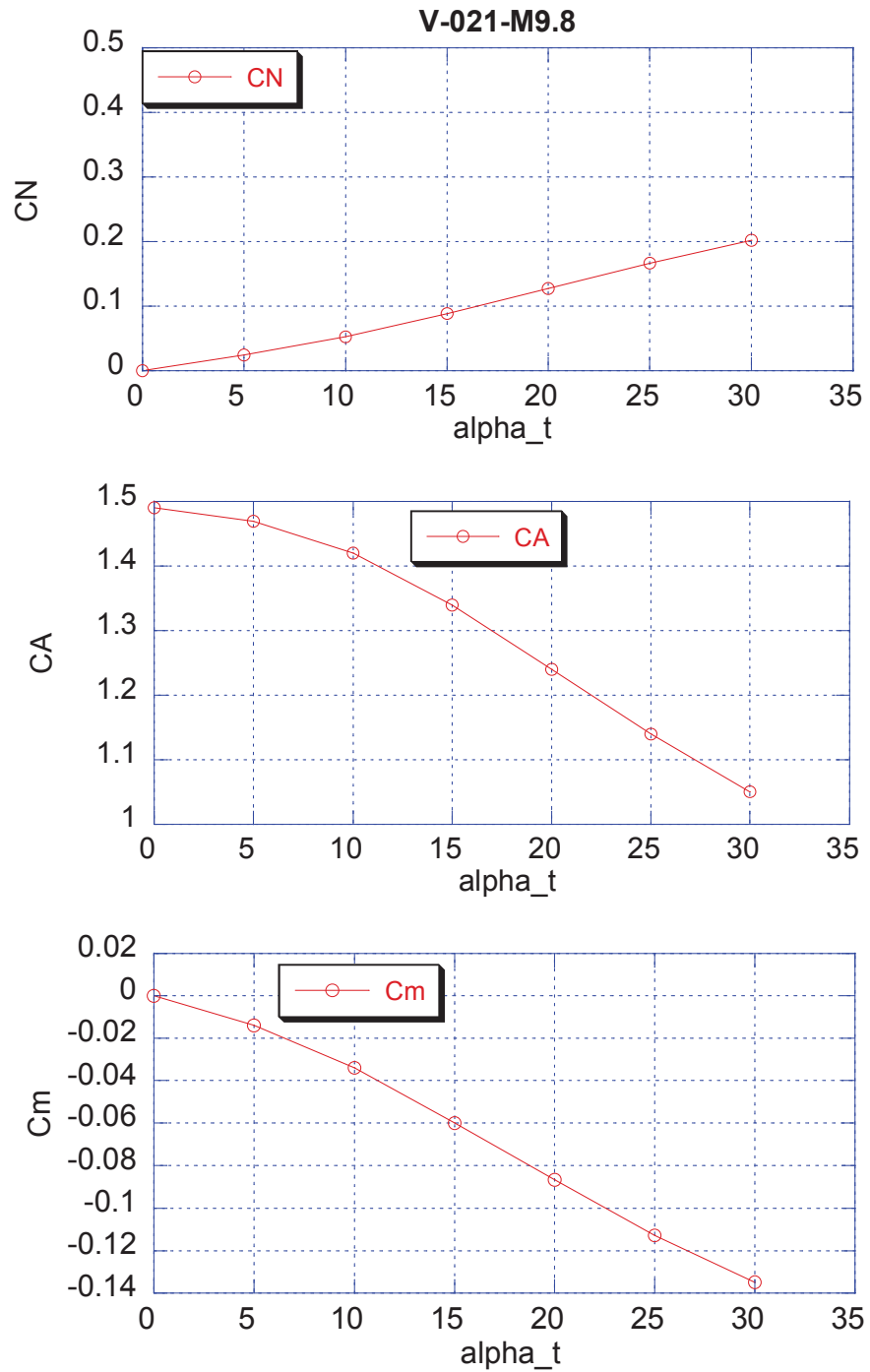


Figure A3 - MMEEV Aero Database for M=9.8. Moment Reference Point is the Vehicle Virtual Nose Apex.

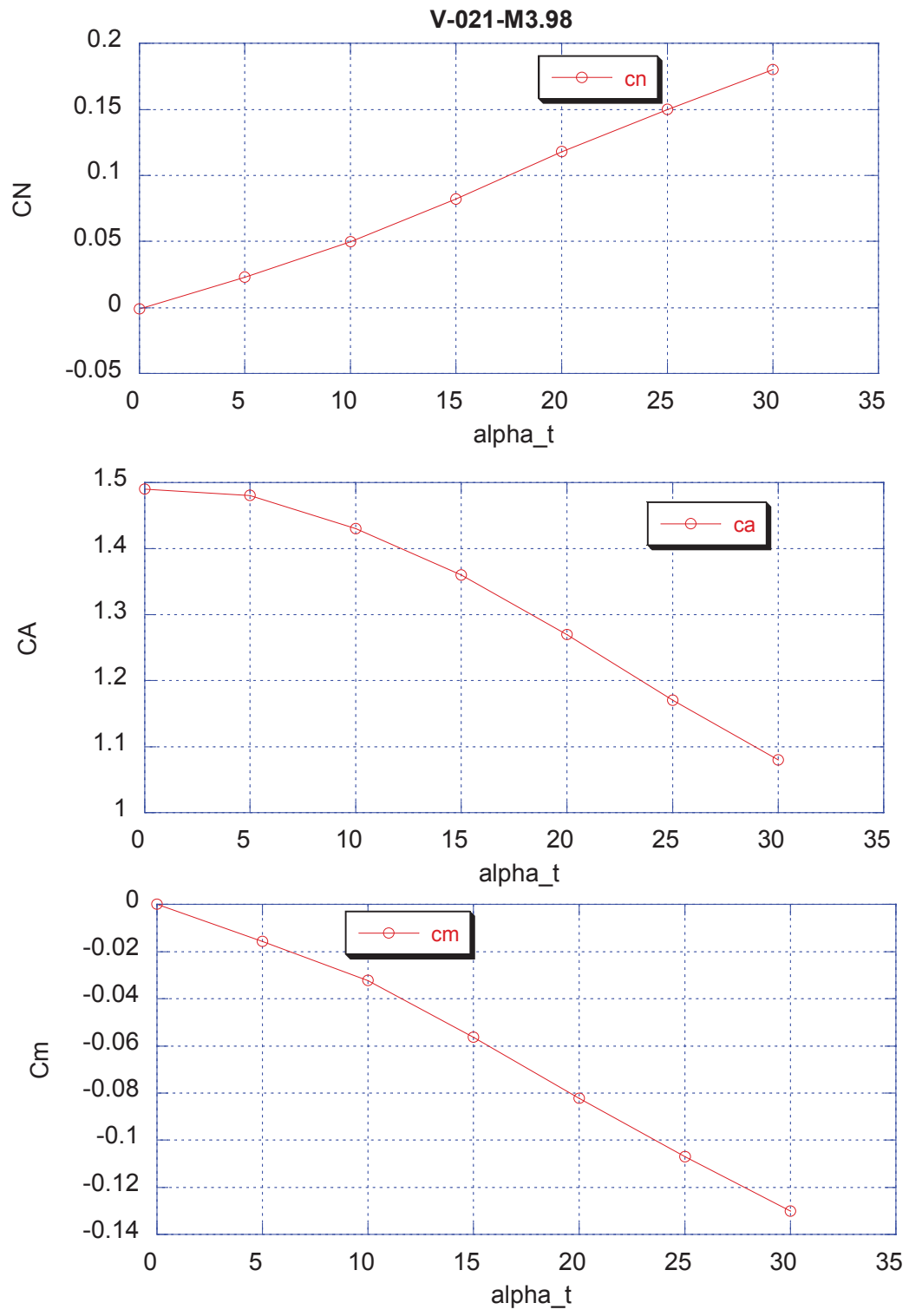


Figure A4 - MMEEV Aero Database for M=3.98. Moment Reference Point is the Vehicle Virtual Nose Apex.

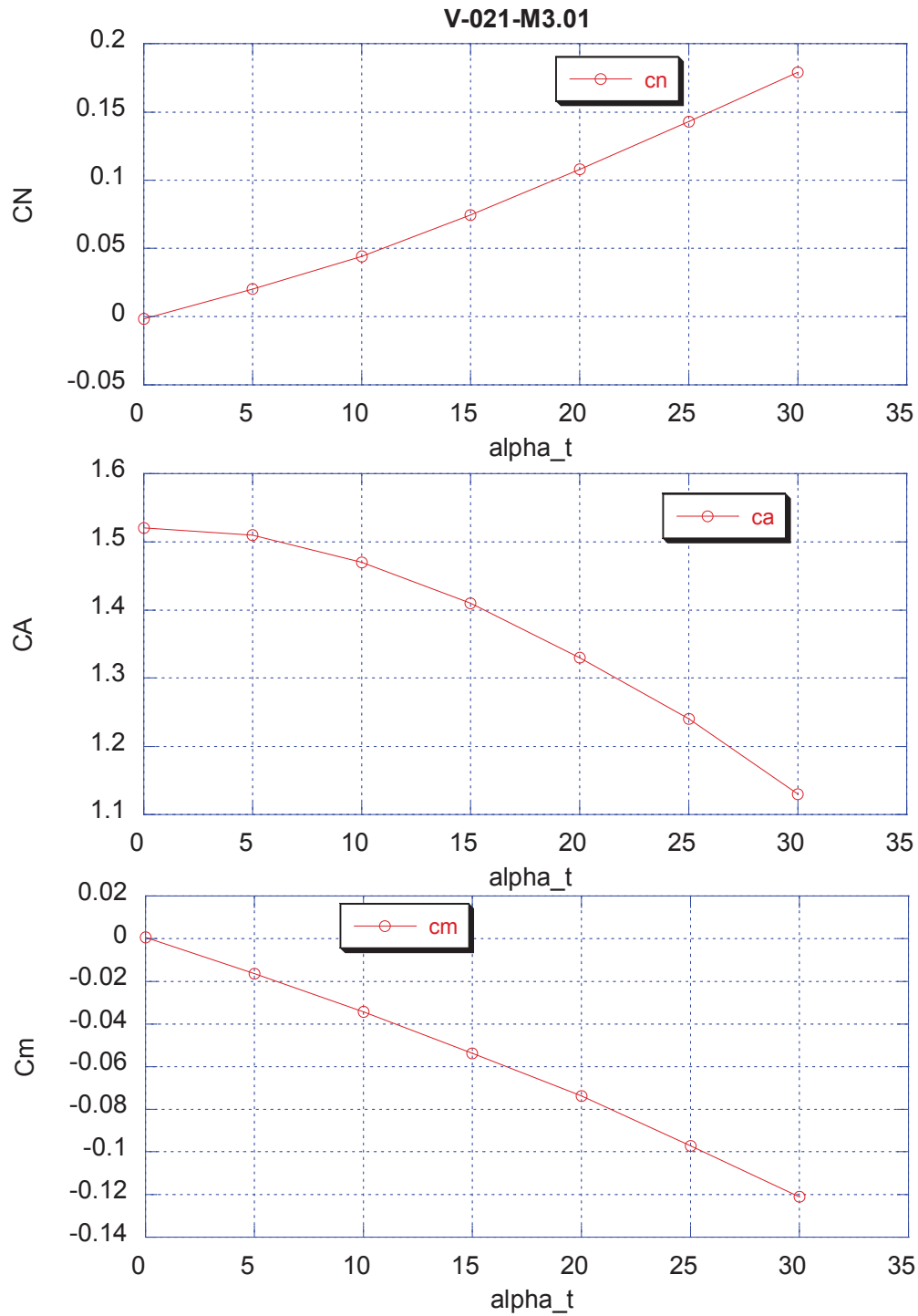


Figure A5 - MMEEV Aero Database for M=1.3. Moment Reference Point is the Vehicle Virtual Nose Apex.

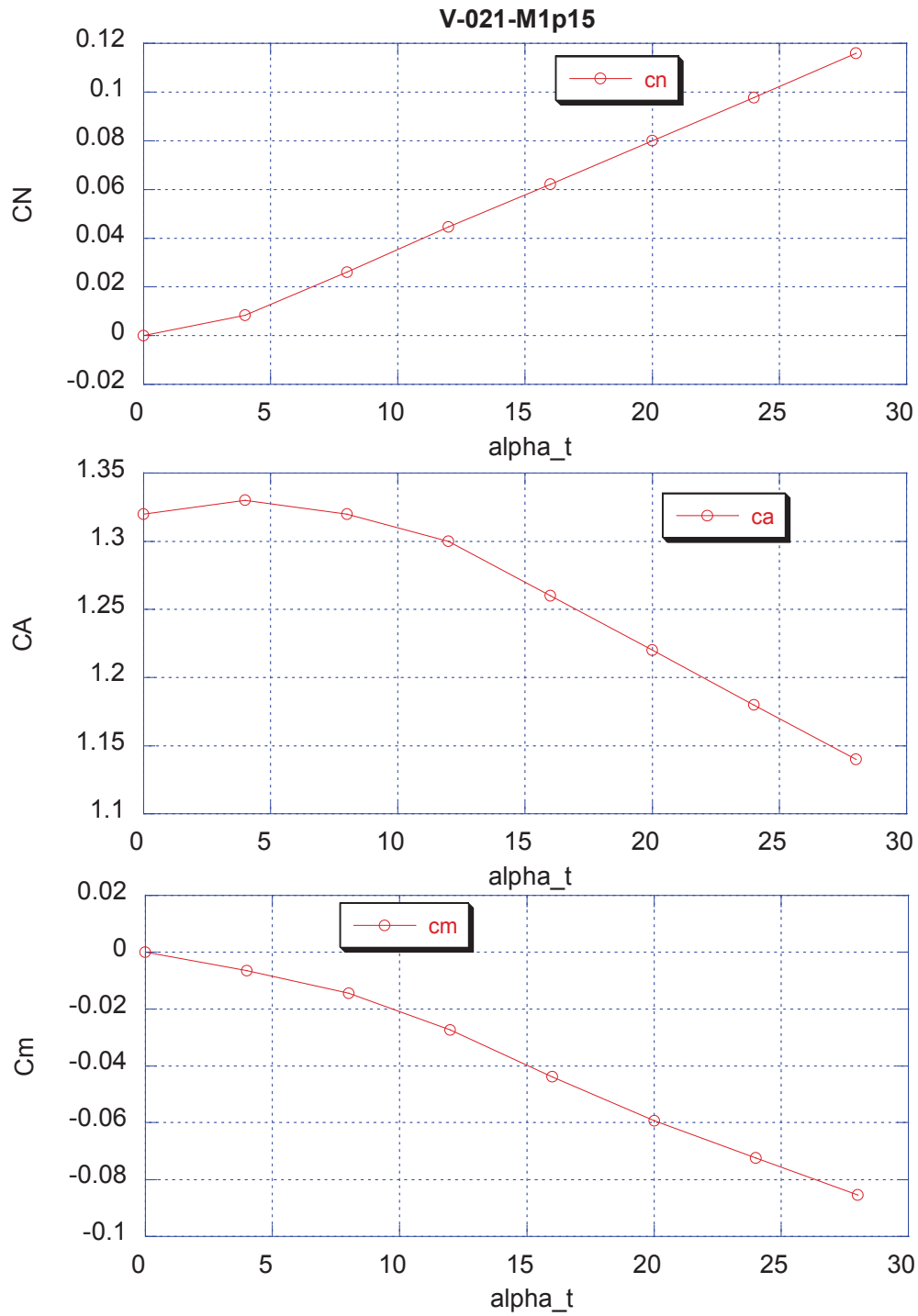


Figure A6 - MMEEV Aero Database for M=1.15. Moment Reference Point is the Vehicle Virtual Nose Apex.

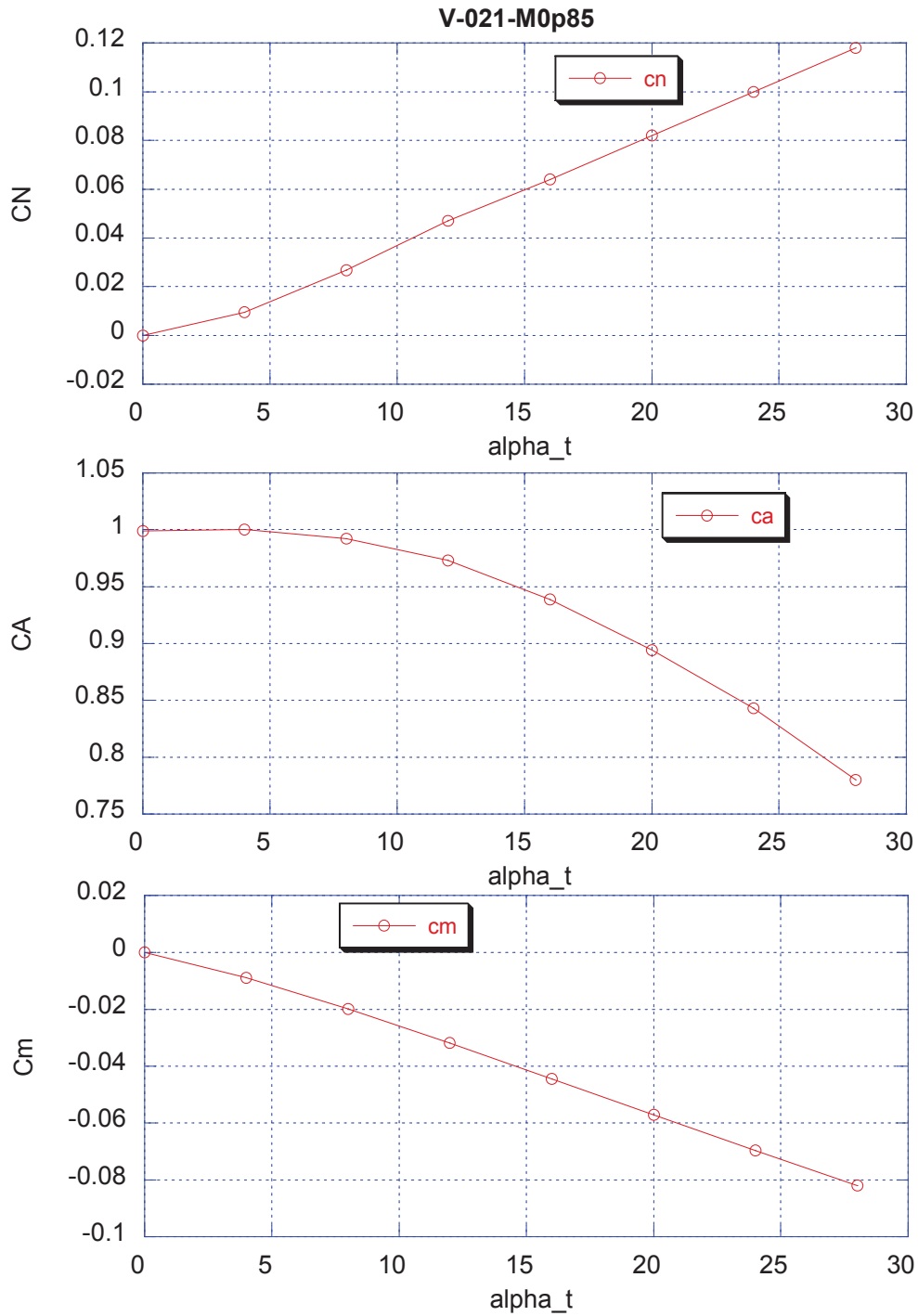


Figure A7 - MMEEV Aero Database for M=0.85. Moment Reference Point is the Vehicle Virtual Nose Apex.

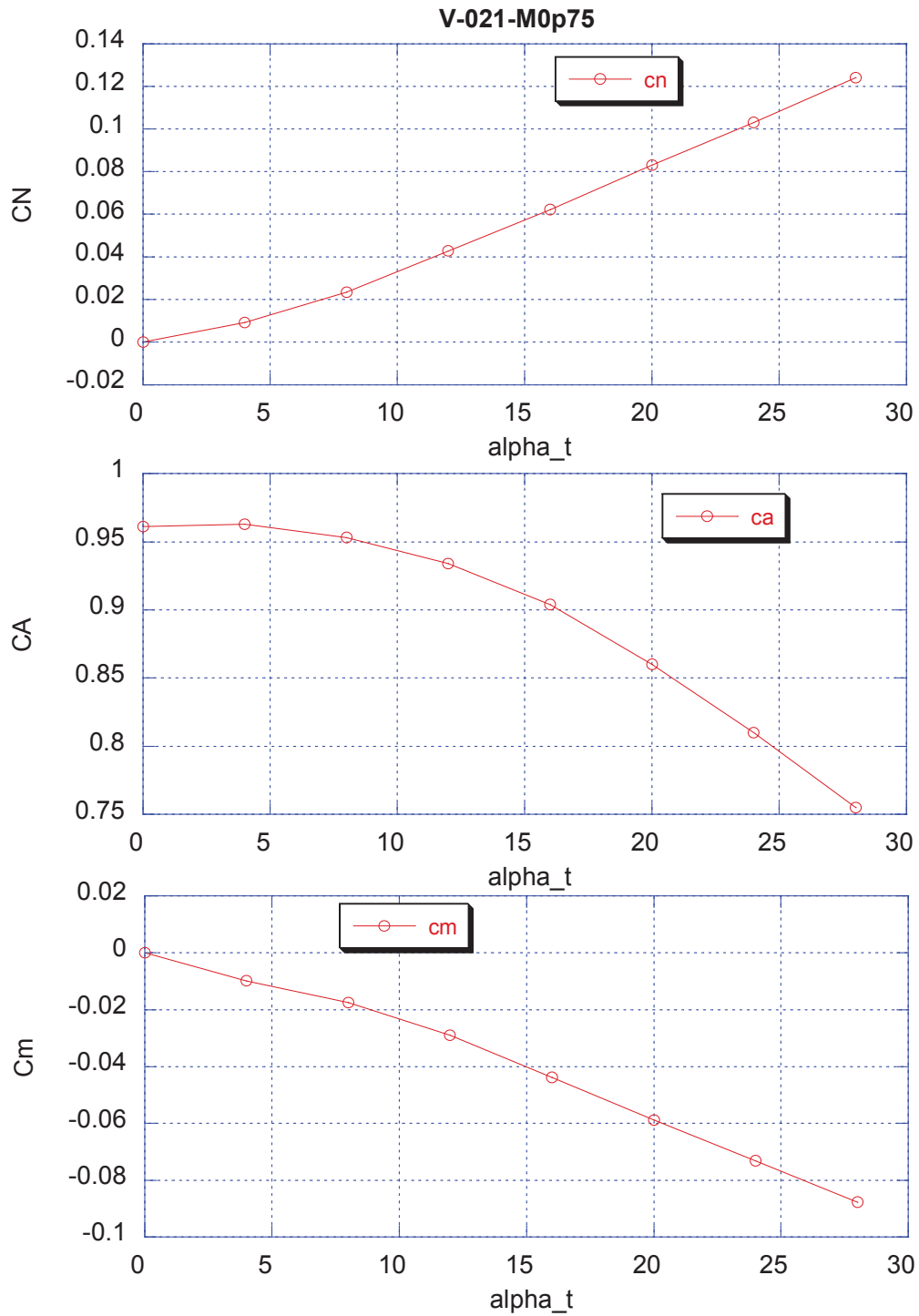


Figure A8 - MMEEV Aero Database for M=0.75. Moment Reference Point is the Vehicle Virtual Nose Apex.

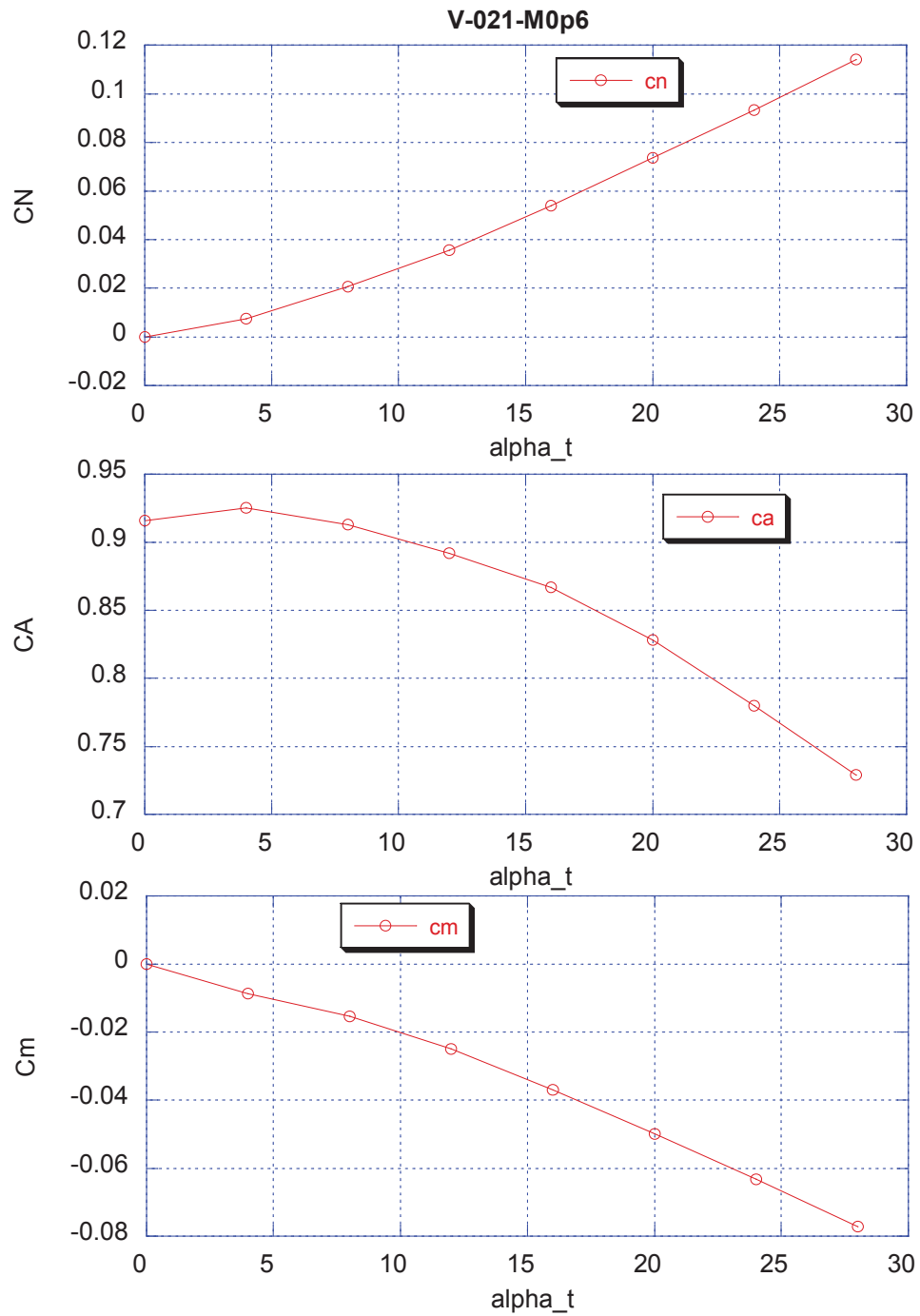


Figure A9 - MMEEV Aero Database for M=0.6. Moment Reference Point is the Vehicle Virtual Nose Apex.

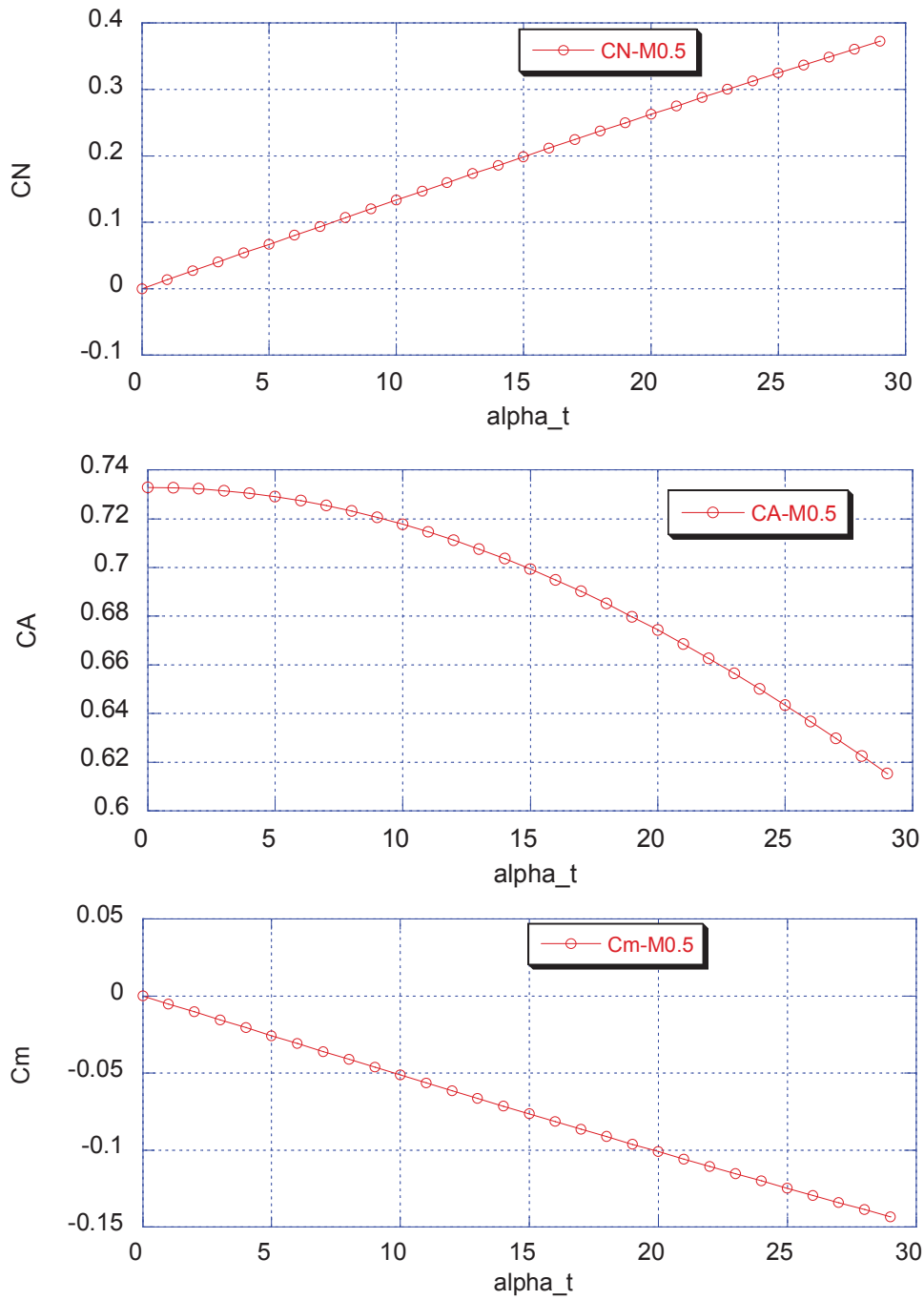


Figure A10 - MMEEV Aero Database for M=0.5. Moment Reference Point is the Vehicle Virtual Nose Apex.

APPENDIX B: MERS DEVELOPMENTAL DATA

PICA-Only

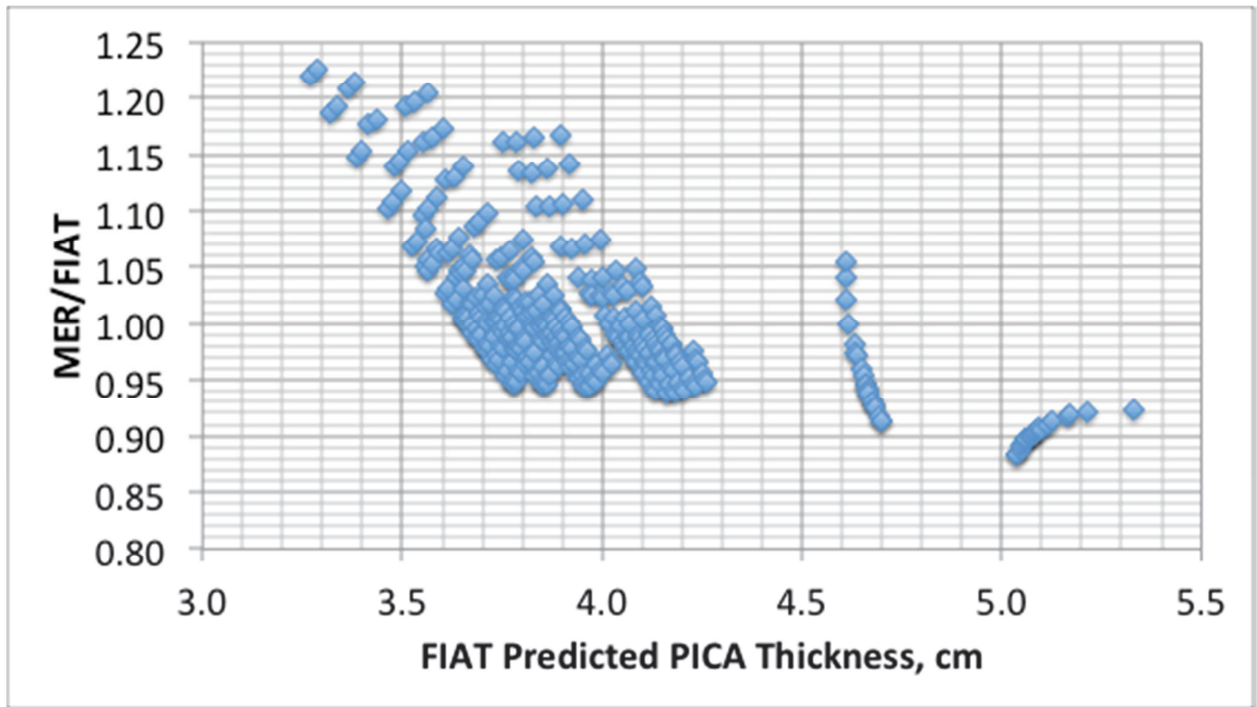


Figure B1. PICA-only MER GoF vs. FIAT-predicted PICA Thickness

Carbon Phenolic Atop Advanced Carbon-Carbon 6

Table B1. Material Stack-up for Carbon Phenolic Atop Advanced Carbon-Carbon 6

Material	Thickness, cm
Carbon Phenolic	variable
HT-424 (adhesive)	0.0381
Advanced Carbon-Carbon (ACC) version 6	0.250

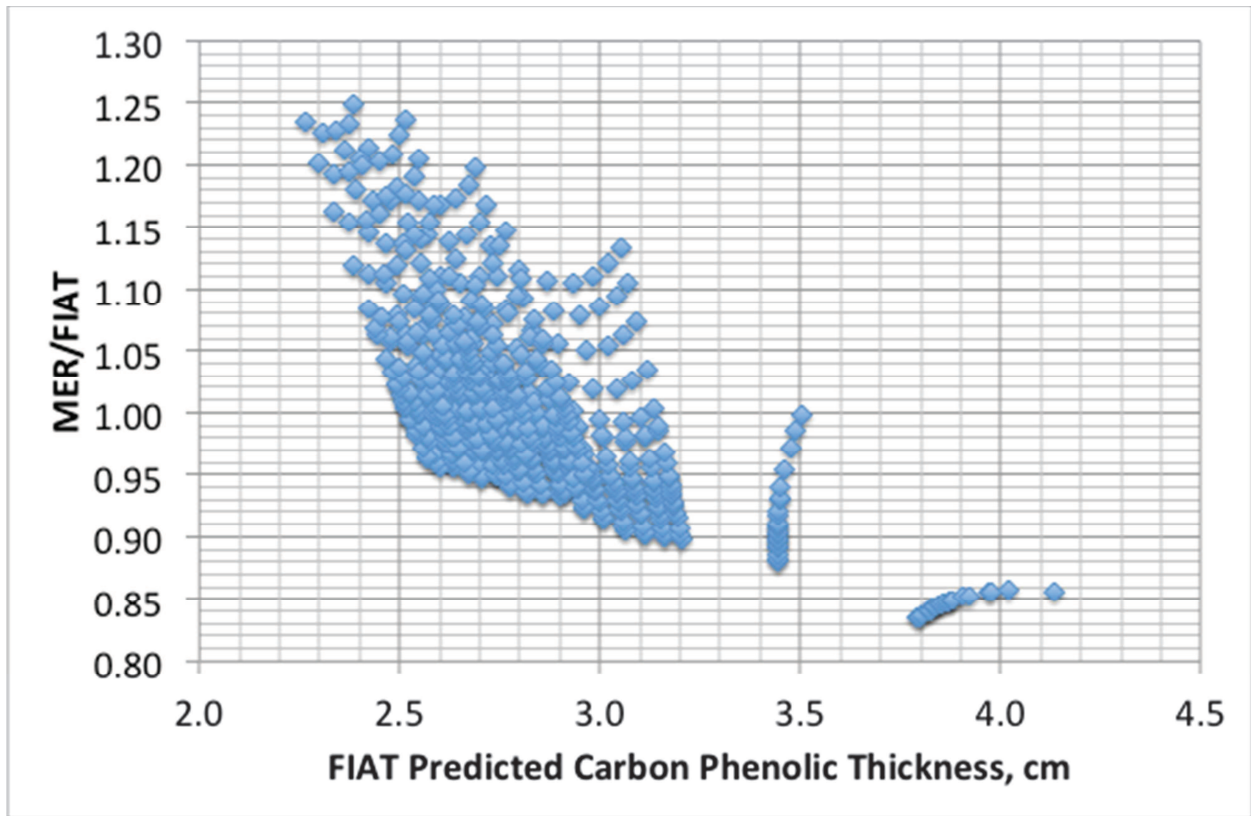


Figure B2. Carbon Phenolic over ACC6 MER, GoF (need your latest result in here)

SIRCA-Only

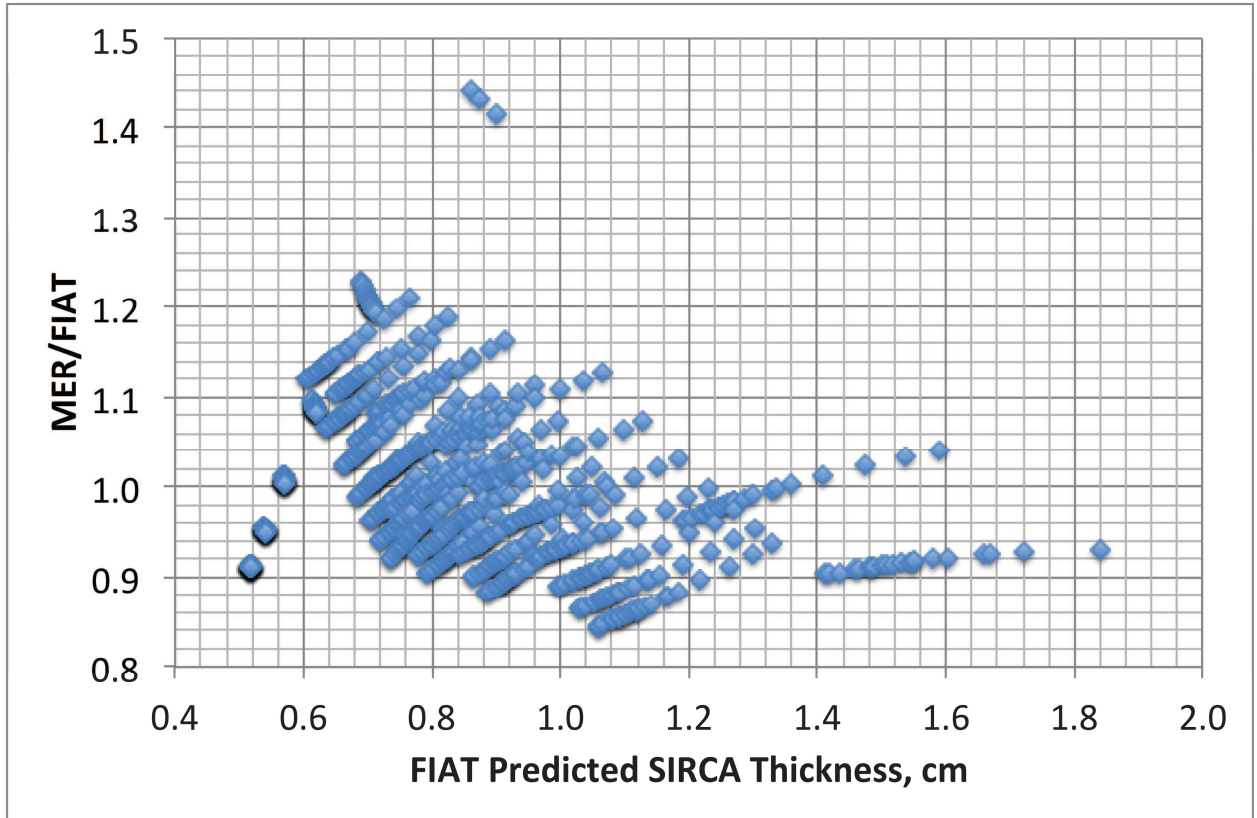


Figure B3. SIRCA MER GoF

Acusil II MER

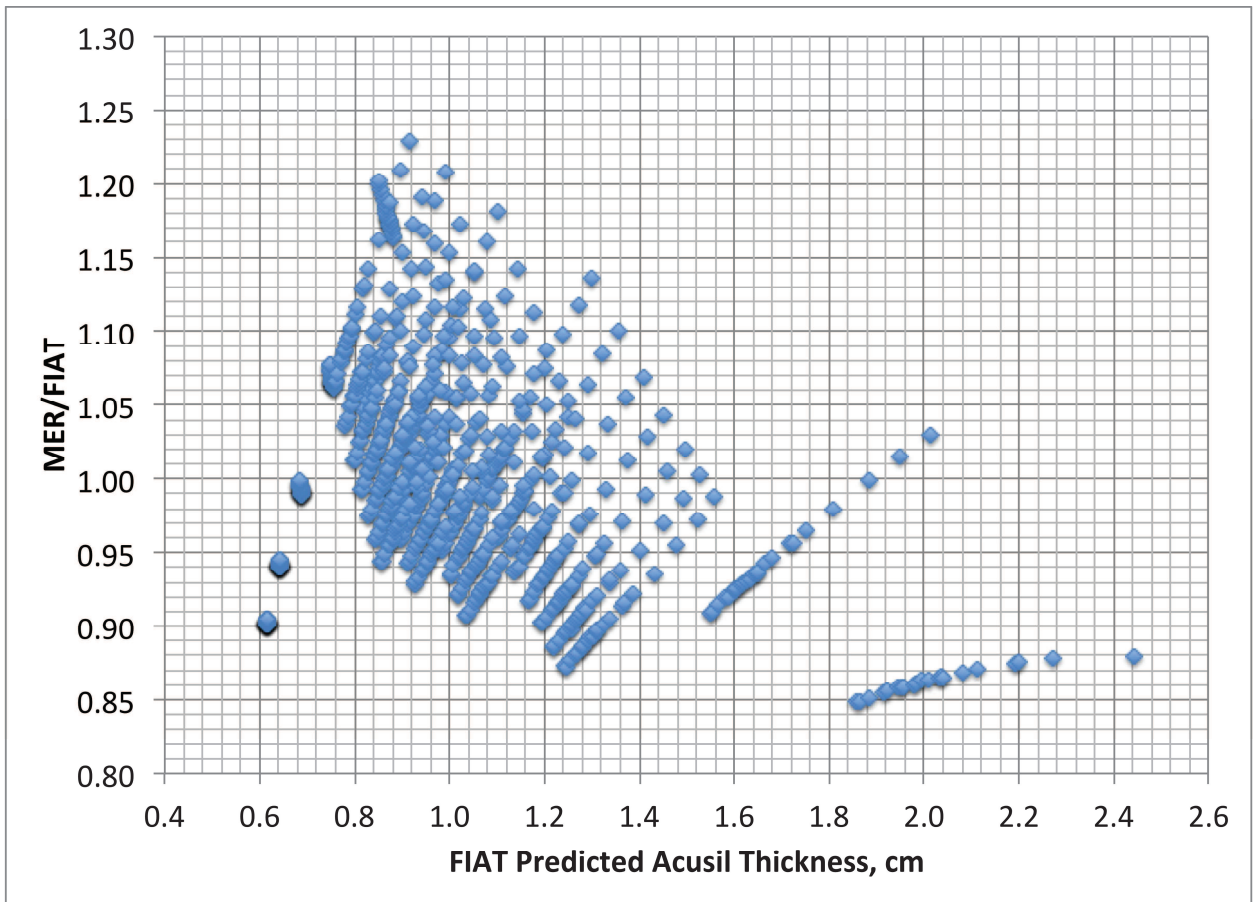


Figure B4. Acusil II MER GoF

SLA-561V-Only

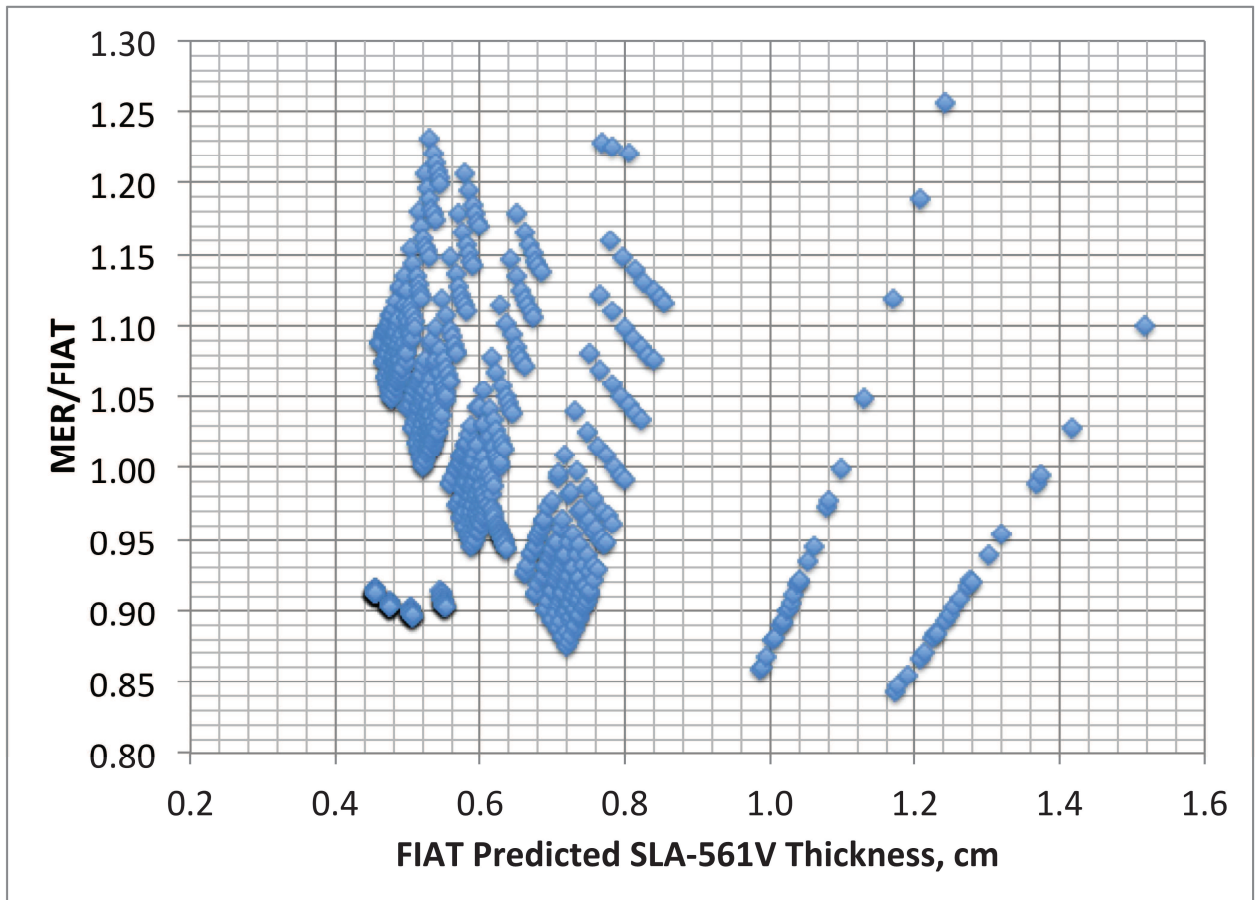


Figure B5. SLA-561V MER GoF

LI-900

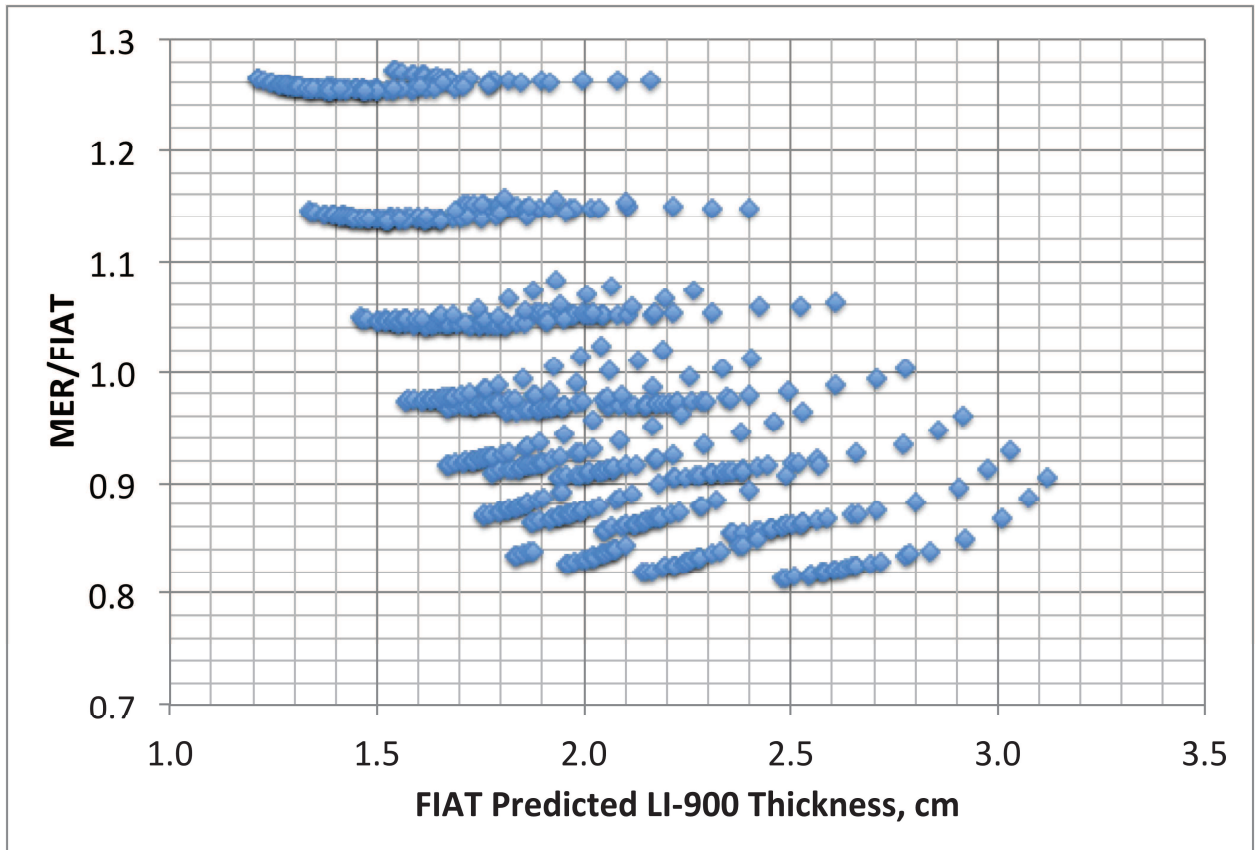


Figure B6. LI-900 MER GoF

APPENDIX C

THERMAL SOAK ANALYSES DATA

Entry Environments and Boundary Conditions

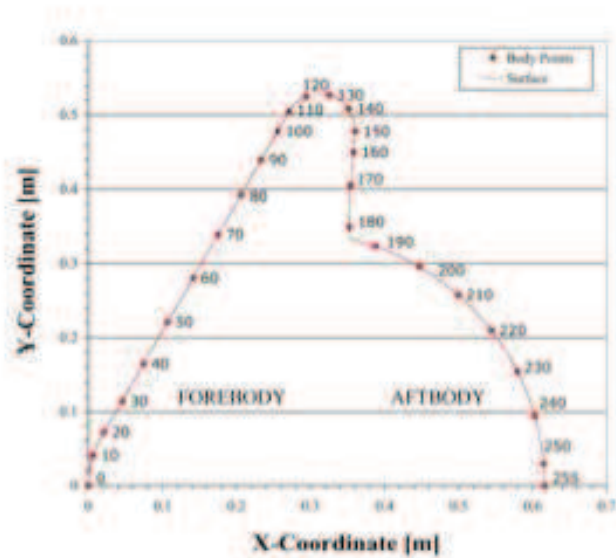


Figure C1 - The 256 Surface Body Points for Full Body Aerothermal Analysis

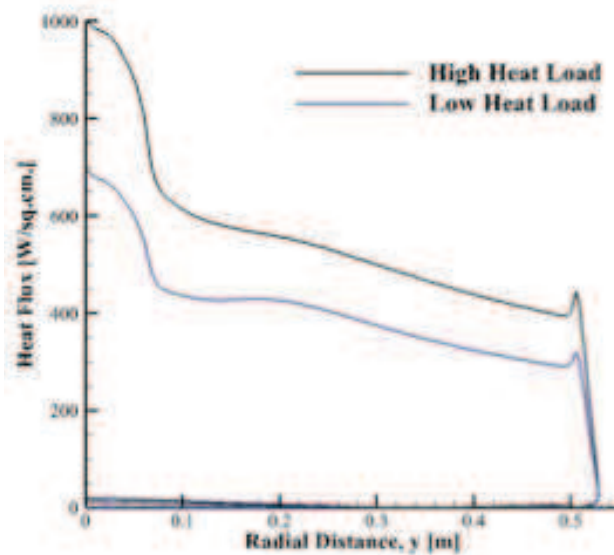


Figure C2 - Heat Flux Distribution Along Vehicle at Peak Heating

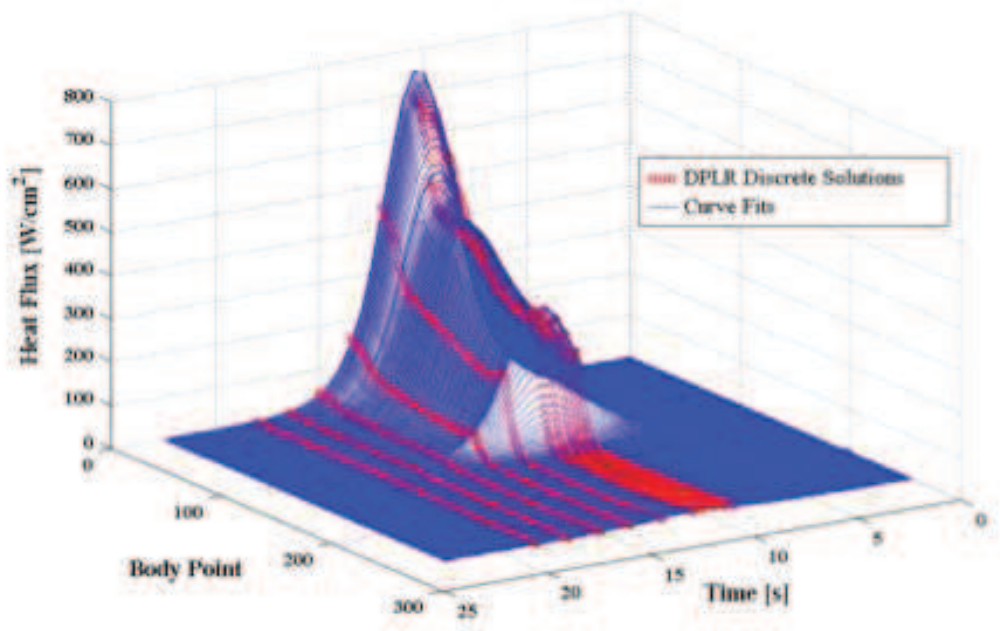


Figure C3 - DPLR Solutions with the Curve Fits Superimposed for the Low Heat Load Trajectory

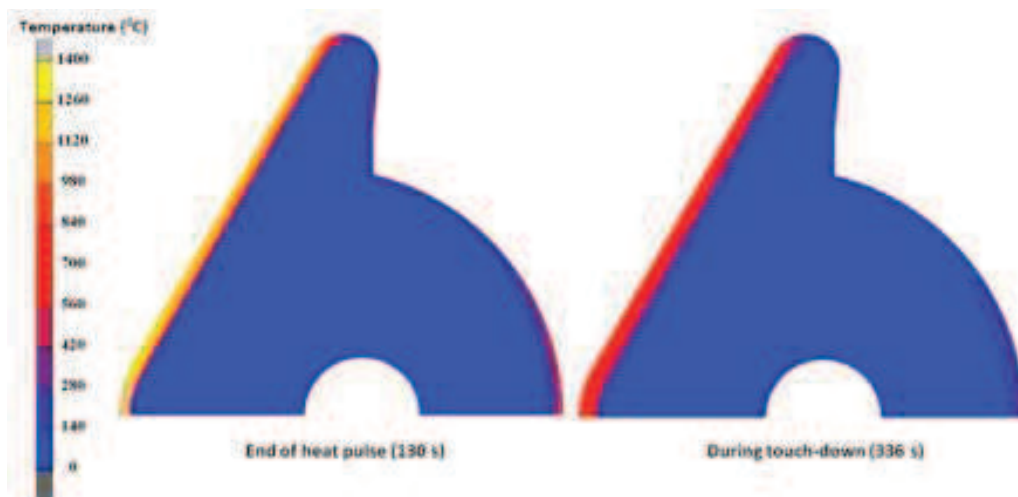


Figure C4 – Temperature Contours for the High Heat Load Trajectory

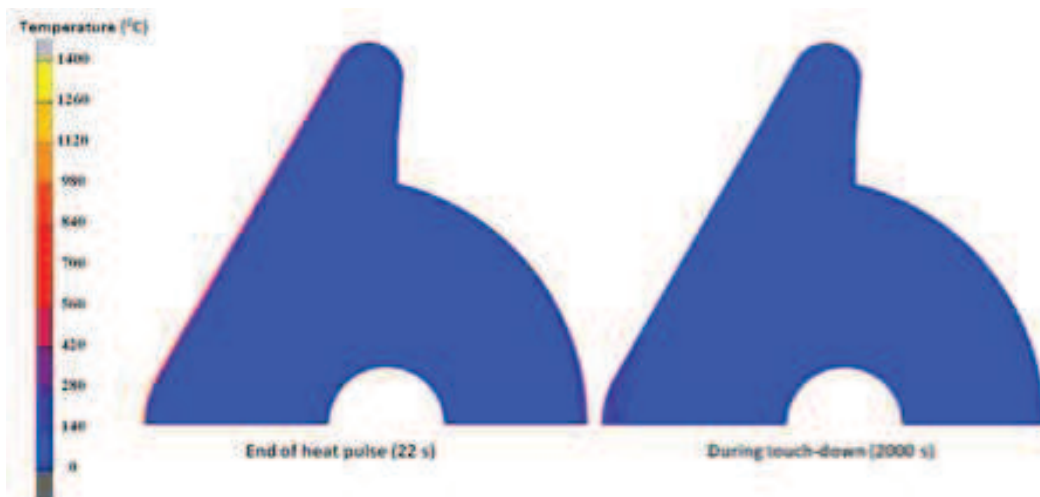


Figure C5 - Temperature Contours for the Low Heat Load Trajectory

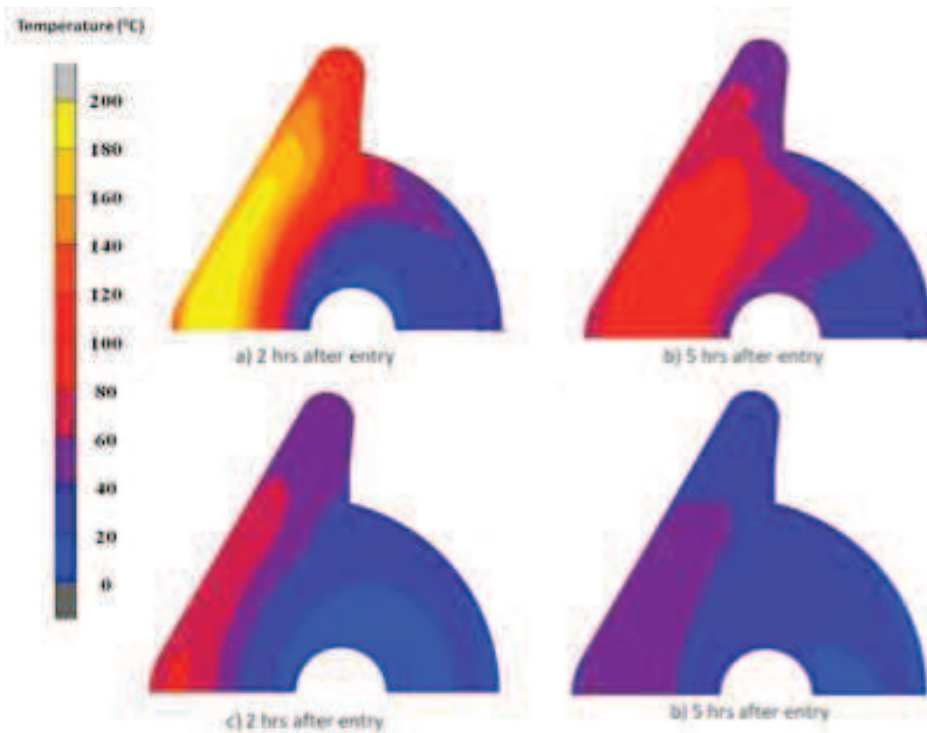


Figure C6 - Temperature Contours in the Probe After Touchdown. a and b Correspond to the High Heat Load Trajectory; c and d Correspond to the Low Heat Load Trajectory

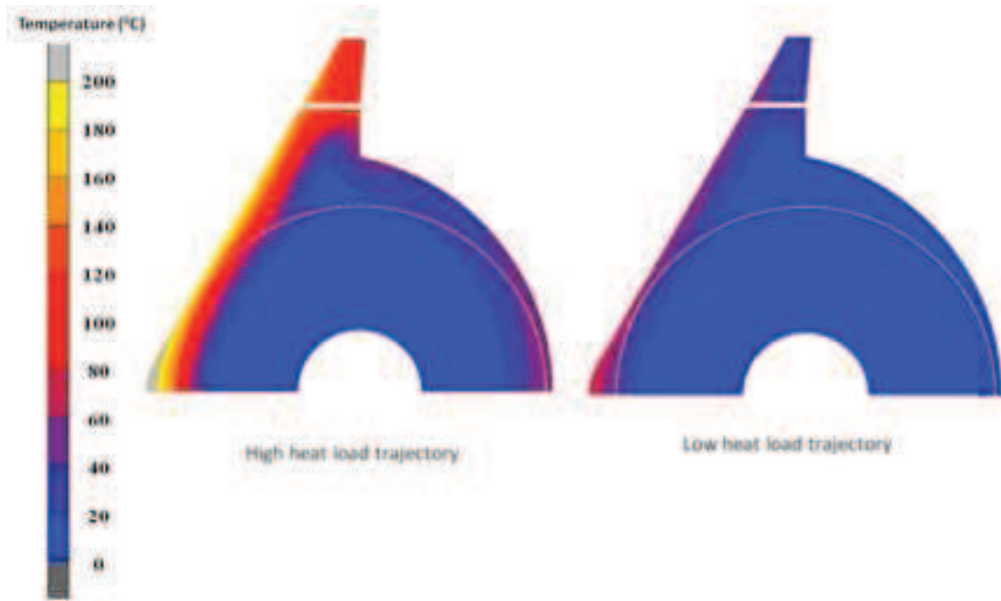


Figure C7 - Peak Foam Temperature for the Two Trajectories

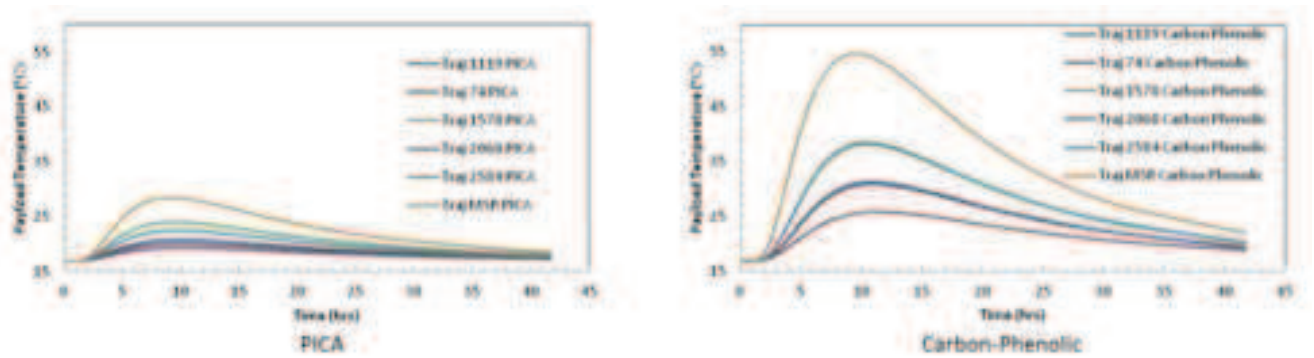
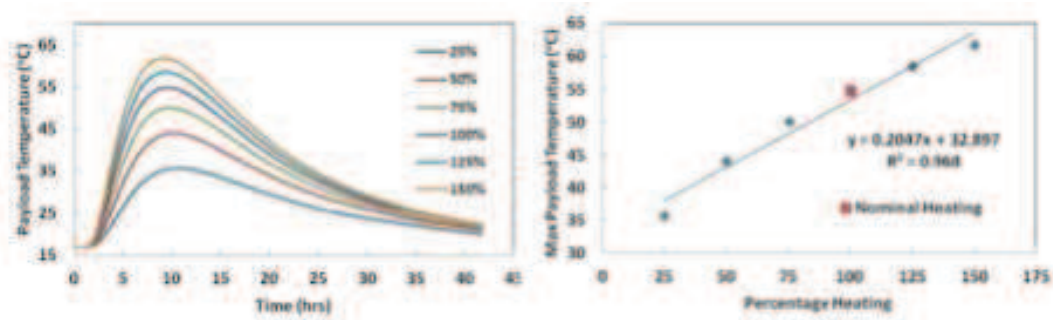
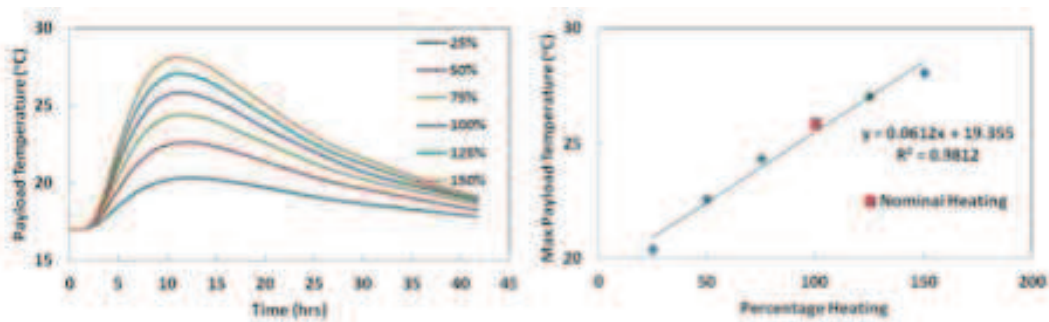


Figure C8 - Payload Temperature History and Peak Payload Temperature for Various Trajectories



a. b.

Figure C9 - Parametric Studies for Heat Flux Magnitude Variation for the High Heat Load Trajectory



a. b.

Figure C10 - Parametric Studies for Heat Flux Magnitude Variation for the Low Heat Load Trajectory

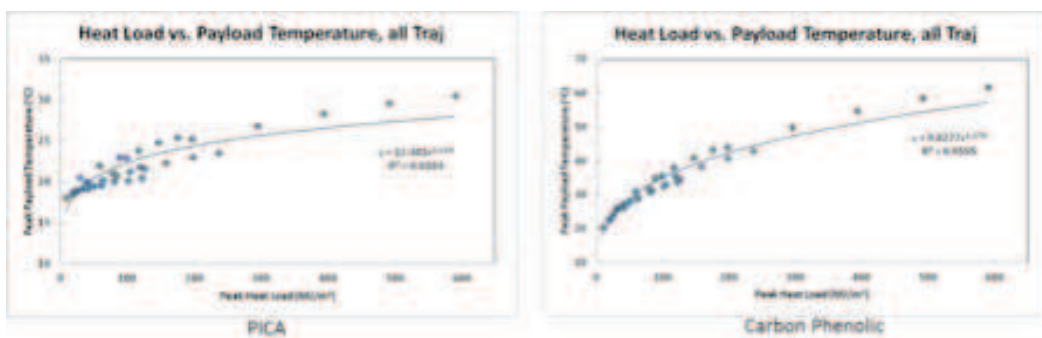


Figure C11 - Peak Payload Temperature Variations with Heat-load for a Given Vehicle Diameter

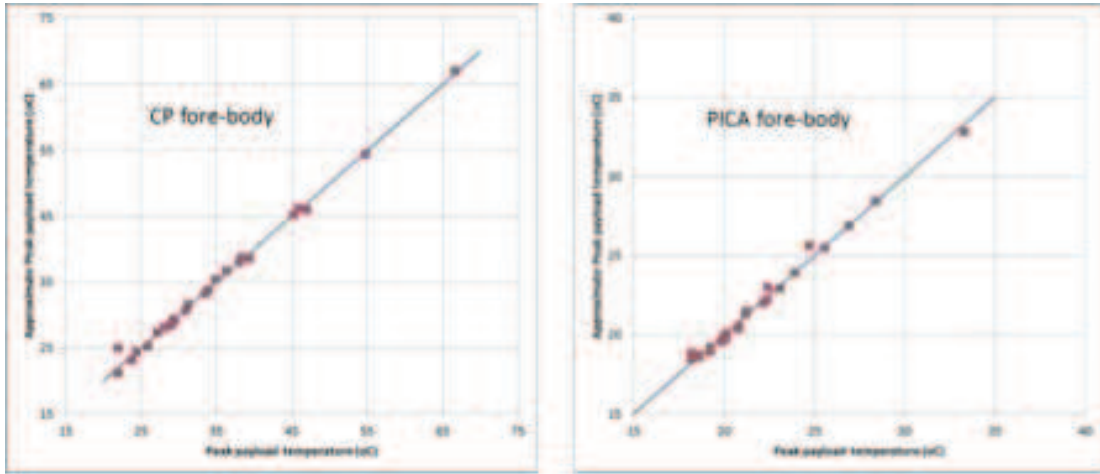


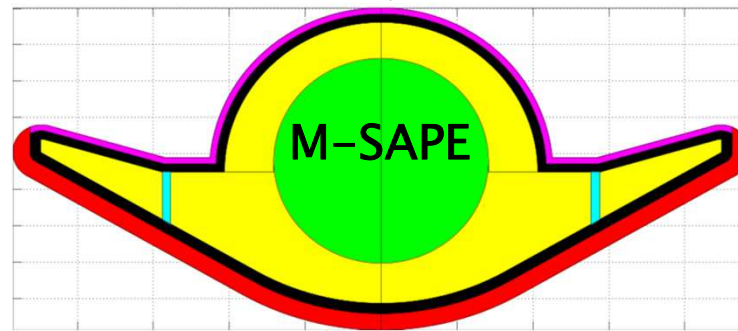
Figure C12 - The GoF for Established Correlations for Peak Payload Temperature with Vehicle Diameter, Peak Stagnation Heat Flux and Heat-load

APPENDIX D
M-SAPE USER GUIDE

M-SAPE Entry Vehicle User Guide

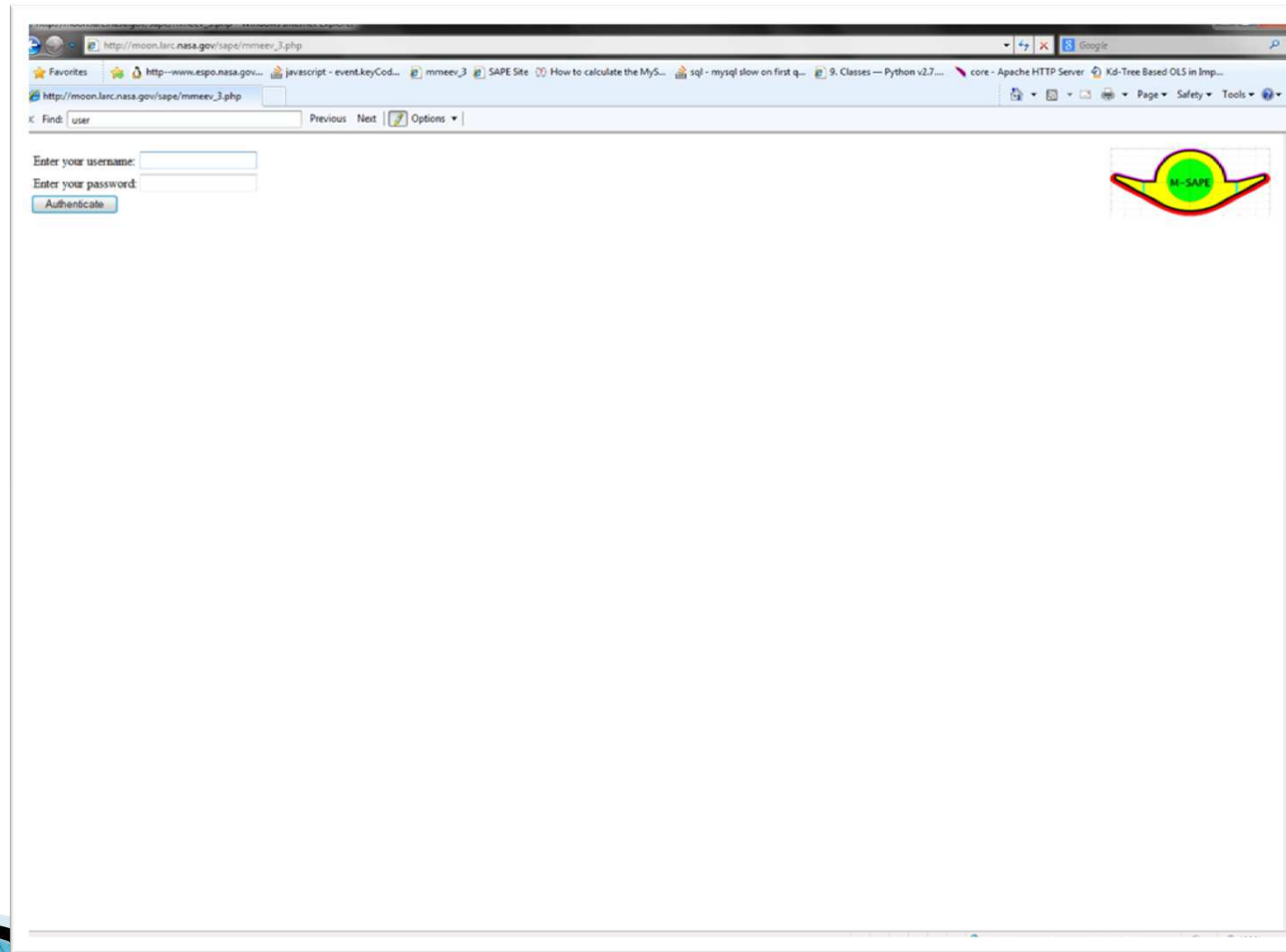
Project Lead: Dr. Jamshid A. Samareh
Database Design and User Interface
Development: Charles A. Liles

Mar 19, 2014



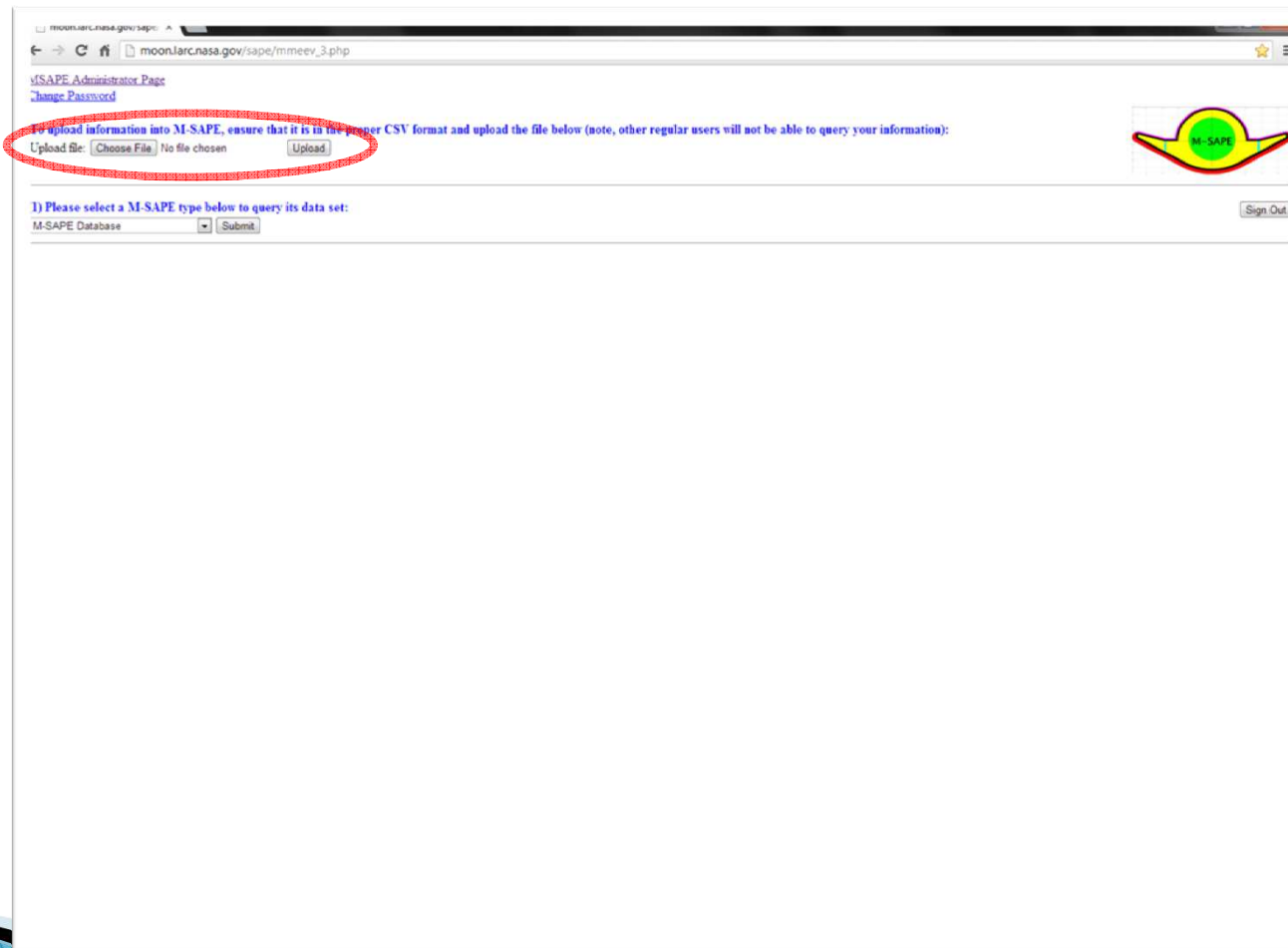
Accessing M-SAPE

- ▶ New users must sign in before accessing the system



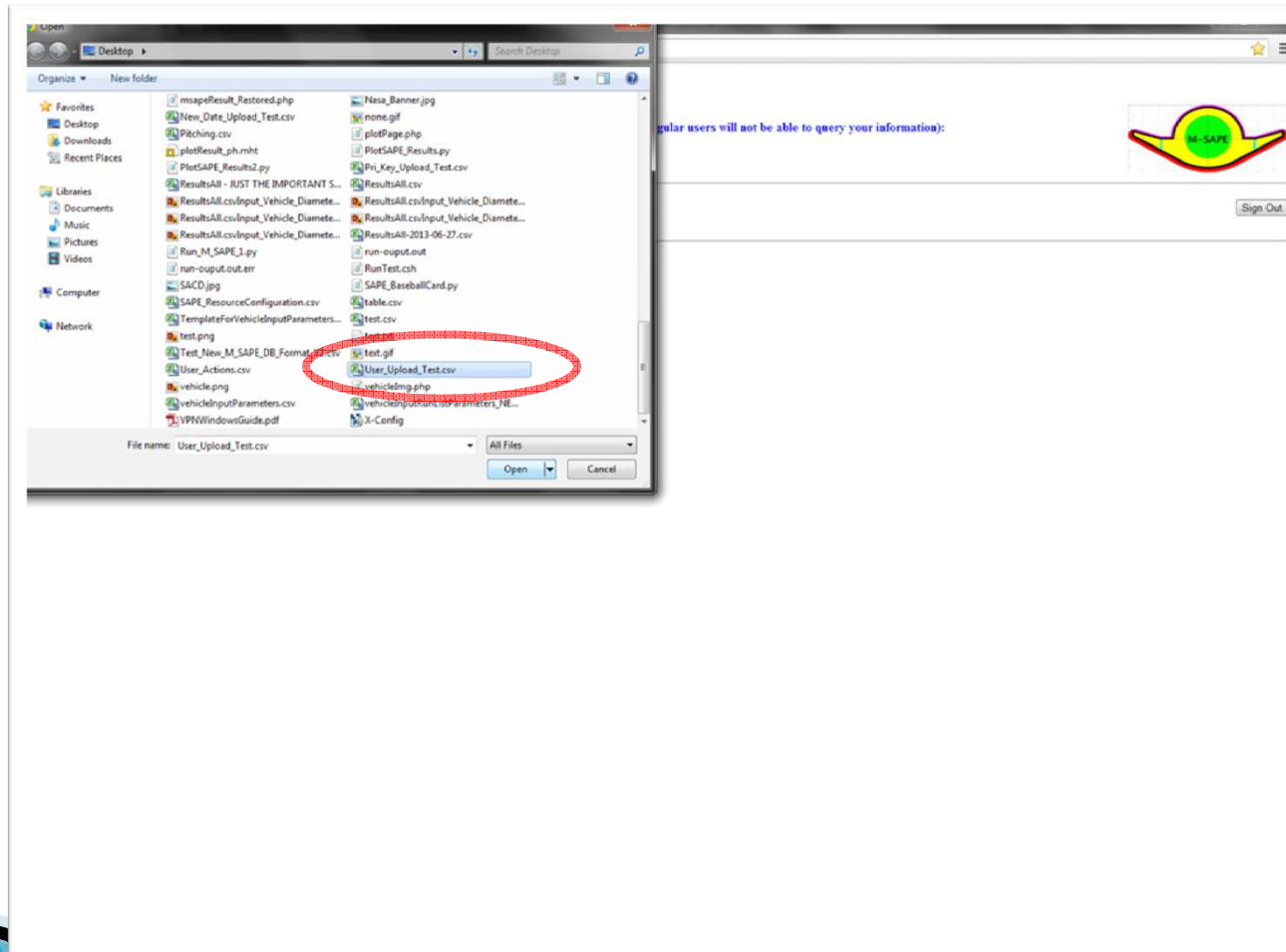
Main Query Page and Uploading Data

- ▶ Once you are logged in, you will be directed to the main query page
- ▶ You can supplement pre-existing database data with your own data; your uploaded data will not be visible to other regular users
- ▶ To upload your data, select “Choose File”



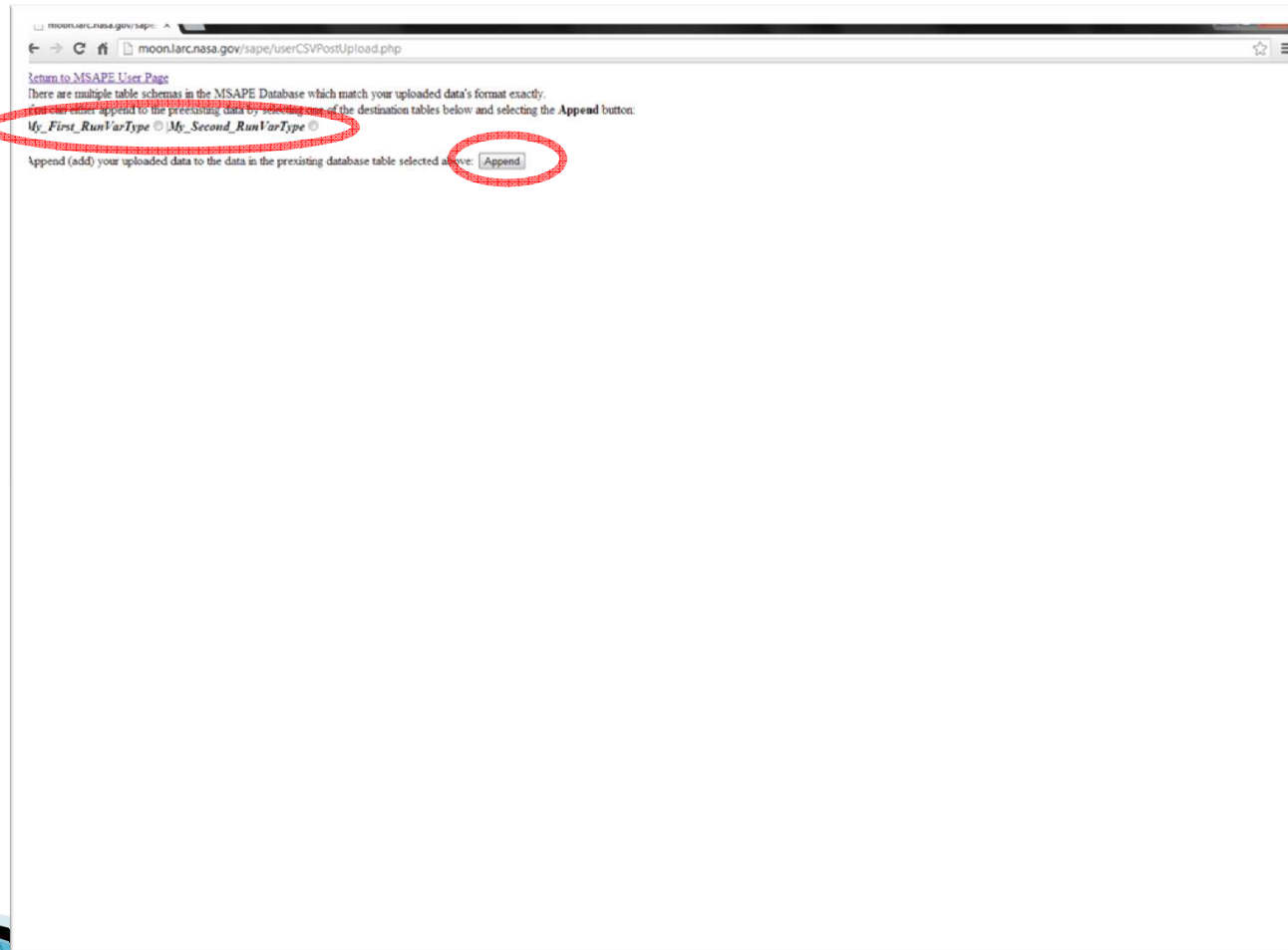
Uploading Data

- ▶ Then select the file that you would like to upload
- ▶ Only CSV formatted files can be uploaded



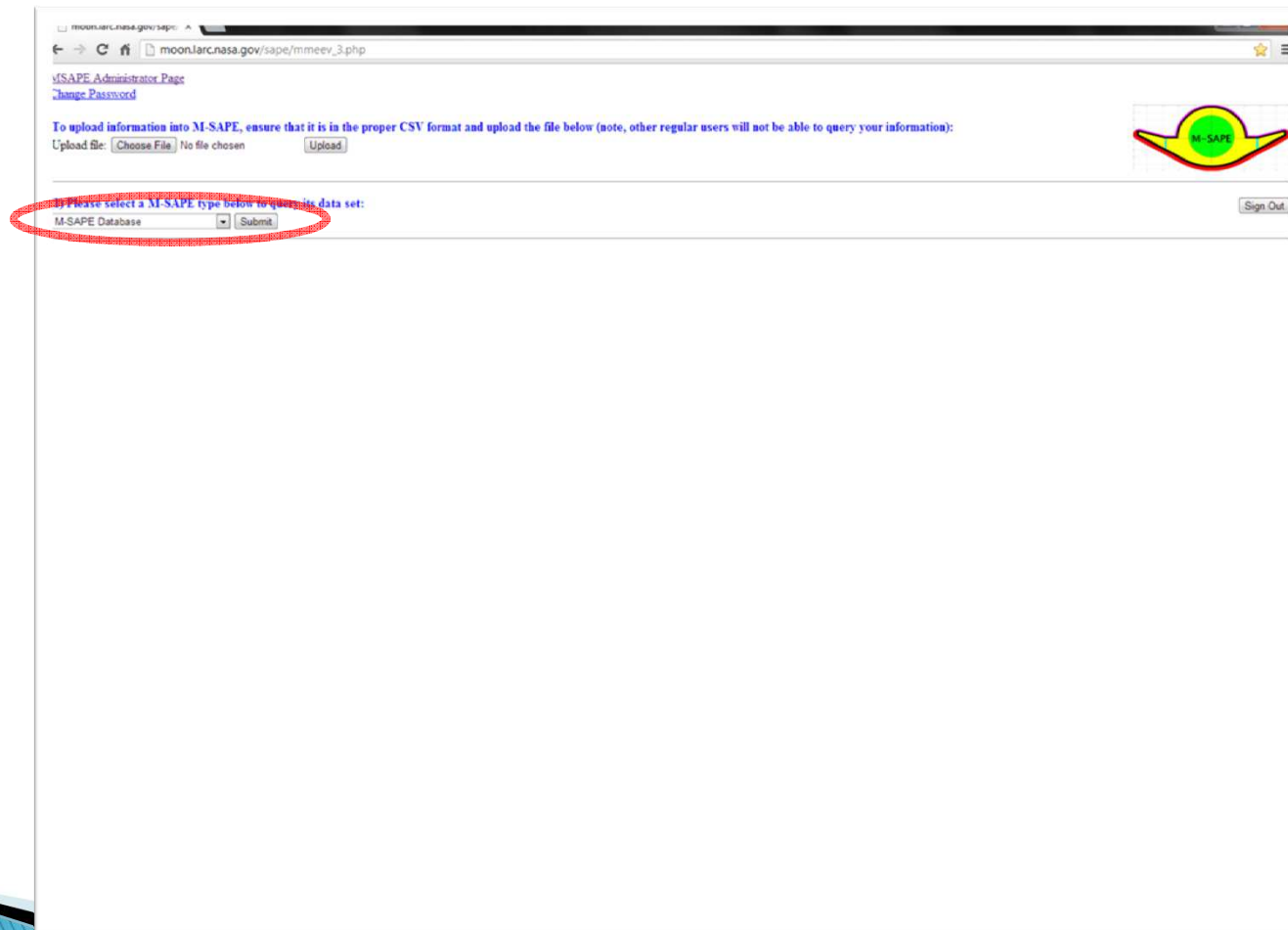
Uploading Data

- ▶ Assuming the file uploads correctly, you will be given an option of which datasets match your input data's format
- ▶ Select the radio button next to the dataset name to which you want to append your data
- ▶ Press "Append"
- ▶ Make sure that you wait for the process to finish; DO NOT CLOSE OR REFRESH THE BROWSER



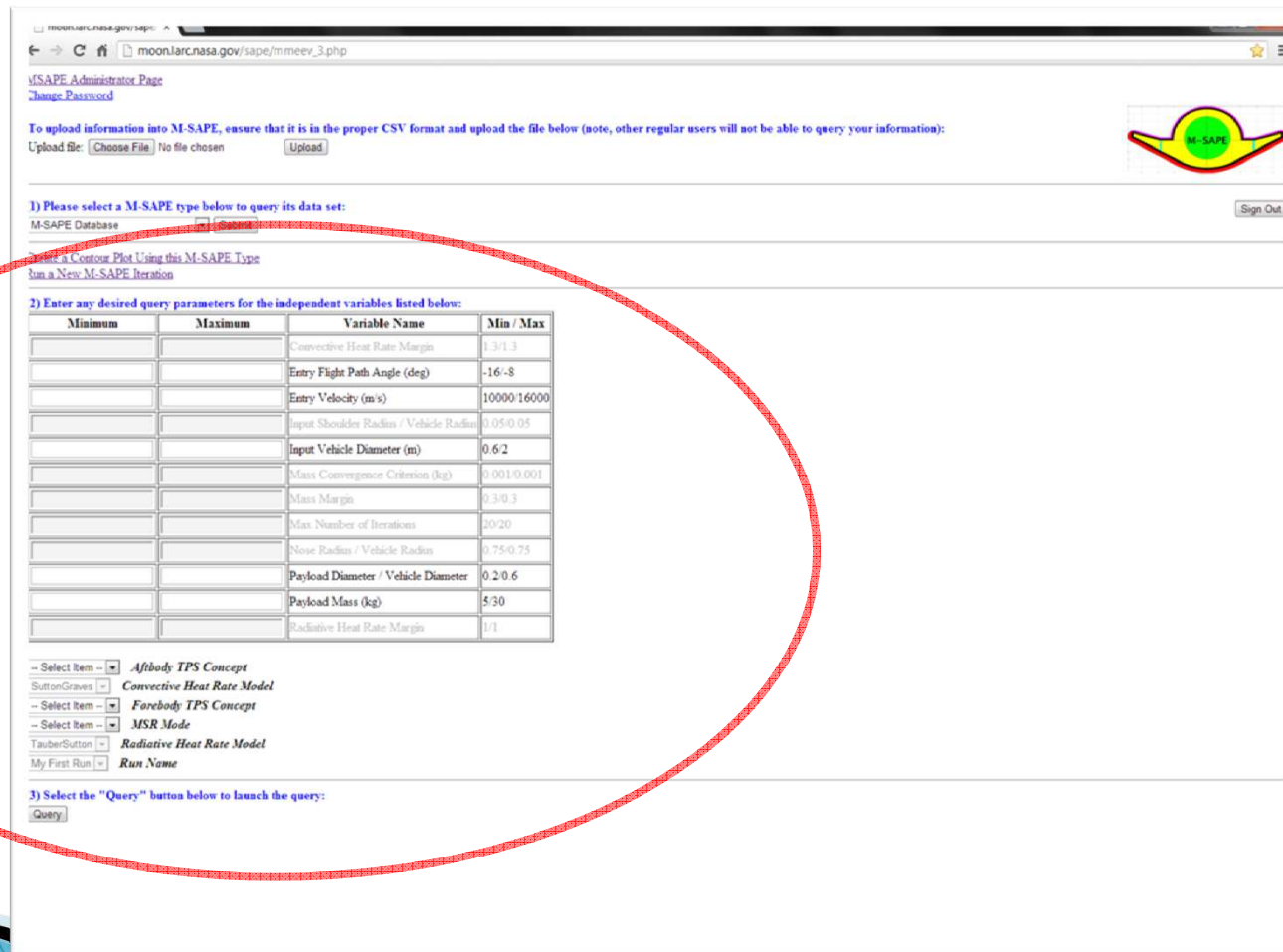
Querying Datasets

- ▶ To query a data set, select the dataset's name in Section (1) of the Main Query Page and then click "Submit"



Querying Datasets

- ▶ In Section (2), you may enter min/max values for numeric variables and select specific values for nominal variables
- ▶ Each value that you specify will have to be true in the query result (*Logical And*)
- ▶ Select the “Query” button in Section (3) to start the query



The screenshot shows the M-SAPE web interface. A red oval highlights the query parameter section. The interface includes a browser address bar, navigation links, an upload section, a sign-out button, and a table for query parameters. Below the table are dropdown menus for selecting concepts and models, and a 'Query' button.

1) Please select a M-SAPE type below to query its data set:

M-SAPE Database

2) Enter any desired query parameters for the independent variables listed below:

Minimum	Maximum	Variable Name	Min / Max
		Convective Heat Rate Margin	1.3/1.3
		Entry Flight Path Angle (deg)	-16/-8
		Entry Velocity (m/s)	10000/16000
		Input Shoulder Radius / Vehicle Radius	0.05/0.05
		Input Vehicle Diameter (m)	0.6/2
		Mass Convergence Criterion (kg)	0.001/0.001
		Mass Margin	0.3/0.3
		Max Number of Iterations	20/20
		Nose Radius / Vehicle Radius	0.75/0.75
		Payload Diameter / Vehicle Diameter	0.2/0.6
		Payload Mass (kg)	5/30
		Radiative Heat Rate Margin	1/1

3) Select the “Query” button below to launch the query:

Querying Datasets

- ▶ Wait for the query results to return (it may take some time)
- ▶ Only the first 200 results will be displayed on the screen
- ▶ You can export all results to a CSV file by selecting “Export Results to CSV”

moon.jarc.nasa.gov/sape

moon.jarc.nasa.gov/sape/mmeev_3.php

3) Select the "Query" button below to launch the query:

[Query](#)

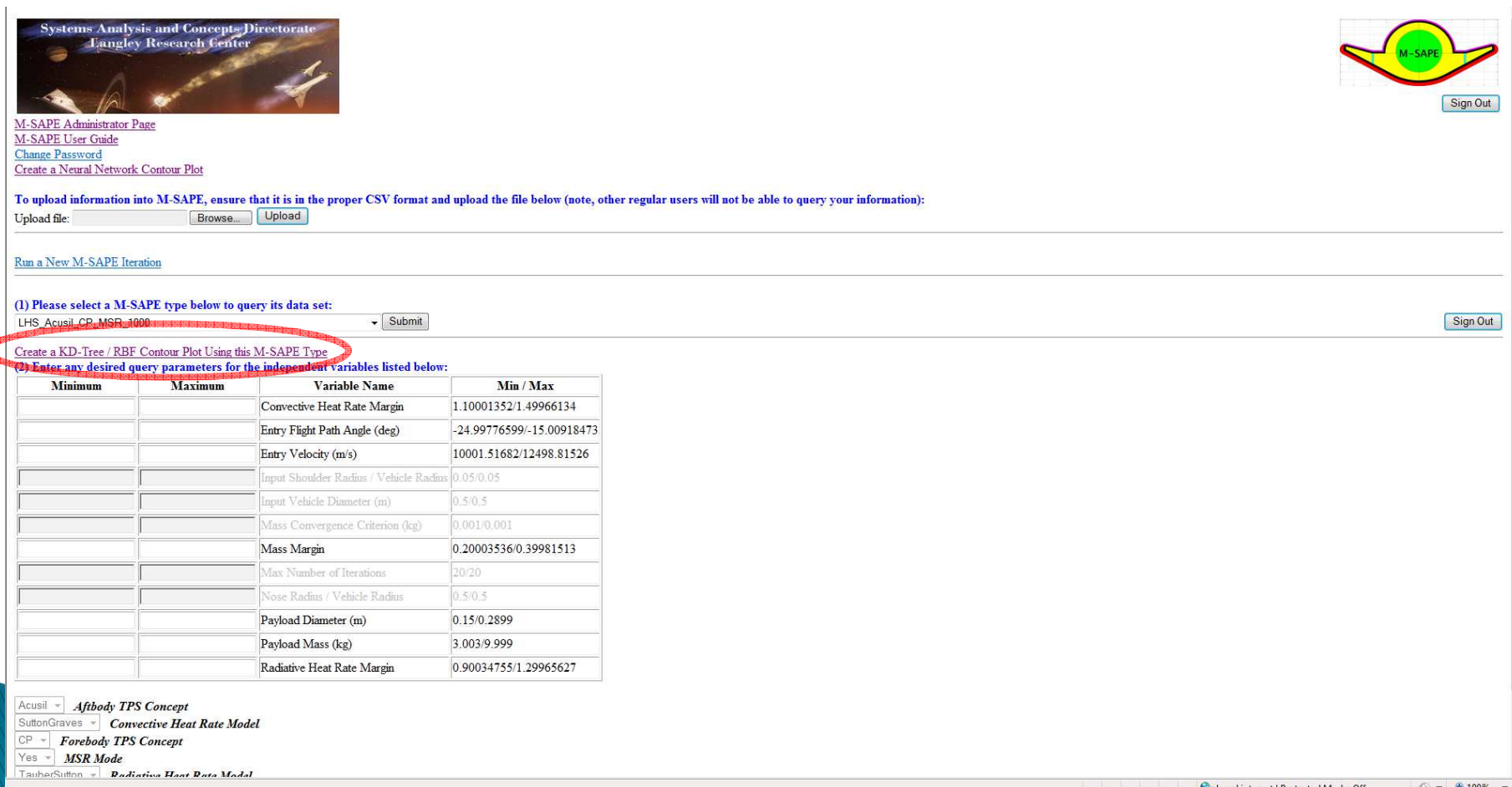
[Export Results to CSV](#)

There are 80639 cases available. Only the first 200 results are shown below. You may view all results by selecting [Export Results to CSV](#) above.

Adjusted Shoulder Radius (m)	Adjusted Shoulder Radius / Vehicle Radius	Adjusted Vehicle Diameter (m)	Aeroshell Type	Aftbody Angle (deg)	Aftbody Carrier Structure Density (kg/m ³)	Aftbody Carrier Structure Mass (kg)	Aftbody Carrier Structure Thickness (cm)	Aftbody Max Heat Rate (W/cm ²)	Aftbody TPS Concept	Aftbody TPS Density (kg/m ³)	Aftbody TPS Mass (kg)	Aftbody TPS Message	Aftbody TPS Thickness (cm)	Aftbody Total Heat Load (J/cm ²)	Atta Stru De (0)
0.0288	0.096	0.6	Sphere-Cone	28.5956	218	0.898357	1.1	8.05381104404	SIRCA	260	0.539316	None	0.545525372596	110.691584496	0.11
0.0284	0.0709	0.8	Sphere-Cone	24.2663	218	1.60671	1.1	6.13328977654	SIRCA	260	0.929652	SIRCA TPS model limits violated value 41.297 is not between 41.94 128.74;	0.5	82.6682717337	0.13

KD-Tree Contour Plots

- ▶ To Run a KD-Tree / RBF contour plot, select the “Create a KD-Tree / RBF Contour Plot Using this M-SAPE Type” hyperlink from the Main Query Page



Systems Analysis and Concepts Directorate
Langley Research Center

M-SAPE Administrator Page
M-SAPE User Guide
Change Password
Create a Neural Network Contour Plot

To upload information into M-SAPE, ensure that it is in the proper CSV format and upload the file below (note, other regular users will not be able to query your information):
Upload file:

[Run a New M-SAPE Iteration](#)

(1) Please select a M-SAPE type below to query its data set:
LHS_Acusil_CP_MSR_1000

Create a KD-Tree / RBF Contour Plot Using this M-SAPE Type
(2) Enter any desired query parameters for the independent variables listed below:

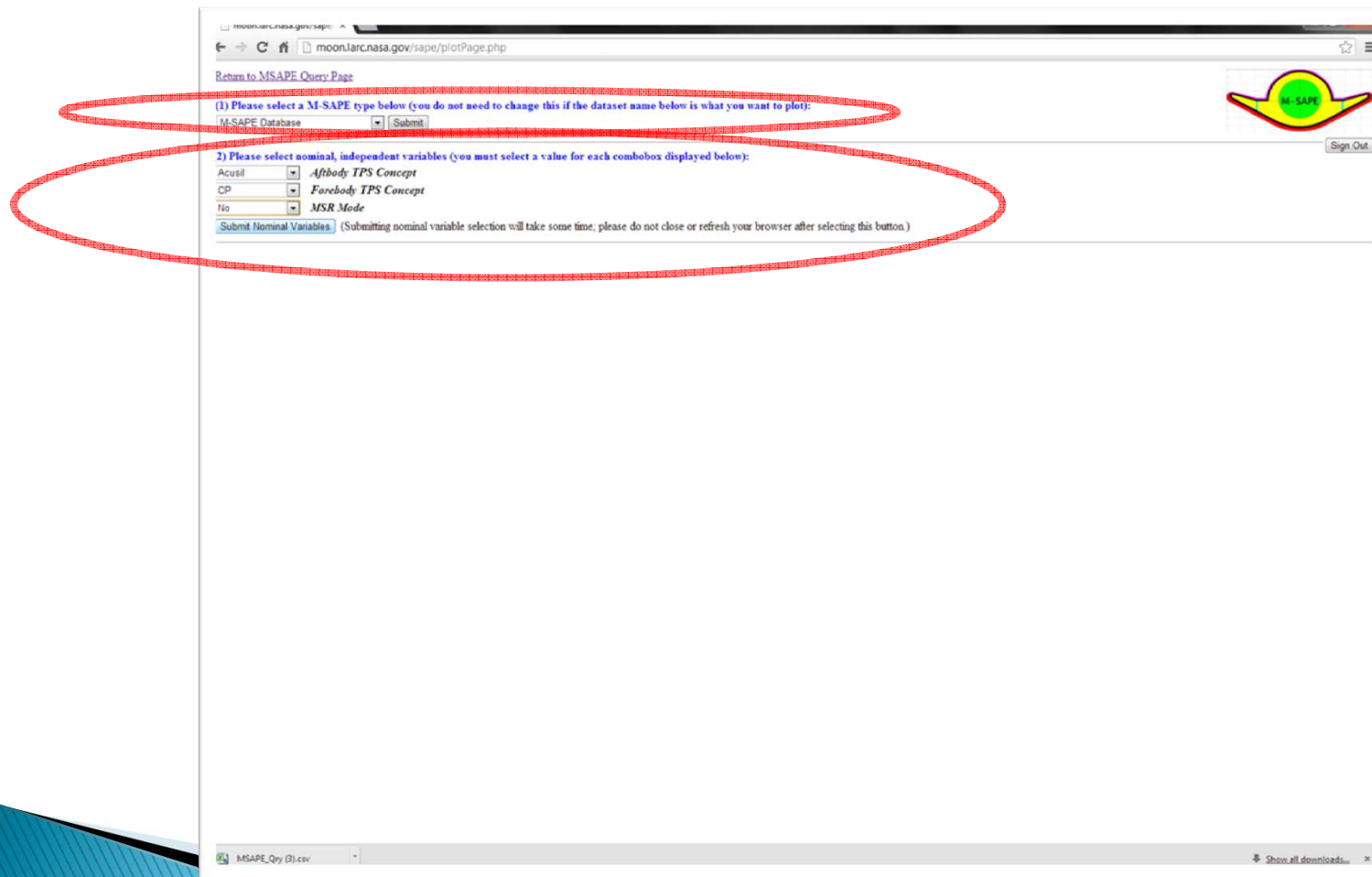
Minimum	Maximum	Variable Name	Min / Max
		Convective Heat Rate Margin	1.10001352/1.49966134
		Entry Flight Path Angle (deg)	-24.99776599/-15.00918473
		Entry Velocity (m/s)	10001.51682/12498.81526
		Input Shoulder Radius / Vehicle Radius	0.05/0.05
		Input Vehicle Diameter (m)	0.5/0.5
		Mass Convergence Criterion (kg)	0.001/0.001
		Mass Margin	0.20003536/0.39981513
		Max Number of Iterations	20/20
		Nose Radius / Vehicle Radius	0.5/0.5
		Payload Diameter (m)	0.15/0.2899
		Payload Mass (kg)	3.003/9.999
		Radiative Heat Rate Margin	0.90034755/1.29965627

Acusil *Aftbody TPS Concept*
SuttonGraves *Convective Heat Rate Model*
CP *Forebody TPS Concept*
Yes *MSR Mode*
TauherSutton *Radiative Heat Rate Model*

Local intranet | Protected Mode: Off | 100%

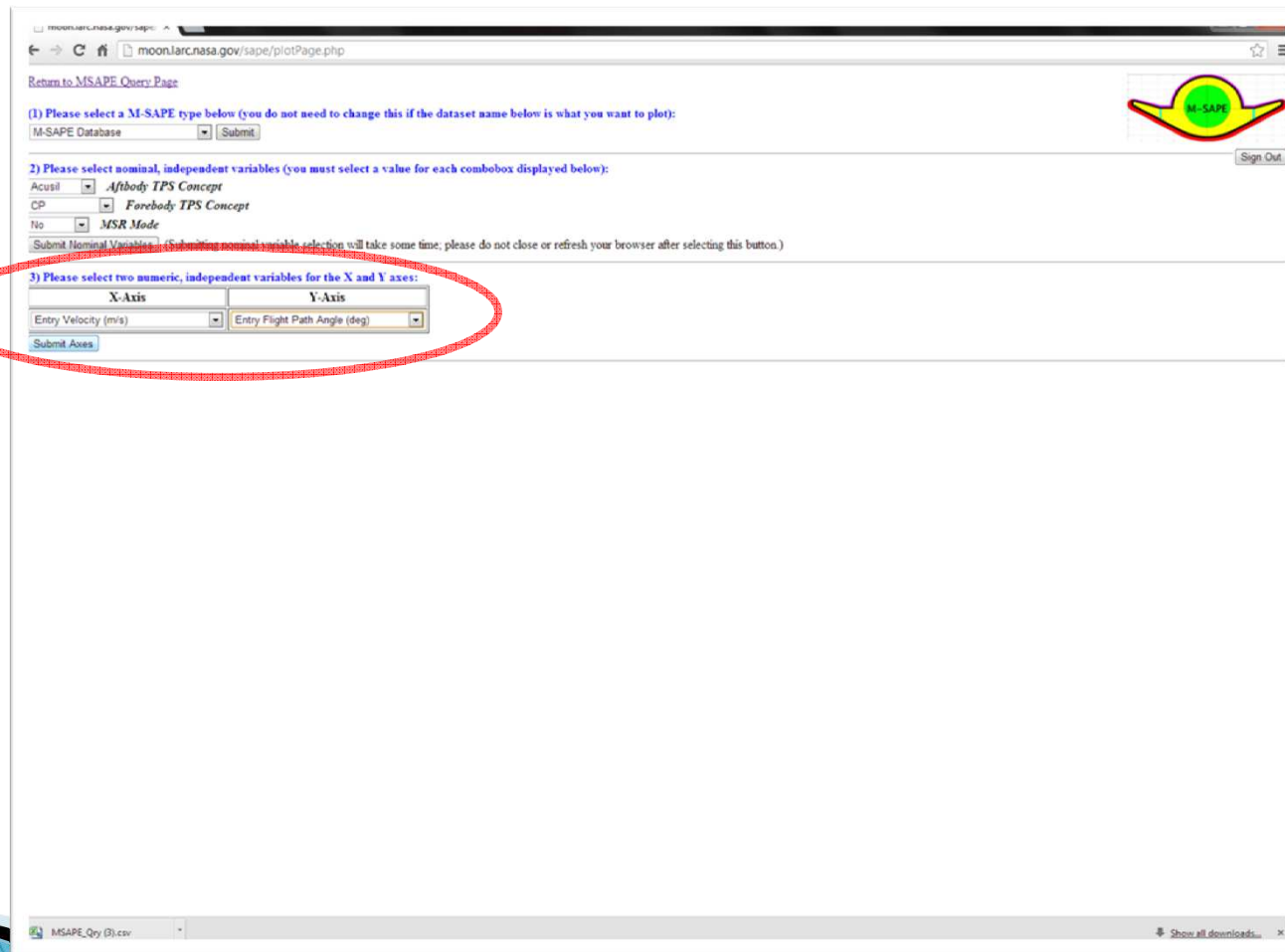
KD-Tree Contour Plots

- ▶ When the KD-Tree Contour Plot Page loads, the M-SAPE type which you had previously selected will be the default in Section (1)
- ▶ You can change the M-SAPE type in Section (1) by selecting it in the combo box and then by clicking “Submit”
- ▶ In Section (2), you must select a nominal value for EACH combo box before proceeding by clicking “Submit Nominal Variables” (be patient, it may take some time before the page reloads)



KD-Tree Contour Plots

- ▶ When the page reloads, you can then select variables for the X and Y axes
- ▶ These variables must be different from each other
- ▶ Hit “Submit Axes” to continue



KD-Tree Contour Plots

- ▶ Next, you can enter values for independent, numeric variables in Section (4)
- ▶ In Section (5), check all variables that you would like to see plotted
- ▶ Then click “Plot” in Section (6)

moon.larc.nasa.gov/sape/plotPage.php

No **MSR Mode**

[Submit Nominal Variables](#) (Submitting nominal variable selection will take some time, please do not close or refresh your browser after selecting this button.)

3) Please select two numeric, independent variables for the X and Y axes:

X-Axis	Y-Axis
Entry Velocity (m/s)	Entry Flight Path Angle (deg)

[Submit Axes](#)

4) Please enter in a value for each numeric, independent variable below. These values will be fixed when generating the contour plot:

	Input Vehicle Diameter (m)	Payload Diameter / Vehicle Diameter	Payload Mass (kg)
Min/Max:	0.6 / 2	0.2 / 0.6	5 / 30
Input:	2	6	30

5) Check the boxes of the dependent, numeric variables below for the contour plot:

<input type="checkbox"/> Adjusted Shoulder Radius (m)	<input type="checkbox"/> Adjusted Shoulder Radius / Vehicle Radius	<input type="checkbox"/> Adjusted Vehicle Diameter (m)	<input type="checkbox"/> Aftbody Angle (deg)	<input type="checkbox"/> Aftbody Carrier Structure Density (kg/m ³)
<input type="checkbox"/> Aftbody Carrier Structure Mass (kg)	<input type="checkbox"/> Aftbody Carrier Structure Thickness (cm)	<input type="checkbox"/> Aftbody Max Heat Rate (W/cm ²)	<input type="checkbox"/> Aftbody TPS Density (kg/m ³)	<input type="checkbox"/> Aftbody TPS Mass (kg)
<input type="checkbox"/> Aftbody TPS Thickness (cm)	<input type="checkbox"/> Aftbody Total Heat Load (J/cm ²)	<input type="checkbox"/> Attached Structure Depth (m)	<input type="checkbox"/> Ballistic Coefficient at Impact (kg/m ²)	<input type="checkbox"/> Body Foam Density (kg/m ³)
<input type="checkbox"/> Crush Load Limit (g's)	<input type="checkbox"/> Downrange (km)	<input type="checkbox"/> Drag Coefficient at Impact	<input type="checkbox"/> Estimated Impact Load (g's)	<input type="checkbox"/> Foam Density (kg/m ³)
<input type="checkbox"/> Foam Thickness (cm)	<input type="checkbox"/> Forebody Carrier Structure Density (kg/m ³)	<input type="checkbox"/> Forebody Carrier Structure Mass (kg)	<input type="checkbox"/> Forebody Carrier Structure Thickness (cm)	<input type="checkbox"/> Forebody Cone Angle (deg)
<input type="checkbox"/> Forebody Convective Heat Load (Margined) (J/cm ²)	<input type="checkbox"/> Forebody Max Convective Heat Rate (Margined) (W/cm ²)	<input type="checkbox"/> Forebody Max Convective Heat Rate (Margined) at Density (kg/m ³)	<input type="checkbox"/> Forebody Max Convective Heat Rate (Margined) at Geodetic Altitude (m)	<input type="checkbox"/> Forebody Max Convective Heat Rate (Margined) at Relative Velocity (m/s)
<input type="checkbox"/> Forebody Max Convective Heat Rate (Margined) at Time (s)	<input type="checkbox"/> Forebody Max Goullard Number	<input type="checkbox"/> Forebody Max Radiative Heat Rate (Margined) (W/cm ²)	<input type="checkbox"/> Forebody Max Radiative Heat Rate (Margined) at Density (kg/m ³)	<input type="checkbox"/> Forebody Max Radiative Heat Rate (Margined) at Geodetic Altitude (m)
<input type="checkbox"/> Forebody Max Radiative Heat Rate (Margined) at Relative Velocity (m/s)	<input type="checkbox"/> Forebody Max Radiative Heat Rate (Margined) at Time (s)	<input type="checkbox"/> Forebody Max Stagnation Pressure (atm)	<input type="checkbox"/> Forebody Max Stagnation Pressure at Density (kg/m ³)	<input type="checkbox"/> Forebody Max Stagnation Pressure at Geodetic Altitude (m)
<input type="checkbox"/> Forebody Max Stagnation Pressure at Relative Velocity (m/s)	<input type="checkbox"/> Forebody Max Stagnation Pressure at Time (s)	<input type="checkbox"/> Forebody Max Total Heat Rate (Margined) (W/cm ²)	<input type="checkbox"/> Forebody Max Total Heat Rate (Margined) at Density (kg/m ³)	<input type="checkbox"/> Forebody Max Total Heat Rate (Margined) at Geodetic Altitude (m)
<input type="checkbox"/> Forebody Max Total Heat Rate (Margined) at Relative Velocity (m/s)	<input type="checkbox"/> Forebody Max Total Heat Rate (Margined) at Time (s)	<input type="checkbox"/> Forebody Radiative Heat Load (Margined) (J/cm ²)	<input type="checkbox"/> Forebody Radiative Heat Rate (coupled) / Radiative Adiabatic	<input type="checkbox"/> Forebody TPS Density (kg/m ³)
<input type="checkbox"/> Forebody TPS Mass (kg)	<input type="checkbox"/> Forebody TPS Thickness (cm)	<input type="checkbox"/> Forebody Total Heat Load (Margined) (J/cm ²)	<input type="checkbox"/> Impact Foam Density (kg/m ³)	<input type="checkbox"/> Impact Foam Mass (kg)
<input type="checkbox"/> Impact Shell Density (kg/m ³)	<input type="checkbox"/> Input Shoulder Radius (m)	<input type="checkbox"/> Ixx (kg-m ²)	<input type="checkbox"/> Iyy (kg-m ²)	<input type="checkbox"/> Izz (kg-m ²)
<input type="checkbox"/> Lid Density (kg/m ³)	<input type="checkbox"/> Lid Height (m)	<input type="checkbox"/> Lid Insulation Mass (kg)	<input type="checkbox"/> Lid Radius (m)	<input type="checkbox"/> Max Dynamic Pressure (Pa)
<input checked="" type="checkbox"/> Max Entry Load (Earth g's)	<input type="checkbox"/> Max Payload Temperature (C)	<input type="checkbox"/> Nose Radius (m)	<input type="checkbox"/> Number of Iterations	<input type="checkbox"/> Payload Density (kg/m ³)
<input type="checkbox"/> Payload Diameter (m)	<input type="checkbox"/> Payload Height (m)	<input type="checkbox"/> Primary Structure Mass (kg)	<input type="checkbox"/> Primary Structure Thickness (cm)	<input type="checkbox"/> Required Stroke (cm)
<input type="checkbox"/> Terminal Velocity (m/s)	<input type="checkbox"/> Time of Flight (s)	<input type="checkbox"/> Total Entry Mass (kg)	<input type="checkbox"/> Vehicle CG Location from Nose (m)	<input type="checkbox"/> Vehicle Height (m)
<input type="checkbox"/> Vertical C.G. Location (X/D)	<input type="checkbox"/> Vertical C.G. Location (m)	<input type="checkbox"/> Wing Insulation Density (kg/m ³)	<input type="checkbox"/> Wing Insulation Mass (kg)	

6) Finally, click "Plot" button below to begin generating the contour plot:

[Plot](#)

MSAPE Onv (3) csv

Show all download...

KD-Tree Contour Plots

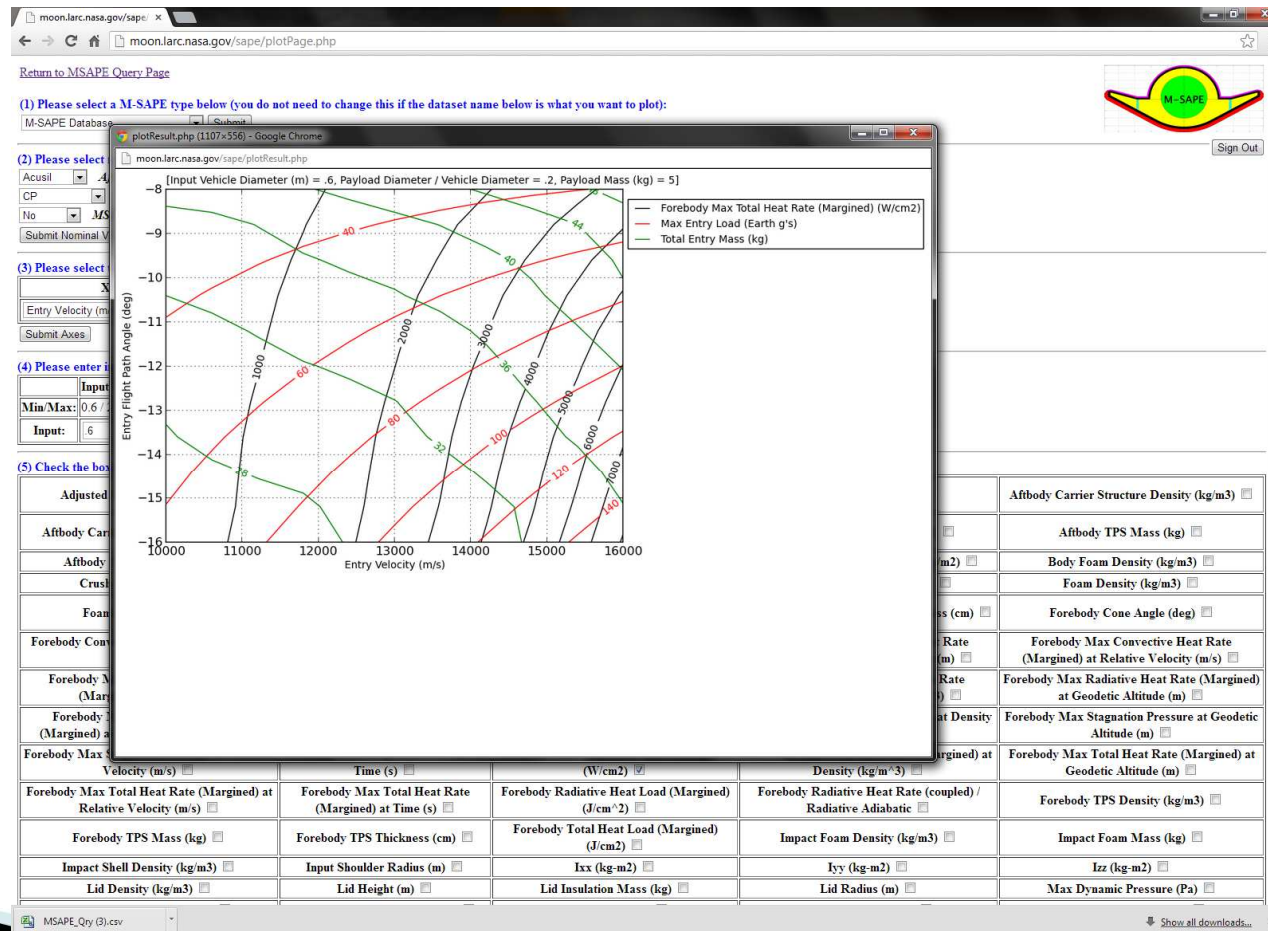
- ▶ A new window will then pop up (you may have to enable the pop up in some browsers, i.e. Opera)
- ▶ The new window will continuously refresh until the image has been created
- ▶ Do not close the pop up window until the image loads or you get an error message

The screenshot shows a web browser window with a large white box containing the text: "Please wait; the image is being generated. Please do not close or refresh the browser." To the right of this box is a NASA logo and a "Sign Out" button. Below the message is a table of parameters, each with a checkbox. The table is organized into columns and rows, listing various physical and engineering parameters.

<input type="checkbox"/> Forebody Max Convective Heat Rate (Margined) at Time (s)	<input type="checkbox"/> Forebody Max Goulard Number	<input type="checkbox"/> Forebody Max Radiative Heat Rate (Margined) (W/cm ²)	<input type="checkbox"/> Forebody Max Radiative Heat Rate (Margined) at Density (kg/m ³)	<input type="checkbox"/> Forebody Max Radiative Heat Rate (Margined) at Geodetic Altitude (m)
<input type="checkbox"/> Forebody Max Radiative Heat Rate (Margined) at Relative Velocity (m/s)	<input type="checkbox"/> Forebody Max Radiative Heat Rate (Margined) at Time (s)	<input type="checkbox"/> Forebody Max Stagnation Pressure (atm)	<input type="checkbox"/> Forebody Max Stagnation Pressure at Density (kg/m ³)	<input type="checkbox"/> Forebody Max Stagnation Pressure at Geodetic Altitude (m)
<input type="checkbox"/> Forebody Max Stagnation Pressure at Relative Velocity (m/s)	<input type="checkbox"/> Forebody Max Stagnation Pressure at Time (s)	<input type="checkbox"/> Forebody Max Total Heat Rate (Margined) (W/cm ²)	<input type="checkbox"/> Forebody Max Total Heat Rate (Margined) at Density (kg/m ³)	<input type="checkbox"/> Forebody Max Total Heat Rate (Margined) at Geodetic Altitude (m)
<input type="checkbox"/> Forebody Max Total Heat Rate (Margined) at Relative Velocity (m/s)	<input type="checkbox"/> Forebody Max Total Heat Rate (Margined) at Time (s)	<input type="checkbox"/> Forebody Radiative Heat Load (Margined) (J/cm ²)	<input type="checkbox"/> Forebody Radiative Heat Rate (coupled) / Radiative Adiabatic	<input type="checkbox"/> Forebody TPS Density (kg/m ³)
<input type="checkbox"/> Forebody TPS Mass (kg)	<input type="checkbox"/> Forebody TPS Thickness (cm)	<input type="checkbox"/> Forebody Total Heat Load (Margined) (J/cm ²)	<input type="checkbox"/> Impact Foam Density (kg/m ³)	<input type="checkbox"/> Impact Foam Mass (kg)
<input type="checkbox"/> Impact Shell Density (kg/m ³)	<input type="checkbox"/> Input Shoulder Radius (m)	<input type="checkbox"/> Ixx (kg-m ²)	<input type="checkbox"/> Iyy (kg-m ²)	<input type="checkbox"/> Izz (kg-m ²)
<input type="checkbox"/> Lid Density (kg/m ³)	<input type="checkbox"/> Lid Height (m)	<input type="checkbox"/> Lid Insulation Mass (kg)	<input type="checkbox"/> Lid Radius (m)	<input type="checkbox"/> Max Dynamic Pressure (Pa)

KD-Tree Contour Plots

- ▶ The image should look something like the one below
- ▶ You can plot multiple images and leave them open in their respective pop up windows
- ▶ **Do not try to run two plots at once**
- ▶ Once you close the pop up window, you will not be able to access it again unless you run the same contour plot again



KD-Tree Contour Plots

- ▶ After proceeding past Section (2), if you decide to change a nominal variable in Section (2), **YOU MUST THEN SELECT “Submit Nominal Variables” AGAIN FOR THE CHANGE TO TAKE EFFECT**
- ▶ Click the “Return to MSAPE Query Page” hyperlink at the top to get back to the Main Query Page

moon.larc.nasa.gov/sape/plotPage.php

[Return to MSAPE Query Page](#)

(1) Please select a MSAPE type below (you do not need to change this if the dataset name below is what you want to plot):
M-MSAPE Database

(2) Please select nominal, independent variables (you must select a value for each combobox displayed below):
Acusil
PICA-AL-5056
No
 (Submitting nominal variable selection will take some time, please do not close or refresh your browser after selecting this button.)

(3) Please select two numeric, independent variables for the X and Y axes:

X-Axis	Y-Axis
Entry Velocity (m/s)	Entry Flight Path Angle (deg)

(4) Please enter in a value for each numeric, independent variable below. These values will be fixed when generating the contour plot:

	Input Vehicle Diameter (m)	Payload Diameter / Vehicle Diameter	Payload Mass (kg)
Min/Max:	0.6 / 2	0.2 / 0.6	5 / 30
Input:	6	.2	5

(5) Check the boxes of the dependent, numeric variables below for the contour plot:

<input type="checkbox"/> Adjusted Shoulder Radius (m)	<input type="checkbox"/> Adjusted Shoulder Radius / Vehicle Radius	<input type="checkbox"/> Adjusted Vehicle Diameter (m)	<input type="checkbox"/> Aftbody Angle (deg)	<input type="checkbox"/> Aftbody Carrier Structure Density (kg/m ³)
<input type="checkbox"/> Aftbody Carrier Structure Mass (kg)	<input type="checkbox"/> Aftbody Carrier Structure Thickness (cm)	<input type="checkbox"/> Aftbody Max Heat Rate (W/cm ²)	<input type="checkbox"/> Aftbody TPS Density (kg/m ³)	<input type="checkbox"/> Aftbody TPS Mass (kg)
<input type="checkbox"/> Aftbody TPS Thickness (cm)	<input type="checkbox"/> Aftbody Total Heat Load (J/cm ²)	<input type="checkbox"/> Attached Structure Depth (m)	<input type="checkbox"/> Ballistic Coefficient at Impact (kg/m ²)	<input type="checkbox"/> Body Foam Density (kg/m ³)
<input type="checkbox"/> Crush Load Limit (g's)	<input type="checkbox"/> Downrange (km)	<input type="checkbox"/> Drag Coefficient at Impact	<input type="checkbox"/> Estimated Impact Load (g's)	<input type="checkbox"/> Foam Density (kg/m ³)
<input type="checkbox"/> Foam Thickness (cm)	<input type="checkbox"/> Forebody Carrier Structure Density (kg/m ³)	<input type="checkbox"/> Forebody Carrier Structure Mass (kg)	<input type="checkbox"/> Forebody Carrier Structure Thickness (cm)	<input type="checkbox"/> Forebody Cone Angle (deg)
<input type="checkbox"/> Forebody Convective Heat Load (Margined) (J/cm ²)	<input type="checkbox"/> Forebody Max Convective Heat Rate (Margined) (W/cm ²)	<input type="checkbox"/> Forebody Max Convective Heat Rate (Margined) at Density (kg/m ³)	<input type="checkbox"/> Forebody Max Convective Heat Rate (Margined) at Geodetic Altitude (m)	<input type="checkbox"/> Forebody Max Convective Heat Rate (Margined) at Relative Velocity (m/s)
<input type="checkbox"/> Forebody Max Convective Heat Rate (Margined) at Time (s)	<input type="checkbox"/> Forebody Max Goulard Number	<input type="checkbox"/> Forebody Max Radiative Heat Rate (Margined) (W/cm ²)	<input type="checkbox"/> Forebody Max Radiative Heat Rate (Margined) at Density (kg/m ³)	<input type="checkbox"/> Forebody Max Radiative Heat Rate (Margined) at Geodetic Altitude (m)
<input type="checkbox"/> Forebody Max Radiative Heat Rate (Margined) at Relative Velocity (m/s)	<input type="checkbox"/> Forebody Max Radiative Heat Rate (Margined) at Time (s)	<input type="checkbox"/> Forebody Max Stagnation Pressure (atm)	<input type="checkbox"/> Forebody Max Stagnation Pressure at Density (kg/m ³)	<input type="checkbox"/> Forebody Max Stagnation Pressure at Geodetic Altitude (m)
<input type="checkbox"/> Forebody Max Stagnation Pressure at Relative Velocity (m/s)	<input type="checkbox"/> Forebody Max Stagnation Pressure at Time (s)	<input type="checkbox"/> Forebody Max Total Heat Rate (Margined) (W/cm ²)	<input type="checkbox"/> Forebody Max Total Heat Rate (Margined) at Density (kg/m ³)	<input type="checkbox"/> Forebody Max Total Heat Rate (Margined) at Geodetic Altitude (m)
<input type="checkbox"/> Forebody Max Total Heat Rate (Margined) at Relative Velocity (m/s)	<input type="checkbox"/> Forebody Max Total Heat Rate (Margined) at Time (s)	<input type="checkbox"/> Forebody Radiative Heat Load (Margined) (J/cm ²)	<input type="checkbox"/> Forebody Radiative Heat Rate (coupled) / Radiative Adiabatic	<input type="checkbox"/> Forebody TPS Density (kg/m ³)
<input type="checkbox"/> Forebody TPS Mass (kg)	<input type="checkbox"/> Forebody TPS Thickness (cm)	<input type="checkbox"/> Forebody Total Heat Load (Margined) (J/cm ²)	<input type="checkbox"/> Impact Foam Density (kg/m ³)	<input type="checkbox"/> Impact Foam Mass (kg)
<input type="checkbox"/> Impact Shell Density (kg/m ³)	<input type="checkbox"/> Input Shoulder Radius (m)	<input type="checkbox"/> Ixx (kg-m ²)	<input type="checkbox"/> Iyy (kg-m ²)	<input type="checkbox"/> Izz (kg-m ²)
<input type="checkbox"/> Lid Density (kg/m ³)	<input type="checkbox"/> Lid Height (m)	<input type="checkbox"/> Lid Insulation Mass (kg)	<input type="checkbox"/> Lid Radius (m)	<input type="checkbox"/> Max Dynamic Pressure (Pa)

MSAPE_Qry (3).csv

Neural Network Contour Plots

- ▶ To Run a Neural Network contour plot, select the “Create a Neural Network Contour Plot” hyperlink from the Main Query Page



Sign Out

- [M-SAPE Administrator Page](#)
- [M-SAPE User Guide](#)
- [Change Password](#)
- [Create a Neural Network Contour Plot](#)

To upload information into M-SAPE, ensure that it is in the proper CSV format and upload the file below (note, other regular users will not be able to query your information):

Upload file:

[Run a New M-SAPE Iteration](#)

(1) Please select a M-SAPE type below to query its data set:

LHS_Acusil_CP_MSR_1000

Sign Out

Create a KD-Tree / RBF Contour Plot Using this M-SAPE Type

(2) Enter any desired query parameters for the independent variables listed below:

Minimum	Maximum	Variable Name	Min / Max
		Convective Heat Rate Margin	1.10001352/1.49966134
		Entry Flight Path Angle (deg)	-24.99776599/-15.00918473
		Entry Velocity (m/s)	10001.51682/12498.81526
		Input Shoulder Radius / Vehicle Radius	0.05/0.05
		Input Vehicle Diameter (m)	0.5/0.5
		Mass Convergence Criterion (kg)	0.001/0.001
		Mass Margin	0.20003536/0.39981513
		Max Number of Iterations	20/20
		Nose Radius / Vehicle Radius	0.5/0.5
		Payload Diameter (m)	0.15/0.2899
		Payload Mass (kg)	3.003/9.999
		Radiative Heat Rate Margin	0.90034755/1.29965627

- Acusil *Aftbody TPS Concept*
- SuttonGraves *Convective Heat Rate Model*
- CP *Forebody TPS Concept*
- Yes *MSR Mode*
- TauberSutton *Radiative Heat Rate Model*

Neural Network Contour Plots

- ▶ Select the dataset which you want to plot from the dropdown menu
- ▶ On the right is a list of dataset's with associated neural networks which have not been enabled for plotting by an Administrator
- ▶ Contact an administrator to enable these neural networks for plotting



The screenshot displays the M-SAPE web interface. At the top left is a banner for the Systems Analysis and Concepts Directorate at Langley Research Center. On the top right is the M-SAPE logo and a 'Sign Out' button. Below the banner are links for 'Return to M-SAPE Query Page' and 'M-SAPE User Guide'. A red oval highlights a dropdown menu with the text '(1) Please select a dataset type below:' and the current selection '-- Select a Dataset for Training --'. Below the dropdown is a 'Submit' button. To the right of the dropdown is a table of datasets:


Datasets	
1000 LHS for SLA-561V CP MSR	
LHS_Acusil_CP_MSR_1000	
Medical	

Below the table is a blue notice: 'The dataset(s) listed below have trained neural networks which have not been enabled by an administrator. Please contact an M-SAPE administrator to enable these networks:'.

Neural Network Contour Plots

- ▶ If your selected dataset has nominal independent variables, select a value for each variable in its appropriate dropdown menu
- ▶ If your selected dataset has shading for nominal variables, the nominal shading table will appear with all variable shades selected
- ▶ Uncheck the nominal shading checkboxes if you do not want to plot nominal shading
- ▶ Select X and Y Axes variables for your contour plot and click “Submit”

Systems Analysis and Concepts Directorate
Langley Research Center



Sign Out

[Return to M-SAPE Query Page](#)
[M-SAPE User Guide](#)

The dataset(s) listed below have trained neural networks which have not been enabled by an administrator. Please contact an M-SAPE administrator to enable these networks:

Datasets	
1000 LHS for SLA-561V CP MSR	
LHS_Acusi_CP_MSR_1000	
Medical	

(1) Please select a dataset type below:
My First Run 2014-02-21 09:01:59

Nominal Independent Variables	Selection
Aftbody TPS Concept	-- Select a Nominal Variable --
Forebody TPS Concept	-- Select a Nominal Variable --
MSR Mode	-- Select a Nominal Variable --

Nominal Shading Variables	Color
Converged	Red <input checked="" type="checkbox"/>
Forebody TPS Message	Yellow <input checked="" type="checkbox"/>
Aftbody TPS Message	Magenta <input checked="" type="checkbox"/>

X-Axis	Y-Axis
-- Select an X-Axis Variable --	-- Select an Y-Axis Variable --

Neural Network Contour Plots

- ▶ Next input specific values for any numeric, independent variables which are not used for the X or Y axes
- ▶ Check each dependent, numeric variable which you would like to see plotted
- ▶ Finally, hit “Plot”

Aftbody TPS Concept	Acusil
Forebody TPS Concept	CP
MSR Mode	Yes

Nominal Shading Variables	Color
Converged	Red <input checked="" type="checkbox"/>
Forebody TPS Message	Yellow <input checked="" type="checkbox"/>
Aftbody TPS Message	Magenta <input checked="" type="checkbox"/>

X-Axis	Y-Axis
Entry Velocity (m/s)	Entry Flight Path Angle (deg)

Input Vehicle Diameter (m)	Nose Radius / Input Vehicle Radius	Payload Diameter / Vehicle Diameter	Payload Mass (kg)
Min/Max: 0.6 / 2	0.75 / 0.78222	0.2 / 0.6	5 / 30
Input: 1	.75	2	6

<input type="checkbox"/> Adjusted Shoulder Radius (m)	<input type="checkbox"/> Adjusted Shoulder Radius / Vehicle Radius	<input type="checkbox"/> Adjusted Vehicle Diameter (m)	<input type="checkbox"/> Aftbody Angle (deg)	<input type="checkbox"/> Aftbody Carrier Structure Density (kg/m3)
<input type="checkbox"/> Aftbody Carrier Structure Mass (kg)	<input type="checkbox"/> Aftbody Carrier Structure Thickness (cm)	<input type="checkbox"/> Aftbody Max Heat Rate (W/cm2)	<input type="checkbox"/> Aftbody TPS Density (kg/m3)	<input type="checkbox"/> Aftbody TPS Mass (kg)
<input type="checkbox"/> Aftbody TPS Thickness (cm)	<input type="checkbox"/> Aftbody Total Heat Load (J/cm2)	<input type="checkbox"/> Attached Structure Depth (m)	<input type="checkbox"/> Ballistic Coefficient at Impact (kg/m2)	<input type="checkbox"/> Body Foam Density (kg/m3)
<input type="checkbox"/> Crush Load Limit (g's)	<input type="checkbox"/> Downrange (km)	<input type="checkbox"/> Drag Coefficient at Impact	<input type="checkbox"/> Estimated Impact Load (g's)	<input type="checkbox"/> Foam Density (kg/m3)
<input type="checkbox"/> Foam Thickness (cm)	<input type="checkbox"/> Forebody Carrier Structure Density (kg/m3)	<input type="checkbox"/> Forebody Carrier Structure Mass (kg)	<input type="checkbox"/> Forebody Carrier Structure Thickness (cm)	<input type="checkbox"/> Forebody Cone Angle (deg)
<input type="checkbox"/> Forebody Convective Heat Load (Margined) (J/cm^2)	<input type="checkbox"/> Forebody Max Convective Heat Rate (Margined) (W/cm^2)	<input type="checkbox"/> Forebody Max Convective Heat Rate (Margined) at Density (kg/m^3)	<input type="checkbox"/> Forebody Max Convective Heat Rate (Margined) at Geodetic Altitude (m)	<input type="checkbox"/> Forebody Max Convective Heat Rate (Margined) at Relative Velocity (m/s)
<input type="checkbox"/> Forebody Max Convective Heat Rate (Margined) at Time (s)	<input type="checkbox"/> Forebody Max Goulard Number	<input type="checkbox"/> Forebody Max Radiative Heat Rate (Margined) (W/cm^2)	<input type="checkbox"/> Forebody Max Radiative Heat Rate (Margined) at Density (kg/m^3)	<input type="checkbox"/> Forebody Max Radiative Heat Rate (Margined) at Geodetic Altitude (m)
<input type="checkbox"/> Forebody Max Radiative Heat Rate (Margined) at Relative Velocity (m/s)	<input type="checkbox"/> Forebody Max Radiative Heat Rate (Margined) at Time (s)	<input type="checkbox"/> Forebody Max Stagnation Pressure (atm)	<input type="checkbox"/> Forebody Max Stagnation Pressure at Density (kg/m^3)	<input type="checkbox"/> Forebody Max Stagnation Pressure at Geodetic Altitude (m)
<input type="checkbox"/> Forebody Max Stagnation Pressure at Relative Velocity (m/s)	<input type="checkbox"/> Forebody Max Stagnation Pressure at Time (s)	<input type="checkbox"/> Forebody Max Total Heat Rate (Margined) (W/cm2)	<input type="checkbox"/> Forebody Max Total Heat Rate (Margined) at Density (kg/m^3)	<input type="checkbox"/> Forebody Max Total Heat Rate (Margined) at Geodetic Altitude (m)
<input type="checkbox"/> Forebody Max Total Heat Rate (Margined) at Relative Velocity (m/s)	<input type="checkbox"/> Forebody Max Total Heat Rate (Margined) at Time (s)	<input type="checkbox"/> Forebody Radiative Heat Load (Margined) (J/cm^2)	<input type="checkbox"/> Forebody Radiative Heat Rate (coupled) / Radiative Adiabatic	<input type="checkbox"/> Forebody TPS Density (kg/m3)
<input type="checkbox"/> Forebody TPS Mass (kg)	<input type="checkbox"/> Forebody TPS Thickness (cm)	<input type="checkbox"/> Forebody Total Heat Load (Margined) (J/cm2)	<input type="checkbox"/> Impact Foam Density (kg/m3)	<input type="checkbox"/> Impact Foam Mass (kg)
<input type="checkbox"/> Impact Shell Density (kg/m3)	<input type="checkbox"/> Input Shoulder Radius (m)	<input type="checkbox"/> Ixx (kg-m2)	<input type="checkbox"/> Iyy (kg-m2)	<input type="checkbox"/> Izz (kg-m2)
<input type="checkbox"/> Lid Density (kg/m3)	<input type="checkbox"/> Lid Height (m)	<input type="checkbox"/> Lid Insulation Mass (kg)	<input type="checkbox"/> Lid Radius (m)	<input type="checkbox"/> Max Dynamic Pressure (Pa)
<input checked="" type="checkbox"/> Max Entry Load (Earth g's)	<input type="checkbox"/> Max Payload Temperature (C)	<input type="checkbox"/> Nose Radius (m)	<input type="checkbox"/> Number of Iterations	<input type="checkbox"/> Payload Density (kg/m3)
<input type="checkbox"/> Payload Diameter (m)	<input type="checkbox"/> Payload Height (m)	<input type="checkbox"/> Primary Structure Mass (kg)	<input type="checkbox"/> Primary Structure Thickness (cm)	<input type="checkbox"/> Required Stroke (cm)
<input type="checkbox"/> Terminal Velocity (m/s)	<input type="checkbox"/> Time of FLight (s)	<input type="checkbox"/> Total Entry Mass (kg)	<input type="checkbox"/> Vehicle CG Location from Nose (m)	<input type="checkbox"/> Vehicle Height (m)
<input type="checkbox"/> Vertical C.G. Location (X/D)	<input type="checkbox"/> Vertical C.G. Location (m)	<input type="checkbox"/> Wing Insulation Density (kg/m3)	<input type="checkbox"/> Wing Insulation Mass (kg)	

Plot

Neural Network Contour Plots

- ▶ Your plot should appear shortly afterwards in a pop-up window
- ▶ If you get the error message: “An error occurred while generating your image.”, try deselecting some numeric, dependent variable checkboxes and then attempt plotting again (errors may be due to a faulty neural network specific to one or more numeric, dependent variable(s))

Systems Analysis and Concepts Directorate
Langley Research Center

Return to M-SAPE Query Page
M-SAPE User Guide

(1) Please select a dataset type below:
My First Run 2014-02-21 09:01:59

Nominal Independent Variables	Selection
Aftbody TPS Concept	Acusil
Forebody TPS Concept	CP
MSR Mode	Yes

Nominal Shading Variables	Color
Converged	Red <input checked="" type="checkbox"/>
Forebody TPS Message	Yellow <input checked="" type="checkbox"/>
Aftbody TPS Message	Magenta <input checked="" type="checkbox"/>

X-Axis: Entry Velocity (m/s)
Y-Axis: Entry Flight Path Angle (deg)

Input Vehicle Diameter (m) = 1, Nose Radius / Input Vehicle Radius = .75, Payload Diameter / Vehicle Diameter = .2, Payload Mass (kg) = 6

Min/Max: 0.6 / 2
Input: 1

0.75 / 0.78222
Input: .75

Forebody Max Total Heat Rate (Margined) (W/cm2)
Max Entry Load (Earth g's)
Total Entry Mass (kg)

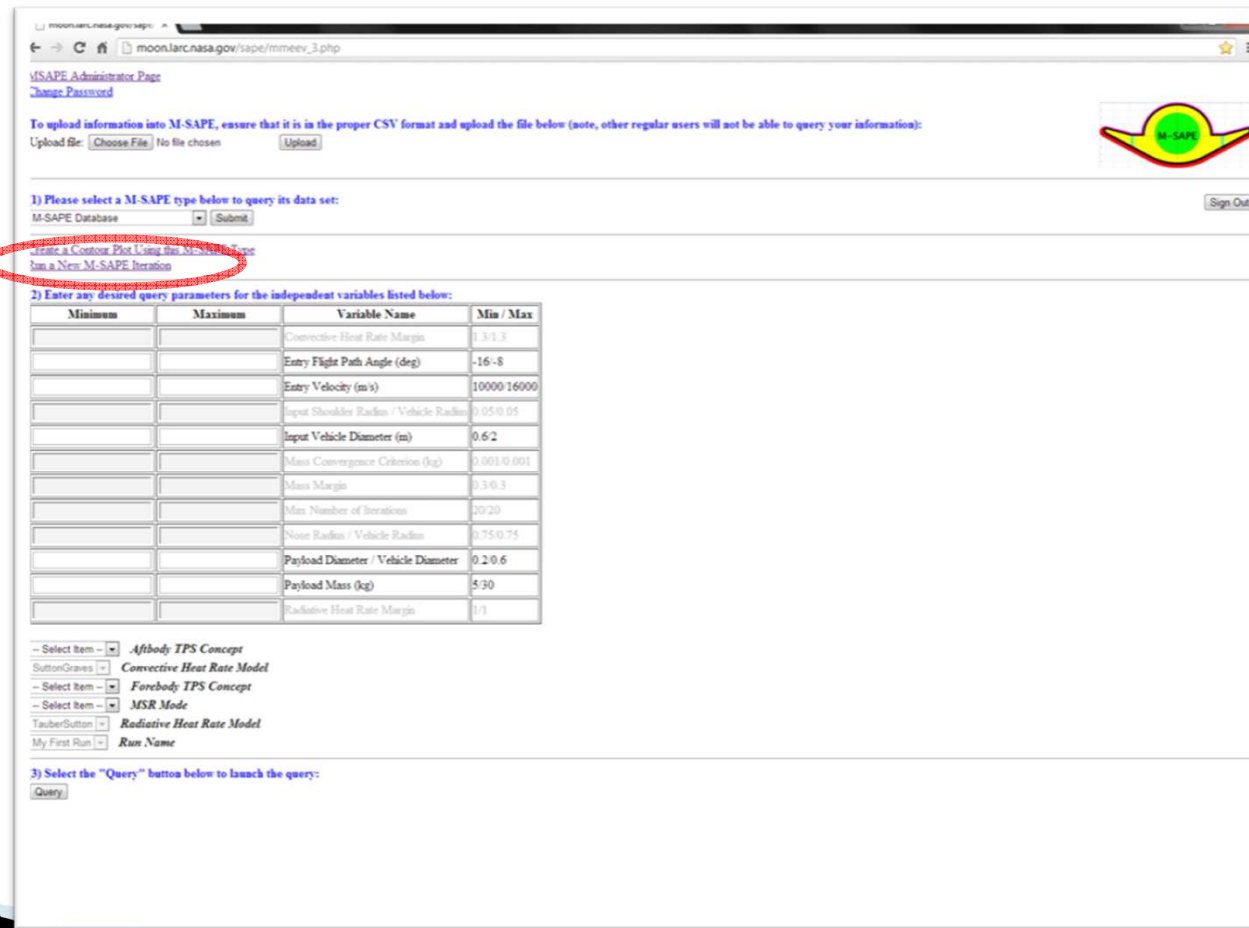
Nominal Shading:
Converged
Forebody TPS Message
Aftbody TPS Message

Aftbody TPS Concept = Acusil, Forebody TPS Concept = CP, MSR Mode = Yes
Dataset: My First Run 2014-02-21 09:01:59
M-SAPE Neural Net Contour Plot Ver 1.0 2014-03-19-10:47:45

<input type="checkbox"/> Adjusted Shoulder Radius (m)	<input type="checkbox"/> Adjusted Shoulder Radius / Vehicle Radius	<input type="checkbox"/> Adjusted Vehicle Diameter (m)	<input type="checkbox"/> Aftbody Angle (deg)	<input type="checkbox"/> Aftbody Carrier Structure Density (kg/m3)
<input type="checkbox"/> Aftbody Carrier Structure Mass (kg)	<input type="checkbox"/> Aftbody Carrier Structure Thickness (cm)	<input type="checkbox"/> Aftbody Max Heat Rate (W/cm2)	<input type="checkbox"/> Aftbody TPS Density (kg/m3)	<input type="checkbox"/> Aftbody TPS Mass (kg)
<input type="checkbox"/> Aftbody TPS Thickness (cm)	<input type="checkbox"/> Aftbody Total Heat Load (J/cm2)	<input type="checkbox"/> Attached Structure Depth (m)	<input type="checkbox"/> Ballistic Coefficient at Impact (kg/m2)	<input type="checkbox"/> Body Foam Density (kg/m3)
<input type="checkbox"/> Crush Load Limit (g's)	<input type="checkbox"/> Downrange (km)	<input type="checkbox"/> Drag Coefficient at Impact	<input type="checkbox"/> Estimated Impact Load (g's)	<input type="checkbox"/> Foam Density (kg/m3)

Single M-SAPE Iteration

- ▶ To run M-SAPE with user input, select the “Run a New M-SAPE Iteration” hyperlink from the Main Query Page



The screenshot shows the M-SAPE Administrator Page in a web browser. The page includes a navigation menu, a file upload section, and a section for selecting an M-SAPE type. A red circle highlights the "Run a New M-SAPE Iteration" link. Below this, there is a table for entering query parameters for independent variables, followed by several dropdown menus for selecting models and concepts.

1) Please select a M-SAPE type below to query its data set:
M-SAPE Database: Submit

2) Enter any desired query parameters for the independent variables listed below:

Minimum	Maximum	Variable Name	Min / Max
		Convective Heat Rate Margin	1.3/1.3
		Entry Flight Path Angle (deg)	-16/-8
		Entry Velocity (m/s)	10000 16000
		Input Shoulder Radius / Vehicle Radius	0.05/0.05
		Input Vehicle Diameter (m)	0.6/2
		Mass Convergence Criterion (kg)	0.001/0.001
		Mass Margin	0.3/0.3
		Max Number of Iterations	10/20
		Nose Radius / Vehicle Radius	0.75/0.75
		Payload Diameter / Vehicle Diameter	0.2/0.6
		Payload Mass (kg)	5/30
		Radiative Heat Rate Margin	1/1

3) Select the "Query" button below to launch the query:

Single M-SAPE Iteration

- ▶ On the M-SAPE Call page, enter a descriptive name for your run in Section (1) (it does not have to be unique)
- ▶ In Section (2), enter input parameters for your entry vehicle design (default values will be selected on page load)
- ▶ Click the “Run M-SAPE” button in Section (3) to start the run

moon.larc.nasa.gov/sape/ x
moon.larc.nasa.gov/sape/msapeCall.php

[Return to MSAPE Query Page](#)
M-SAPE Database

(1) Please enter an identifying name for this run below:

(2) Please enter valid values for numeric and nominal independent variables below:

Enter Value Below:	Variable Name	Min / Max
1.3	Convective Heat Rate Margin	0 / 10
-8	Entry Flight Path Angle (deg)	-90 / -1
12000	Entry Velocity (m/s)	10000 / 16000
0.05	Input Shoulder Radius / Vehicle Radius	0.02 / 0.1
1	Input Vehicle Diameter (m)	0.5 / 2
0.001	Mass Convergence Criterion (kg)	0.0001 / 1
0.3	Mass Margin	0 / 1
20	Max Number of Iterations	1 / 200
0.75	Nose Radius / Vehicle Radius	0.25 / 0.9
0.6	Payload Diameter / Vehicle Diameter	0.2 / 0.6
15	Payload Mass (kg)	5 / 20
1	Radiative Heat Rate Margin	0 / 2

SIRCA *Aftbody TPS Concept*
SuttonGraves *Convective Heat Rate Model*
PICA-AL-5056 *Forebody TPS Concept*
Yes *MSR Mode*
TauberSutton *Radiative Heat Rate Model*
My First *Run Name*

(3) Press the "Run M-SAPE" button below to start the run:

[Previous User M-SAPE Runs:](#)

Run Name	Date
Test3	2013-08-01 12:15:18
cables2013-07-31_1115_15	2013-07-31 11:15:15
Test2	2013-07-31 11:12:13
Test1	2013-07-31 11:08:18

MSAPE_Qry (3).csv Show all downloads... x

Single M-SAPE Iteration

- ▶ A pop up page will appear (once again, you may need to enable pop ups depending on your browser)
- ▶ Depending on your design and the number of iterations you selected in Section (2), it may take some time for the design to close (i.e. four minutes for an 18 iteration run); be patient

The screenshot shows a web browser window with the URL `moon.larc.nasa.gov/sape/msapeCall.php`. The page contains a form for entering parameters for an M-SAPE iteration. A pop-up window is overlaid on the page, displaying the text: "Please wait; M-SAPE is still running. Please do not close or refresh the browser." The pop-up window has a yellow border and a "Sign Out" button. The background page shows a table of input variables and a "Run M-SAPE" button.

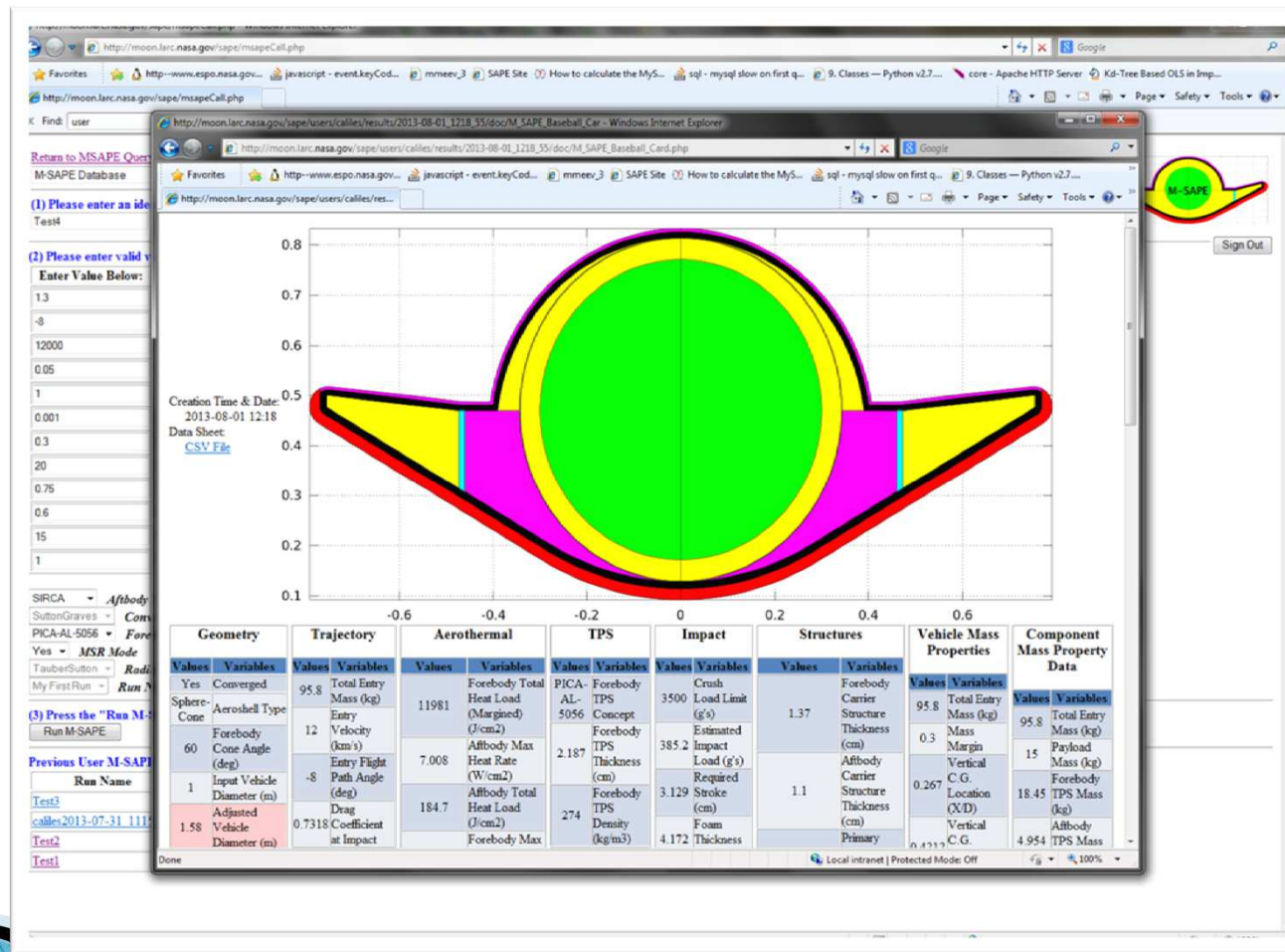
Enter Value Below:	Variable Name
1.3	Convective Heat Rate Margin
-8	Entry Flight Path Angle (deg)
12000	Entry Velocity (m/s)
0.05	Input Shoulder Radius / Vehicle Radius
1	Input Vehicle Diameter (m)
0.001	Mass Convergence Criterion (kg)
0.3	Mass Margin
20	Max Number of Iterations
0.75	Nose Radius / Vehicle Radius
0.6	Payload Diameter / Vehicle Diameter
15	Payload Mass (kg)
1	Radiative Heat Rate Margin

Buttons: SIRCA, Aftbody TPS Concept, SuttonGraves, Convective Heat Rate Model, PICA-AL-5056, Forebody TPS Concept, Yes, MSR Mode, TauberSutton, Radiative Heat Rate Model, My First Run, Run Name, Run M-SAPE

Run Name	Date
Test3	2013-08-01 12:15:18
calbes2013-07-31_1115_15	2013-07-31 11:15:15
Test2	2013-07-31 11:12:13
Test1	2013-07-31 11:08:18

Single M-SAPE Iteration

- ▶ If the design closed successfully, you will see a the pop up page eventually displayed like the one below
- ▶ Otherwise, you should see an error message; contact a M-SAPE administrator for assistance



Single M-SAPE Iteration

- ▶ Unlike the Contour Plotting page, your previous M-SAPE runs will be stored in the system
- ▶ Previous M-SAPE runs can be accessed from the hyperlinks in the table below Section (3)
- ▶ Select the “Return to MSAPE Query Page” at the top to navigate to the Main Query Page

The screenshot shows the M-SAPE web interface. At the top, there is a navigation bar with a link "Return to MSAPE Query Page" circled in red. Below this is a form for entering an identifying name for the run. The main section contains a table of input parameters with their current values and min/max ranges. Below the table are dropdown menus for selecting various models and concepts. At the bottom, there is a "Run M-SAPE" button and a table of previous user runs, also circled in red.

(1) Please enter an identifying name for this run below:

(2) Please enter valid values for numeric and nominal independent variables below:

Enter Value Below:	Variable Name	Min / Max
1.3	Convective Heat Rate Margin	0 / 10
-8	Entry Flight Path Angle (deg)	-90 / -1
12000	Entry Velocity (m/s)	10000 / 16000
0.05	Input Shoulder Radius / Vehicle Radius	0.02 / 0.1
1	Input Vehicle Diameter (m)	0.5 / 2
0.001	Mass Convergence Criterion (kg)	0.0001 / 1
0.3	Mass Margin	0 / 1
20	Max Number of Iterations	1 / 200
0.75	Nose Radius / Vehicle Radius	0.25 / 0.9
0.6	Payload Diameter / Vehicle Diameter	0.2 / 0.6
15	Payload Mass (kg)	5 / 20
1	Radiative Heat Rate Margin	0 / 2

SIRCA *Aftbody TPS Concept*
 SuttonGraves *Convective Heat Rate Model*
 PICA-AL-5056 *Forebody TPS Concept*
 Yes *MSR Mode*
 TauberSutton *Radiative Heat Rate Model*
 My First Run *Run Name*

(3) Press the "Run M-SAPE" button below to start the run:

Run M-SAPE

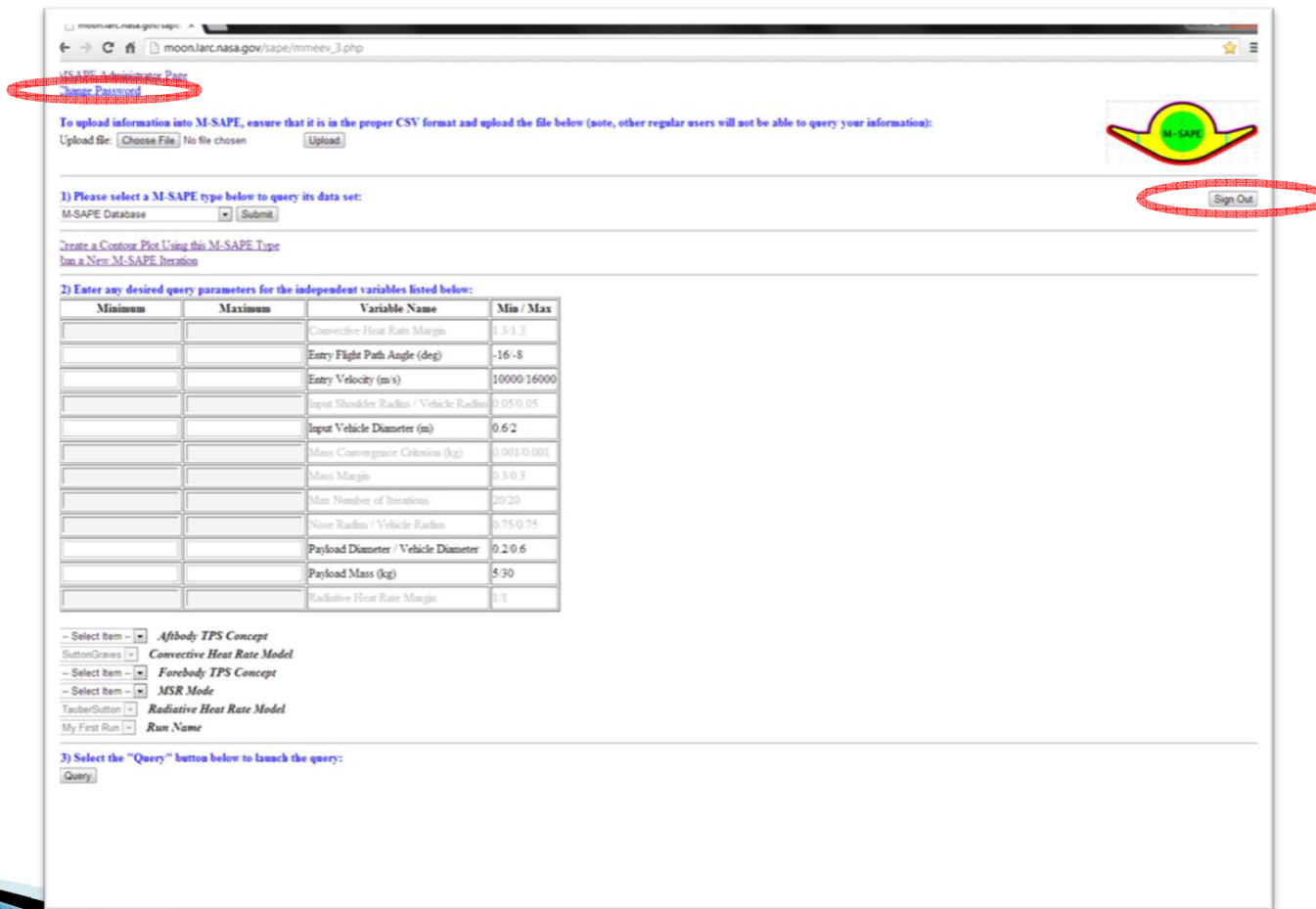
Previous User M-SAPE Runs:

Run Name	Date
Test3	2013-08-01 12:15:18
cables2013-07-31_1115_15	2013-07-31 11:15:15
Test2	2013-07-31 11:12:13
Test1	2013-07-31 11:08:18

MSAPE_Qry (3).csv

Changing Passwords / Signing Out

- ▶ You can change your M-SAPE password from the Main Query Page by selecting the “Change Password” link at the top
- ▶ To exit the system, click the “Sign Out” button in the top right of most pages



The screenshot shows the M-SAPE Administrator Page in a web browser. The browser address bar displays `moon.larc.nasa.gov/sape/mmeev_3.php`. At the top left, the text "M-SAPE Administrator Page" is visible, with a red circle around the "Change Password" link. In the top right corner, there is a yellow and green M-SAPE logo and a "Sign Out" button, both of which are circled in red. Below the logo, there is a section for uploading information into M-SAPE, followed by a dropdown menu for selecting an M-SAPE type. A table of query parameters is provided, and at the bottom, there are several dropdown menus for selecting different TPS concepts and models.

Minimum	Maximum	Variable Name	Min / Max
		Convective Heat Rate Margin	1.3/1.3
		Entry Flight Path Angle (deg)	-16/-8
		Entry Velocity (m/s)	10000 16000
		Input Shoulder Radius / Vehicle Radius	0.05/0.05
		Input Vehicle Diameter (m)	0.6/2
		Mass Convergence Criterion (kg)	0.001/0.001
		Mass Margin	0.3/0.3
		Max Number of Iterations	10/20
		Nose Radius / Vehicle Radius	0.75/0.75
		Payload Diameter / Vehicle Diameter	0.2/0.6
		Payload Mass (kg)	5/30
		Radiative Heat Rate Margin	1/1

REPORT DOCUMENTATION PAGE				Form Approved OMB No. 0704-0188	
<p>The public reporting burden for this collection of information is estimated to average 1 hour per response, including the time for reviewing instructions, searching existing data sources, gathering and maintaining the data needed, and completing and reviewing the collection of information. Send comments regarding this burden estimate or any other aspect of this collection of information, including suggestions for reducing this burden, to Department of Defense, Washington Headquarters Services, Directorate for Information Operations and Reports (0704-0188), 1215 Jefferson Davis Highway, Suite 1204, Arlington, VA 22202-4302. Respondents should be aware that notwithstanding any other provision of law, no person shall be subject to any penalty for failing to comply with a collection of information if it does not display a currently valid OMB control number.</p> <p>PLEASE DO NOT RETURN YOUR FORM TO THE ABOVE ADDRESS.</p>					
1. REPORT DATE (DD-MM-YYYY)		2. REPORT TYPE		3. DATES COVERED (From - To)	
01-08 - 2014		Technical Memorandum			
4. TITLE AND SUBTITLE				5a. CONTRACT NUMBER	
				5b. GRANT NUMBER	
				5c. PROGRAM ELEMENT NUMBER	
6. AUTHOR(S)				5d. PROJECT NUMBER	
				5e. TASK NUMBER	
				5f. WORK UNIT NUMBER	
7. PERFORMING ORGANIZATION NAME(S) AND ADDRESS(ES)				8. PERFORMING ORGANIZATION REPORT NUMBER	
NASA Langley Research Center Hampton, VA 23681-2199				L-20440	
9. SPONSORING/MONITORING AGENCY NAME(S) AND ADDRESS(ES)				10. SPONSOR/MONITOR'S ACRONYM(S)	
				11. SPONSOR/MONITOR'S REPORT NUMBER(S)	
National Aeronautics and Space Administration Washington, DC 20546-0001				NASA	
				NASA/TM-2014-218507	
12. DISTRIBUTION/AVAILABILITY STATEMENT					
Unclassified - Unlimited Subject Category 18 Availability: NASA CASI (443) 757-5802					
13. SUPPLEMENTARY NOTES					
14. ABSTRACT					
<p>This report describes an integrated system for Multi-mission System Analysis for Planetary Entry (M-SAPE). The system in its current form is capable of performing system analysis and design for an Earth entry vehicle suitable for sample return missions. The system includes geometry, mass sizing, impact analysis, structural analysis, flight mechanics, TPS, and a web portal for user access. The report includes details of M-SAPE modules and provides sample results. Current M-SAPE vehicle design concept is based on Mars sample return (MSR) Earth entry vehicle design, which is driven by minimizing risk associated with sample containment (no parachute and passive aerodynamic stability). By M-SAPE exploiting a common design concept, any sample return mission, particularly MSR, will benefit from significant risk and development cost reductions. The design provides a platform by which technologies and design elements can be evaluated rapidly prior to any costly investment commitment.</p>					
15. SUBJECT TERMS					
Entry vehicle; Sample return; System analysis					
16. SECURITY CLASSIFICATION OF:			17. LIMITATION OF ABSTRACT	18. NUMBER OF PAGES	19a. NAME OF RESPONSIBLE PERSON
a. REPORT	b. ABSTRACT	c. THIS PAGE			STI Help Desk (email: help@sti.nasa.gov)
U	U	U	UU	137	19b. TELEPHONE NUMBER (Include area code)
					(443) 757-5802